Fall 2013

Investigating an unusual flavin-dependent mechanism of thymidylate biosynthesis

Eric Michael Koehn
University of Iowa

INVESTIGATING AN UNUSUAL FLAVIN-DEPENDENT MECHANISM OF THYMIDYLATE BIOSYNTHESIS

by

Eric Michael Koehn

A thesis submitted in partial fulfillment
of the requirements for the Doctor of
Philosophy degree in Chemistry
in the Graduate College of
The University of Iowa

December 2013

Thesis Supervisor: Professor Amnon Kohen

Graduate College
The University of Iowa
Iowa City, Iowa

CERTIFICATE OF APPROVAL

PH.D. THESIS

This is to certify that the Ph.D. thesis of

Eric Michael Koehn

has been approved by the Examining Committee
for the thesis requirement for the Doctor of Philosophy
degree in Chemistry at the December 2013 graduation.

Thesis Committee: _____
Amnon Kohen, Thesis Supervisor

_____
Johna Leddy

_____
Daniel M. Quinn

_____
F. Christopher Pigge

_____
Eric E. Nuxoll

To LaVonne Midgley

Don’t gain the world and lose your soul, wisdom is better than silver or gold.
-Bob Marley
Zion Train

ACKNOWLEDGMENTS

I am truly indebted to so many who have helped me achieve a Ph.D., in ways too abundant to appropriately enumerate here. Most of all I'd like to thank God. It's been a long, challenging trip, and it is undoubtedly my faith that has brought me to this point. I thank my wife, Demelza. She is my reason and motivation, the one and only, my inspiration. I thank my family. They have taught me so many personal qualities that have been indispensible during my graduate education.

I extend a special thank you to my adviser, Amnon Kohen. As a mentor, he has exceeded my expectations, and educated me far beyond the scope of science. I am a firm believer that mentors should be someone we want to emulate. Over the years I can say I am truly grateful to have Amnon as a mentor, and I hope that one day I can share some of the qualities I learned from him with my own graduate students.

I would also like to thank my "lab family" and all those in the Kohen group. Akin to how brothers and sisters shape our personality and character, those who I have had the pleasure to work with as a graduate student have likewise provided a similar balance of friendship, support, adversity and accountability that has helped me mature personally and scientifically.

I have had the great opportunity to collaborate with several scientists as a graduate student. I specifically thank Bruce Palfey (UMich) and Irimpan Mathews (Stanford) for their thoughtful discussion and productive data sharing over the years.

Lastly, but certainly not least, I'd like to thank Don Reznicek (Normandale College). I'm not sure exactly when I decided to pursue an advanced degree in Chemistry, but "I would bet my Grandmother's scarf" this guy had something to do with it.

ABSTRACT

Biosynthesis of DNA depends on thymidylate synthase that catalyzes the reductive methylation of uridylate to form the essential base thymidylate. Two classes of thymidylate synthases are known. Humans and all other eukaryotes rely on *thy*A-encoded TSase, whereas, many microorganisms including several severe pathogens rely on the *thy*X-encoded flavin-dependent thymidylate synthase (FDTS). This dissertation describes research conducted to delineate the molecular mechanism of FDTS enzymes, and identify distinguishing features from that of classical TSases. Most notably, the findings presented in Chapter II indicate the mechanism of FDTS catalysis is unique to pyrimidine methylation in that it does not involve a covalent enzyme-substrate complex during the reaction. This work further investigates this unusual mechanism, by constructing a more thorough picture of the reaction through characterization of intermediates as shown in Chapter III. Additional studies regarding the structure, substrate binding patterns, FAD cofactor chemistry, and oxidase activity are presented in Chapters IV and V. Overall, the work presented here impacts our general knowledge about pyrimidine methylation strategies, and could potentially set the groundwork for mechanism-based rational inhibition of FDTS enzymes leading to possible antibiotic compounds.

TABLE OF CONTENTS

LIST OF TABLES

Table

LIST OF FIGURES

Figure

LIST OF SCHEMES

Scheme

CHAPTER I

FLAVIN-DEPENDENT THYMIDYLATE SYNTHASE: A NOVEL PATHWAY TOWARD THYMINE

This chapter was in full or part published in the Archives of Biochemistry and Biophysics Koehn E. M. and Kohen, A., 2010, *Arch. Biochem. Biophys.* 493:96-102. Figures and/or content are used with permission from Elsevier.

Abstract

For several decades, only one chemical pathway was known for the *de novo* biosynthesis of the essential DNA nucleotide, thymidylate. This reaction catalyzed by *thy*A-encoded (denoted *TYMS* in humans and other mammals) thymidylate synthases is the last committed step in the biosynthesis of thymidylate and proceeds *via* the reductive methylation of uridylate. However, many microorganisms have recently been shown to produce a novel, flavin-dependent thymidylate synthase encoded by the *thy*X gene. Preliminary structural and mechanistic studies have shown substantial differences between these deoxyuridylate-methylating enzymes. Recently, both the chemical and kinetic mechanisms of FDTS have provided further insight into the distinctions between *thy*A and *thy*X encoded thymidylate synthases. Since FDTSs are found in several severe human pathogens their unusual mechanism offers a promising future for the development of antibiotic and antiviral drugs with little effect on human thymidylate biosynthesis.

Introduction

Thymidylate is one of the four DNA building blocks and is crucial for survival of all organisms. This essential nucleotide is the product of the enzyme thymidylate synthase, which catalyzes the reductive methylation of 2'-deoxyuridine-5'-monophosphate (dUMP) to form thymidylate (2'-deoxythymidine-5'-monophosphate or dTMP). Until recently, it was thought that *thy*A-encoded (denoted *TYMS* in humans and

other mammals) thymidylate synthases were the sole means to the *de novo* biosynthesis of thymidylate. These enzymes, called classical thymidylate synthases, have a well studied chemical and kinetic mechanism and have been the target of several chemotherapeutic and antimicrobial agents (1, 2).

In 2002, the identification of several organisms that lacked the *thy*A and *TdK* (the gene coding for thymidine kinase, a thymidine-scavenging enzyme) genes led to the discovery of an alternate flavin-dependent thymidylate sythase (FDTS) (3-5). FDTSs are coded by the *thy*X gene, which is present in ~30% of all microorganisms including several severe human pathogens (see http://www.cdc.gov) (6). Many organisms depend solely on FDTS to produce thymidylate (e.g. all *Rikettasia*) and it has recently been suggested that dependence on the *thy*X gene limits chromosomal replication in these organisms (7-9).

FDTSs share no structure or sequence homology with classical thymidylate synthases. The first crystal structure of FDTS obtained was from the organism *T. maritima* and is presented with the crystal structure of *E. coli* thymidylate synthase in Fig. 1.1 (10, 11). Classical thymidylate sythases are homodimers with one active site per subunit (Fig. 1.1 A) (1). This contrasts FDTSs, which are homotetramers with four active sites, each located at the interface of three subunits (Fig 1.1B). Catalytically important residues differ between these two enzymes, and an extended *thy*X motif has recently been characterized for FDTS enzymes (12). Perhaps the most distinguishable feature of the FDTS structure is the short distance (< 4Å) between the isoalloxazine moiety of the coenzyme flavin adenosine dinucleotide (FAD) and the substrate dUMP (Fig.1.1 B).

The overall chemical conversion catalyzed by thymidylate synthases is the net substitution of the C5 hydrogen of dUMP by a methyl group to form the product dTMP (Fig. 1.2). Although FDTSs catalyze the conversion of dUMP to dTMP, early biochemical studies determined that the FDTS-catalyzed reaction differs from that seen in classical thymidylate synthases. Classical thymidylate synthases use N^5,N^{10}-

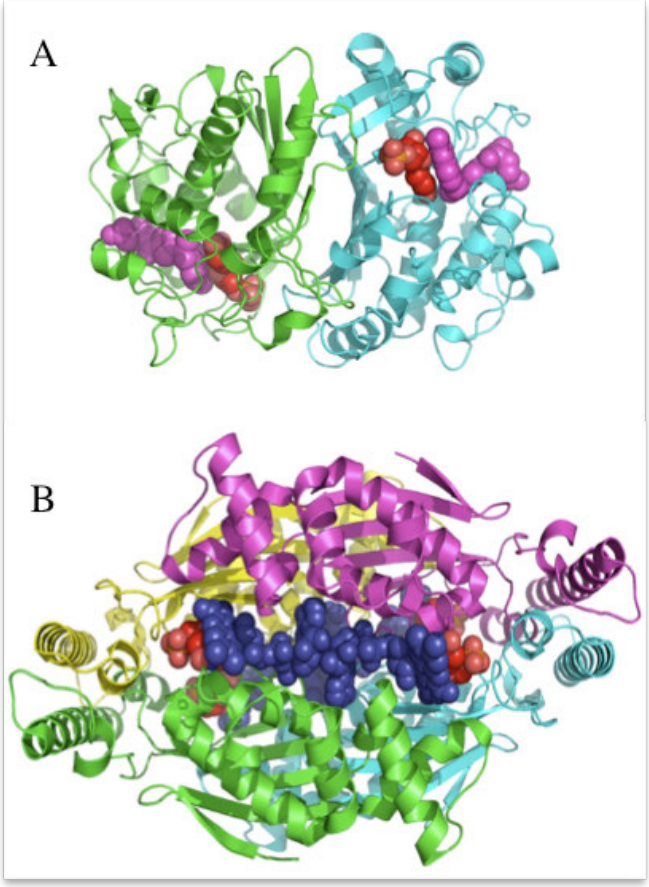

Figure 1.1. Thymidylate synthase structures. A) Classical thymidylate synthase dimer from *E. coli* (PDB entry 2KCE). The substrate dUMP is red and the cofactor analogue (Zd1694, Ralitrexed) is magenta and are highlighted as space filling shapes. B) *T. maritima* FDTS tetramer (PDB entry 1O26). FAD (blue) and dUMP (red) are highlighted as space filling shapes.

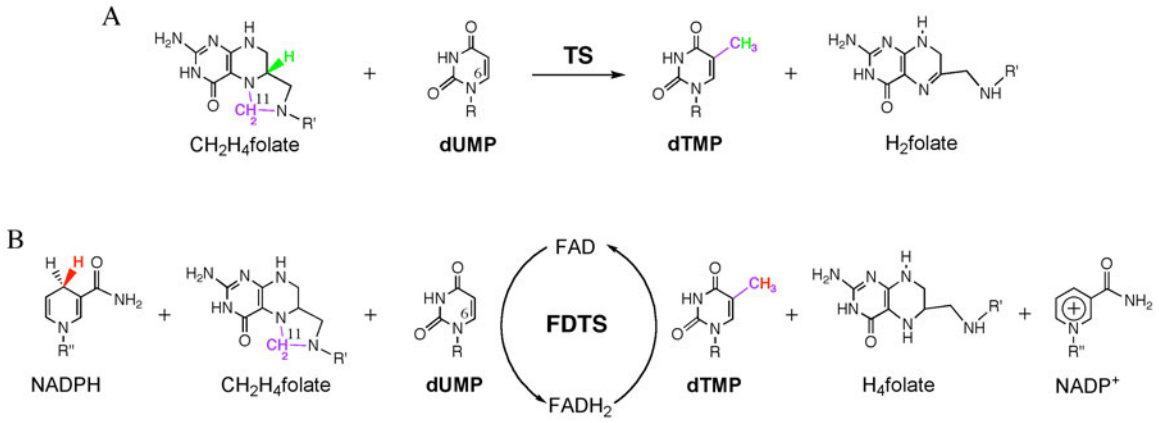

Figure 1.2. Thymidylate synthase reactions. A) The reaction catalyzed by classical thymidylate sythases (TSs). B) The reaction catalyzed by FDTS enzymes. R = 2′-deoxyribose-5′-phosphate; R′ = (*p*-aminobenzoyl)-glutamate; R″ = adenosine-5′-pyrophosphate-ribityl.

methylene-5,6,7,8-tetrahydrofolate (CH_2H_4folate) and dUMP to produce dihydrofolate (H_2folate) and dTMP (Fig. 1.2A).FDTSs, on the other hand, consume dUMP, CH_2H_4folate and reduced nicotinamide adenine dinucleotide phosphate (NADPH) to produce dTMP, tetrahydrofolate (H_4folate) and $NADP^+$. The FDTS reaction is mediated by a flavin adenosine dinucleotide (FAD) coenzyme that cycles between reduced and oxidized forms (FAD → $FADH_2$) during a catalytic turnover (Fig 1.2B). FDTS activity appears to take the place of both classical thymidylate synthase and dihydrofolate reductase (denoted DHFR, an enzyme which uses NADPH to reduce H_2folate to H_4folate) reactions.

Due to the differences in structure and general reactivity of FDTSs, from mammalian thymidylate synthase, it seems likely that inhibition of these enzymes is possible without disrupting human thymine biosynthesis. Rationally-designed compounds which could lead to selective inhibition of FDTS enzymes present a promising frontier for antibiotic and antiviral drug development. As a principal step in such a drug-development process, the distinctions between the catalytic mechanisms of classical thymidylate sythases and FDTSs need to be clarified.

Chemical mechanisms of classical TS (EC 2.1.1.45) versus FDTS (EC 2.1.1.148)

In Fig. 1.3A, the proposed chemical mechanism (1, 2) of classical thymidylate synthases is presented. A conserved active-site cysteine residue is required for catalysis and has been shown to covalently activate the substrate dUMP *via* Michael-addition to the C6 position of the uracil moiety (step 2, Fig. 1.3A). The resulting enolate anion can behave as a nucleophile and attack *via* Mannich condensation (step 3) the activated iminum form (produced in step 1) of CH_2H_4folate. H_4folate then undergoes Hoffman elimination to form a C5=C7 double bond resulting in a covalently bound exocyclic intermediate (step 4) (13). The reaction is complete when a hydride from H_4folate is

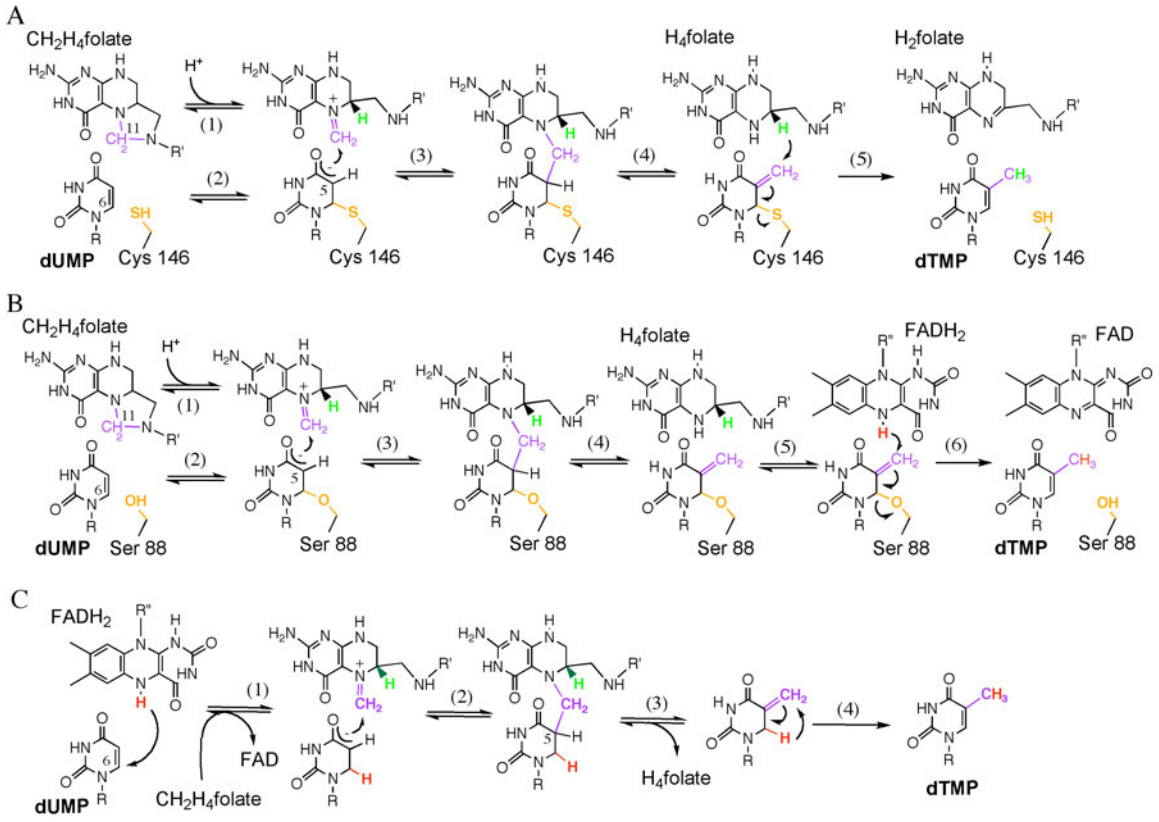

Figure 1.3. Thymidylate synthase mechanisms. A) The chemical mechanism for the classical thymidylate synthase catalyzed reaction. B) The chemical mechanism for the FDTS which depends on an enzymatic nucleophile. C) A mechanism for the FDTS that does not rely on an enzymatic nucleophile. The conserved enzymatic nucleophile is orange, the methylene is purple, the reducing hydride from H_4folate is green, and the hydride from $FADH_2$ is red. R = 2′-deoxyribose-5′-phosphate; R′ = (*p*-aminobenzoyl)-glutamate; R″ = adenosine-5′-pyrophosphate-ribityl.

transferred to the C7 position (step 5), and both dTMP and H_2folate dissociate from the enzyme. Nucleophilic attack and covalent bonding of dUMP to the active site cysteine residue have been clearly demonstrated in the crystal structure of *ec*TS in complex with 5-fluoro-dUMP and CH_2H_4folate (Protein Data Bank accession 1tls (14)). This functionality is an important feature of the classical thymidylate synthase reaction and has been instrumental in inhibitor and chemotherapeutic drug development (e.g. 5-fluoro-dU).

Recent studies have indicated that the mechanism of FDTSs differs substantially from that of classical thymidylate synthase enzymes. Since FDTSs were identified in organisms that lacked the classical thymidylate biosynthesis genes (i.e. *thy*A and *fol*A that codes for DHFR) and produce H_4folate instead of H_2folate (Fig. 1.1B), it was natural to suggest that these enzymes are bifunctional (15, 16). Bifunctional activity would be consistent with classical thymidylate synthase activity and flavin-dependent DHFR activity. The following observations have led to the rejection of this hypothesis: i) when conducting FDTS reactions using (*R*)-6-^{3}H-CH_2H_4folate (17) the tritium remains on the H_4folate (18). This is in direct contrast to experiments with classical thymidylate synthase where this tritium always transfers to the C7 position of dTMP (step 5, Fig. 1.3A)(1, 2, 18, 19); ii) reactions preformed in D_2O result in deuterated dTMP, suggesting that the reduced flavin exchanges protons with the solvent prior to a hydride transfer directly to the nucleotide (18, 20-22); and iii) if tritiated NADPH is used to reduce the flavin, the tritium ends up in the water and not dTMP or H_4folate. These experiments support a mechanism where NADPH reduces FAD to $FADH_2$, and the pyrimidine moiety accepts a hydride equivalent from the $FADH_2$ to form dTMP (Fig. 1.2C). Notably, the FDTS reaction differs from known mechanisms of bifunctional enzymes and classical thymidylate sythases (1, 2, 4, 7, 10, 12, 14-16, 18, 19, 22-29).

Structural studies of FDTS identified a conserved active-site serine that has been proposed to serve as an enzymatic nucleophile, in a manner analogous to the cysteine

residue of classical thymidylate synthases. This suggestion was originally based on sequence alignments of *thy*X genes which exhibited no conserved cysteines, but did show a strictly conserved serine residue (3, 30). Crystal structures of FDTSs from three different organisms indicated that this conserved serine residue is 4Å from the electrophilic C6 position of dUMP (see Fig. 1.4) (10, 23, 31).

Mutagenesis studies of FDTS from *H. pylori* and *M. tuberculosis* have been used to support the putative role of serine as a nucleophile (12, 30). The conserved serine(Ser84) in the *Hp*FDTS enzyme was mutated to alanine and this mutant enzyme retained activity. However, it was reasoned that a neighboring serine (Ser85) was able to rescue the activity of the S84A mutant enzyme. This hypothesis was supported by a double mutant S84A/S85A which had no observed activity. The conserved serine (Ser105) of *Tb*FDTS was mutated to glutamic acid, which resulted in an enzyme which failed to complement in thymidine deficient media. This S105E mutant was shown to slowly oxidize NADPH, however, this rate was less than 1/100 of the rate of oxidation observed for wild-type (12). These results support the conclusion that without serine in the active site, FDTS catalysis cannot take place.

Additionally, a mutation of Ser84 in the *Hp*FDTS and Ser105 in the *Tb*FDTS to cysteine resulted in an active enzymes (12, 30). These observed activities suggest that cysteine can take the place of the serine nucleophile. Further studies using MALDI-TOF mass spectrometry of the *Hp*FDTS-S84C mutant indicated a covalent adduct between the enzymatic cysteine and the product dTMP (30). This S84C-dTMP covalent complex, in addition to the lack of observable synthase activity for both the *Hp*FDTS-S84A/S85A double mutant and the *Tb*FDTS-S105E mutant further support the role of serine as an active site nucleophile.

Taking the suggestion that serine is the active site nucleophile, together with the evidence ruling out a bifunctional enzyme, led to the proposed chemical mechanism for FDTS enzymes presented in Fig. 1.3B (18). This mechanism parallels the classical

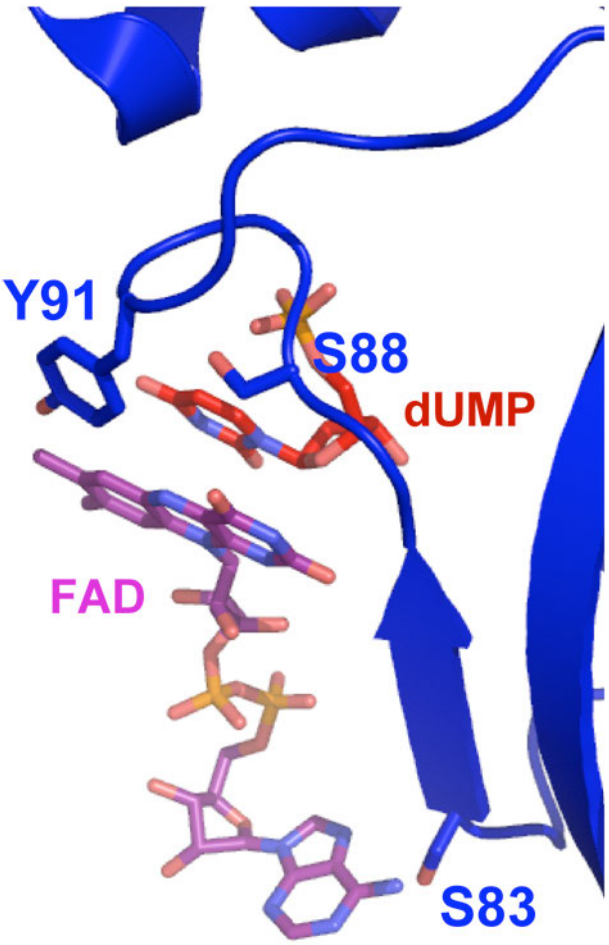

Figure 1.4. Crystal structure of *Tm*FDTS-dUMP-FAD complex. The three possible conserved nucleophiles Y91, S88 and S83 are shown as sticks. The oxygen of the S88 and the N5 of FAD are 4Å and 3.5Å from the electrophilic C6 of dUMP, respectively.

thymidylate synthase mechanism, and differs from it in that a serine residue serves as the enzymatic nucleophile (Fig. 1.3B, step 2) and the reduced flavin cofactor provides the reductive hydride to terminate the reaction (step 4).

We approached the idea that serine was acting as an enzymatic nucleophile with some doubt due to a lack of structural evidence and the ambiguity that may arise from the study of a double mutant *Hp*FDTS enzyme. For serine to act as a nucleophile it must be activated by a general base system in the enzyme's active site (e.g. the catalytic triad present in hydrolytic enzymes). Upon evaluating the available crystal structures of FDTSs, we were unable to identify such a general base system required to deprotonate serine (Fig. 1.4) (10, 22, 31). This observation suggests that the conserved serine of FDTS is much less reactive than its classical cysteine counterpart, thus diminishing the likelihood of its reactivity towards dUMP.

To determine serine's role in the FDTS reaction, we preformed mutation studies using *T. Maritima* FDTS. The active site of *Tm*FDTS contains only the conserved serine (Ser88) and no other strictly conserved nucleophilic residues (10, 23, 31). Mutation of Ser88 to alanine (PDB 3g4a) resulted in an enzyme which surprisingly retained activity (22), an anomaly that could not be explained easily based on the mechanism proposed in Fig. 1.3B.

When Ser88 was mutated to cysteine the resulting enzyme had 1/20 the activity of S88A and 1/400 the activity of the wild-type *Tm*FDTS. The crystal structure of S88C (PDB 3g4c) in complex with dUMP did not show covalent binding to the C6 position of the uracil moiety. Nevertheless, MALDI-TOF mass spectrometry analysis of the *Tm*FDTS-S88C mutant indicated an apparent covalent adduct with the substrate dUMP, consistent with the previous studies on the *Hp*FDTS-S84C mutant. However, even in solution, cysteine has been shown to covalently bind to pyrimidine moieties. This fact, along with the low activity of the cysteine mutants, suggests that covalent binding of

cysteine to the nucleotide may represent a dead-end complex which is not part of the catalytic pathway (22).

The conserved residues, Ser83 and Tyr91, are the only other potential enzymatic nucleophiles besides Ser88 (Fig. 1.4) within *Tm*FDTS. Tyr91 is an unlikely nucleophile, because its mutation to Phe in *Hp*FDTS results in an enzyme that is 50% more active than the wild type (30). The Ser83 residue is 17.7 Å from C6 of dUMP and is hydrogen-bonded to the adenine ring of FAD at the core of the tetramer. For Ser83 to activate dUMP, FAD would need to dissociate, which is inconsistent with both our steady-state results (18, 29) and crystal structures with $NADP^+$ bound instead of FAD (PDB 2GQ2), which show Ser83 still H-bonded to the adenine moiety (32). These points diminish the possibility Ser83 or Tyr91 acting as nucleophiles during the FDTS reaction.

Besides the enzyme residues Ser83, Tyr91 and Ser88, the absence of any other possible enzymatic nucleophile is further supported by experiments using halogenated dUMP analogs. Perhaps the most convincing evidence for Micheal-addition in classical thymidylate synthases is the covalent complex of 5F-dUMP with CH_2H_4folate (PDB 1tls). Similar complexes have not been identified for FDTS as detected by MALDI-TOF mass spectrometry (22) and X-ray crystallography (PDB 1o28) (10, 22). Additionally, FDTS does not catalyze the dehalogenation of 5Br-dUMP a common assay for enzymatic Michael-addition in the classical thymidylate synthase reaction (22, 28). In light of the fact that S88A is an active enzyme, and no other experimental evidence suggests activation of the substrate by an enzyme residue, we have concluded that the FDTS catalyzed reaction does not rely on an enzymatic nucleophile. This feature fundamentally distinguishes the FDTS reaction from that of classical thymidylate synthases (22).

In the absence of an enzymatic nucleophile, the mechanism proposed in Fig. 1.3B does not explain the reaction catalyzed by FDTS. To further elucidate the FDTS reaction we followed the flow of hydrogens from the reduced flavin coenzyme by a range of analytical techniques. Previous experiments used ESI-MS to identify a mono-deuterated

dTMP as a product of FDTS reactions in D_2O (18). We recently revisited these experiments, performing reactions in D_2O at both 37 ºC and 65 ºC and analyzing the product by ^1H and ^2H NMR. At 65 ºC (close to the physiological temperature of *T. maritima*) the product observed was 7-^2H -dTMP. However, the product of the 37 ºC reactions showed a significant percentage (up to 60%) of 6-^2H -dTMP, which is consistent with hydrogen transfer directly to the uracil moiety. Both the lack of enzymatic nucleophile and the observation of deuterium at C6 of dTMP for reactions in D_2O, suggest a strikingly different mechanism for FDTS than for classical TS, or, for that matter, any other known biological methylation.

Besides an enzymatic residue, a hydroxide ion or the flavin coenzyme could activate dUMP. A hydroxide nucleophile is unlikely due to the lack of a general base system in the FDTS active sites required to produce a hydroxide ion by deprotonation of a water molecule. Additional tests with the flavin derivative, 5-carba-daza-FAD, resulted in catalytic activity suggesting that the N5 of the flavin is not the source of nucleophile. These observations, along with the finding that the reduced flavin can transfer a hydrogen to the C6 position of dUMP, are consistent with reduction of the uracil moiety by hydride transfer from the reduced flavin to the dUMP substrate (22).

As a consequence, we have recently proposed a mechanism that is consistent with all currently published data regarding the chemical mechanism of FDTS enzymes (10, 18, 26, 30, 31, 33). Inspired by known flavo-protein reactions (34, 35), we suggested a mechanism wherein a hydride is transferred to the uracil moiety from $FADH_2$ (see Fig. 1.3C, step 1). Such a mechanism would result in a noncovalently bound enolate anion, which could act as a nucleophile and attack the activated iminium form of CH_2H_4folate (step 2). Following elimination of H_4folate (step 3), an isomer of thymine is then formed, which can undergo rearrangement to form the product dTMP (step 4) (22). Since we have no direct evidence regarding the methylene transfer, the steps in this newly proposed

mechanism are presented as the simplest case, and other more complex mechanisms can be envisioned.

The putative exocyclic methylene intermediate formed in step 3 of Fig. 1.3 B is an isomer of thymine and has been shown to be stable in solution (Koehn and Kohen unpublished data and ref (36)).The product dTMP is thermodynamically favored over this isomer, and the enzyme could catalyze its isomerization either by an addition-elimination mechanism or by a sigmatropic 1,3-hydrogen rearrangement (37). Both these isomerization mechanisms have been investigated by following the flow of hydrogens during the FDTS reaction. The observation that 6-^{2}H -dTMP is formed when enzyme reactions are performed in D_2O at reduced temperatures can be explained by reduced stereoselectivity and normal kinetic isotope effect on that step (See Fig 1.5). If there was a loss of stereoselectivity, and the H-transfer is faster than D-transfer during an addition-elimination mechanism, it should be possible to observe 6,7-$^{2}H_2$-dTMP. This product would be formed upon addition of $^{2}H^{+}$ to the C7 position and elimination of H^{+} from the C6, resulting in a di-deuterated product (Fig. 1.5B). Mass spectrometric and NMR analysis of the reaction products has always indicated a mono-deuterated dTMP product, suggesting a concerted rearrangement of the hydrogen between the C6 and C7 positions consistent with a 1,3- hydrogen shift (22). Such an isomerization reaction could be catalyzed by the oxidized flavin in the active site via oxidation of the C6 and reduction of C7.

The suggestion that FDTS does not use an enzymatic nucleophile, and that the reduced flavin transfers a hydride to the pyrimidine ring during the reaction, leads to a strikingly different chemical cascade than the classical thymidylate synthase enzymes. This presents significant opportunities for rational design of selective inhibitors for FDTSs. Since the FDTS reaction appears to follow a reaction path leading to noncovalently bound intermediates, analogs which can mimic these intermediate species

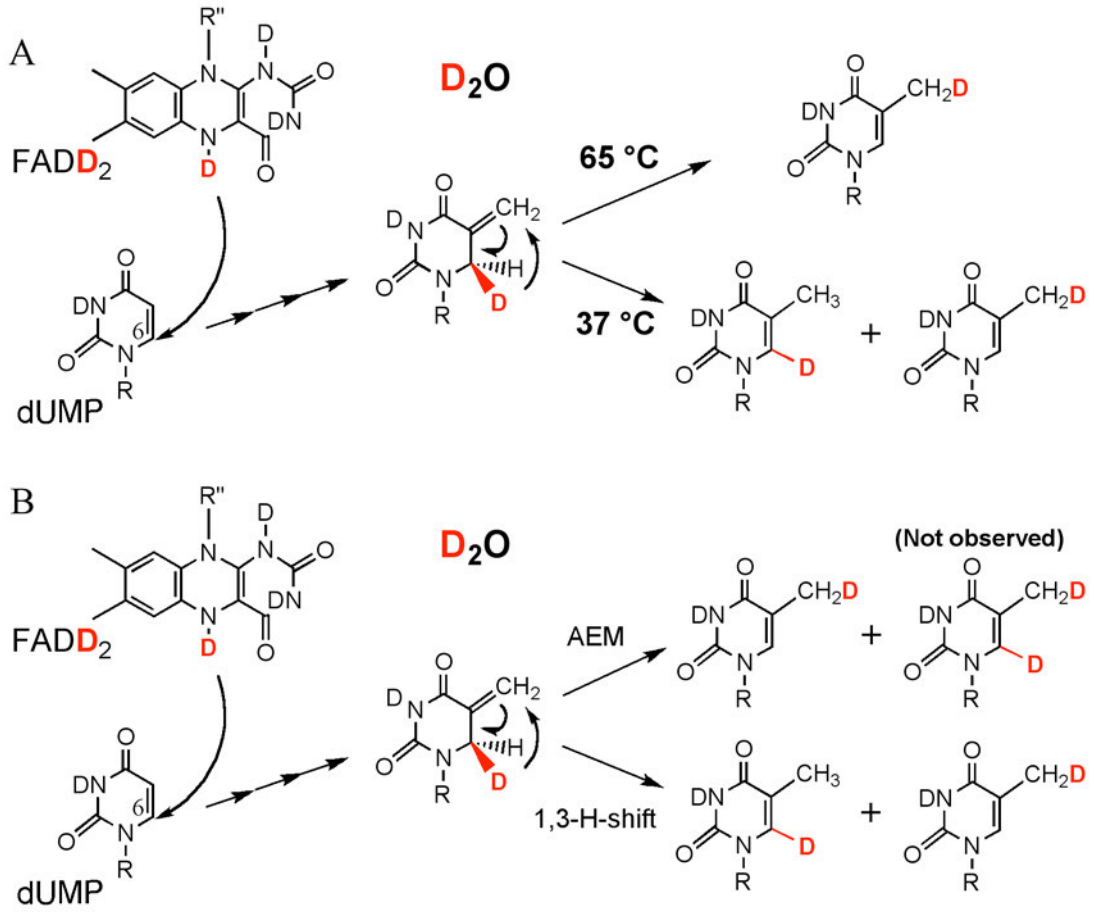

Figure 1.5. FDTS deuterium labeling experiment. (A) An illustration of the observed products of the FDTS-catalyzed reaction when performed in D_2O at both 65 °C and 37 °C. (B) Labeling outcomes of isomerization in D_2O by an addition–elimination mechanism (AEM, top path) or a 1,3-hydrogen rearrangement (1,3-H-shift, bottom path).

or transition states for their formation may bind tightly to FDTS and have little effect on classical thymidylate sythases. Such tight-binding inhibitors of FDTS may also consequently facilitate crystallographic studies, and thus lay the foundations for rational drug design.

Kinetic mechanism of FDTS

Along with efforts to establish the chemical mechanism of the reaction catalyzed by FDTS, the binding and release features of the substrates and products have been investigated. Recently many works have explored the order of substrate binding, product release and their associated binding constants (23, 25, 27, 29, 33, 38, 39). Overall, it appears that FDTS follows a sequential order of binding for all its substrates; however, little information is available regarding the order of product release. Measurement of substrate binding constants has proved to be challenging due to the ability of FDTS to function as an oxidase (catalyzing the conversion of O_2 to H_2O_2) and the ability for the substrate dUMP to function as an activator of the enzyme's oxidative half reaction (25, 29, 33).

Early studies of the substrate binding order offered conflicting results with regard to the kinetic mechanism of FDTSs. Liebl and co-workers determined that the rate of oxidation of NADPH was increased in the presence of dUMP (24). Their results contrasted the mechanism suggested by McClarty and co-workers, wherein NADPH and CH_2H_4folate bind and $NADP^+$ and H_4folate are released from the enzyme prior to dUMP binding. This latter mechanism proposed that an Arg residue serves as a vehicle for the methylene; however, subsequent studies (23, 29, 33, 38) have not been able to confirm methylene transfer to the enzyme experimentally. Furthermore, several recent studies have observed sequential binding between CH_2H_4folate and dUMP during the FDTS reaction, excluding the possibility for the release of H_4folate prior to dUMP binding (23, 29, 33, 38).

Recent investigations of the oxidase activity of FDTS have provided insight into the activation kinetics previously observed for the dUMP-$FADH_2$-FDTS complex (39) and moreover, have provided the means to monitor the binding features of the FDTS synthase reaction (29). FDTS can catalyze the reduction of O_2 to H_2O_2, and displays normal Michealis-Menton kinetics for molecular oxygen with a relatively small K_M. This is unusual for many flavo-proteins that function as oxidases, and may imply that FDTS has a binding site for O_2, or more likely, that some other step becomes rate-limiting under saturating concentrations of oxygen (40).

We have shown that CH_2H_4folate and O_2 competitively bind to the same activated form of the enzyme, namely the dUMP-$FADH_2$-$NADP^+$-FDTS complex (29, 33). Furthermore, we found that the rate of FAD reduction is independent of dUMP concentration. However, oxidation of $FADH_2$ has a strong dependence on dUMP (with a functional activation constant, $K_f \sim 2\mu M$) (33). This observation supports a mechanism were dUMP is not required to bind prior to NADPH, as previously suggested (23, 24, 39). Additionally, a sequential mechanism between NADPH and O_2, along with high affinity of $NADP^+$ for the dUMP-$FADH_2$-FDTS, suggests that $NADP^+$ does not leave the reactive complex prior to CH_2H_4folate binding as previously suggested (18, 23, 27). Overall, the oxidase activity has proved to be a useful tool to probe the substrate-binding features of FDTS synthase activity, and also emphasizes the importance of studying these enzymes under anaerobic conditions in order to avoid artifacts produced by this side reaction.

Using the information obtained during studies of the oxidase reaction (29, 33), along with previous steady state measurements on the synthase reaction of FDTS (23, 27, 33, 38), a kinetic mechanism for the FDTS-catalyzed reaction has been proposed. This mechanism is sequential with respect to all substrates, and can be divided into two half reactions as depicted in Fig. 1.6 (25, 29, 33). In the reductive half reaction it is proposed that NADPH binds first to reduce FAD to $FADH_2$, and then dUMP can bind to form the

dUMP-$FADH_2$-$NADP^+$-FDTS complex. Both molecular oxygen and CH_2H_4folate have been shown to have a high affinity and compete for this quaternary enzyme complex. Binding of CH_2H_4folate (top path, Fig. 1.6) or O_2 (bottom path, Fig. 1.6) begins the oxidative half reaction where these species are converted to H_4folate and H_2O_2, respectively. Since there is no evidence of the order of product release, the dissociation of the enzyme complex after oxidation of the flavin is proposed to proceed by the 'first come, last to leave' principal, and more rigorous experimental study is needed to resolve the question of binding and release order.

Mechanism-based inhibition of FDTSs

The biosynthetic pathways for thymidylate present good targets for antibacterial and antiviral drugs, as nucleotides are essential for cellular reproduction. This, together with the presence of *thy*X in the genome of human pathogens, biowarfare agents and many other microbes makes FDTS attractive for selective inhibition without affecting human thymidylate biosynthesis. Such inhibitors would need to exploit the differences between these enzymes in order to selectively disrupt FDTS function, and not that of classical thymidylate synthases.

A striking difference between FDTS and classical thymidylate synthases is the lack of an enzymatic nucleophile. One of the most effective classical thymidylate synthase inhibitors, 5F-dUMP, has been shown to covalently bind the active-site cysteine in these enzymes. FDTSs however, lack this functionality and consequently do not bind 5F-dUMP covalently. The intermediate proposed after step 3, in Fig 1. 3C, is a noncovalent species that may tightly bind to the enzyme (6, 22). Analogues that mimic this species or the transition state for its formation are likely to have a high affinity for FDTS, but not for classical thymidylate synthases. Compounds that take advantage of covalent versus noncovalent binding modes could comprise one avenue for rational inhibitors of FDTS.

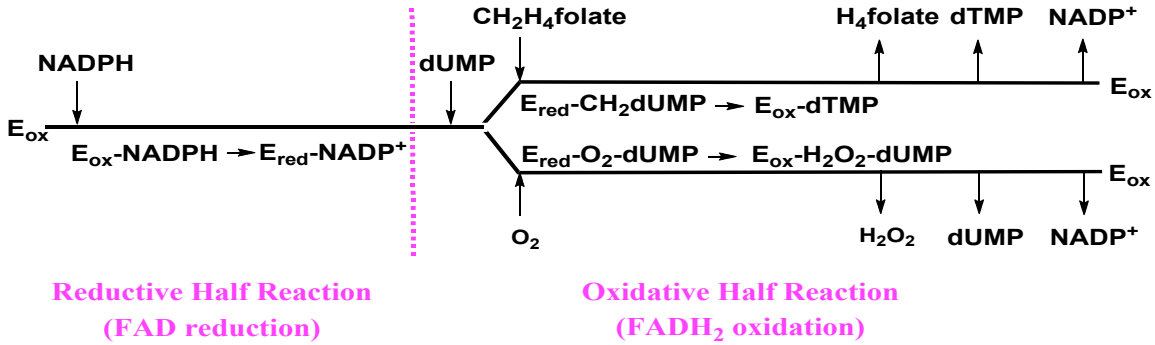

Figure 1.6. Kinetic mechanism of FDTS. A proposed binding and release order for substrates and products of the FDTS catalyzed reaction. E_{ox} and E_{red} correspond to the oxidized (FAD-FDTS) and reduced ($FADH_2$-FDTS) enzyme complexes, respectively.

A notable characteristic of FDTS enzymes is the activation of the enzyme by dUMP, and the high affinity of CH_2H_4folate to the dUMP-$FADH_2$-$NADP^+$-FDTS complex. To date, the only mechanistically relevant complexes for which crystal structures have been solved are with dUMP or its halogenated derivatives bound to the oxidized enzyme (e.g. (5F or 5Br)-dUMP-FAD-FDTS complex). Efforts to crystallize complexes with folate moieties have not been successful, and the only complex with the nicotinamide cofactor indicates that $NADP^+$ has substituted for the FAD (32), and is unlikely to be part of the catalytic pathway. Our recent findings suggest that under strictly anaerobic conditions the possibility to crystallize the reduced form of FDTS bound to folate moieties may be greatly increased. Studies of the activated dUMP-$FADH_2$-$NADP^+$-FDTS complex may provide valuable structural data, such as the location of the binding site for CH_2H_4folate, which could result in the identification of previously unrecognized mechanism-based compounds or inhibitors.

To date there are few inhibitors of FDTS activity (41), and none that show high specificity for FDTS over classical thymidylate synthase. As mentioned above, the chemical and kinetic mechanisms of FDTS have recently been greatly clarified; however, even with current knowledge of these enzymes, the scope of rationally designed inhibitors is limited. Preliminary suggestions of rational inhibitors have included bridged or hybrid ligands, such as linked adenosine moieties (31, 33), which could effectively bind more than one active site, thus inhibiting the enzyme. Also, the linking of dUMP analogs to the pterin ring of NADPH or the isoalloxazine moiety of the FAD may produce bridged ligands that will bind tightly and specifically to FDTS. These conceptually simple inhibitors may give rise to alternate ligands for crystallization, providing access to new structural conformations.

FDTSs represent an under characterized family of enzymes that is critical for the survival of many human pathogens. With the recent advances in the understanding of both the chemical and kinetic mechanism of these enzymes, future antibiotic drug design

looks promising. Advancement towards this goal hinges on the discovery of novel inhibitors selective to FDTSs with little impact upon human thymine biosynthesis and consequently, low toxicity.

Conclusion

Studies of FDTSs are in their early stages, and both the chemical and kinetic mechanisms of these enzymes have not thoroughly been established. However, it has been shown that the mechanism of the FDTS-catalyzed reaction differs greatly from that of the classical thymidylate synthases. Perhaps the most notable distinction between these pathways toward thymidylate, is the role of an enzymatic nucleophile. Classical thymidylate synthases require an active site nucleophile to covalently activate the substrate, dUMP. FDTSs, on the other hand, lack such functionality leading to a chemical cascade where the dUMP and intermediates along the reaction path, do not covalently bind the enzyme. Instead, the FDTS-catalyzed reaction relies on the reduced flavin cofactor, which has been suggested to reduce the uracil moiety by hydride transfer.

The *thy*X gene is present in many microbes, including several pathogens that threaten human life. FDTSs represent an attractive target for antimicrobial drugs due to the structural differences between *thy*A and *thy*X encoded enzymes, and the unusual chemical mechanism observed for FDTSs. Currently, there are several known potent inhibitors of classical thymidylate synthases, which are broadly used clinically, but have little effect on FDTSs. This suggests that it is possible to develop compounds selective to FDTSs. Future research of FDTSs will include crystallization attempts with folate moieties, investigation of the chemical properties and binding modes of noncovalent intermediates, elucidation of the relative timing of events during the FDTS-catalyzed reaction, and foremost, design and combinatorial efforts to find specific inhibitors.

CHAPTER II

A NOVEL MECHANISM OF THYMIDYLATE BIOSYNTHESIS IN ORGANISMS CONTAINING THE *THY*X GENE

This chapter was in full or part published in Nature, Koehn E. M. *et. al.,* 2009, *Nature* 458:919-923. Figures and/or content are used with permission from NPG.

Abstract

Biosynthesis of the DNA base thymine depends on activity of the enzyme thymidylate synthase (TS) to catalyze the methylation of the uracil moiety of 2'-deoxyuridine-5'-monophosphate (dUMP). All known thymidylate synthases (TSs) rely on an active site residue of the enzyme to activate dUMP (1, 2). This functionality has been demonstrated for classical TSs, including human TS, and is instrumental in mechanism-based inhibition of these enzymes. Here we report the first example of thymidylate biosynthesis that occurs without an enzymatic nucleophile. This unusual biosynthetic pathway occurs in organisms containing the *thy*X gene, which encodes for a flavin-dependent thymidylate synthase (FDTS), and is present in several human pathogens (4, 25, 30). Our findings indicate that the putative active site nucleophile is not required for FDTS catalysis, and no alternative nucleophilic residues capable of serving this function can be identified. Instead, our findings suggest that a hydride equivalent (i.e. a proton and two electrons) is transferred from the reduced flavin cofactor directly to the uracil ring, followed by an isomerization of the intermediate to form the product, 2'-deoxythymidine-5'-monophosphate (dTMP). These observations indicate a very different chemical cascade than that of classical TSs or any other known biological methylation. The findings and chemical mechanism proposed here, together with available structural data, suggest that selective inhibition of FDTSs, with little effect on human thymine biosynthesis, should be feasible. Since several human pathogens depend on FDTS for

DNA biosynthesis, its unique mechanism makes it an attractive target for antibiotic drugs.

Research report

Classical thymidylate synthases (TSs), encoded by the *thy*A gene, are present in most eukaryotes, including humans, and their catalytic mechanism has been extensively studied. As a result, classical TSs are frequently targeted by chemotherapeutic and antibiotic drugs. A recently discovered class of TSs, the flavin-dependent thymidylate synthases (FDTSs) (3, 4, 10), is encoded by the *thy*X gene and has been found primarily in prokaryotes and viruses (4, 30), including several pathogens and bio-warfare agents (33). Several organisms, including human pathogens, rely solely on *thy*X for thymidylate synthesis (e.g. all *Rickettsia*, lacking genes encoding for DHFR, TS, and thymine kinase). It has recently been suggested that *thy*X limits chromosomal replication in these organisms (7). FDTSs share no structure or sequence homology with classical TSs, and thus present a promising new frontier for antibacterial/antiviral drug development (3, 10, 25).

The catalytic mechanism of classical TSs has been well established (1, 2) and is presented in Figure 2.1A. A strictly conserved active site cysteine covalently activates the uracil ring by nucleophilic Michael-addition at the C6 position of dUMP (Figure 2.1A, step 2). The resulting enolate then attacks (step 3) the iminium form of N^5,N^{10}-methylene-5,6,7,8-tetrahydrofolate (CH_2H_4folate) that was formed in step 1, followed by elimination of tetrahydrofolate (H_4folate), which results in a C5=C7 double bond (step 4). Finally, a hydride transfer from C6 of the H_4folate yields the products dTMP and dihydrofolate (H_2folate, step 5). Common drugs that target classical TS either covalently bind to the catalytic nucleophile (e.g., 5F-dUMP) or noncovalently bind the folate binding pocket (e.g., Tomudex and other antifolates).

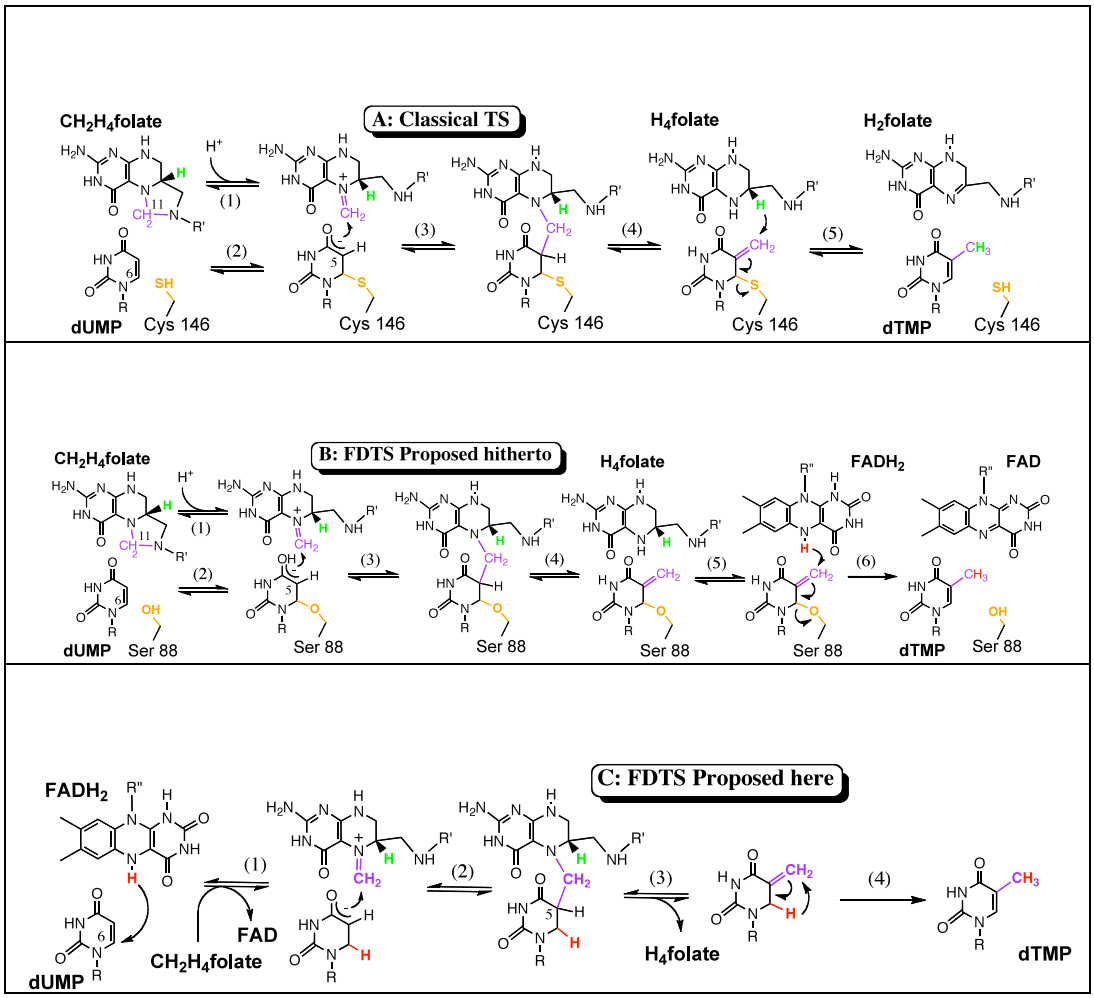

Figure 2.1. TSase mechanisms. A. The chemical mechanism for the classical TS catalyzed reaction (1, 2, 42). B. The chemical mechanism for the FDTS proposed hitherto (18). C. The newly proposed mechanism for the FDTS that does not rely on an enzymatic nucleophile. The conserved enzymatic nucleophile is orange, the methylene is purple, the reducing hydride from H_4folate is green, and hydride from $FADH_2$ is red. R= 2'-deoxyribose-5'-phosphate and R'= (*p*-aminobenzoyl)-glutamate. R"= adenosine-5'-pyroposphate-ribityl.

It has previously been proposed that FDTSs have a chemical mechanism analogous to the classical TS mechanism presented in Figure 2.1A, but with a serine residue acting as a nucleophile (Figure 2.1B, step 2), and a flavin cofactor providing a reductive hydride to terminate the reaction (Figure 2.1B, step 6). This would result in the production of H_4folate (9), suggesting that CH_2H_4folate functions only as a methylene donor and not as a hydride donor (18).The suggestion that a serine serves as the active site nucleophile in FDTS was originally based on sequence alignments of *thy*X genes that indicated no conserved cysteine but a strictly conserved serine. Crystal structures of FDTSs from three very different organisms (10, 23, 31) placed this conserved serine about 4 Å from the C6 position of dUMP (e.g., Figure 2.1A). However, without a neighboring general base this serine will not be deprotonated, decreasing its potential reactivity. This fact may cast doubt on this serine's putative role as a nucleophile.

Point mutation studies were performed with FDTS from *H. pylori* (*hp*FDTS), where the conserved serine residue, Ser84, was mutated to either alanine or cysteine (S84A and S84C). While both mutations were found to retain activity (30), it was assumed that an adjacent serine residue (Ser85) could have rescued the activity of S84A. Abolished enzyme activity of a double mutant (S84A/S85A) supported this hypothesis. Furthermore, MALDI-TOF MS analysis showed that the S84C mutant forms a covalent adduct with dTMP, suggesting that Cys84 binds the product of the catalyzed reaction. These results were used to propose that Ser84 activates dUMP in accordance with Figure 2.1B (18, 30).

To further test this hypothesis, we performed similar mutation studies using FDTS from *T. maritima* (*tm*FDTS). The active site of this enzyme contains a strictly conserved serine, Ser88, and no alternative nucleophilic residues (see refs (3, 10) and the Supplementary Information - SI). Mutations were confirmed by plasmid sequencing, peptide fragment analysis (MALDI-TOF MS), and X-ray crystallography. Activity tests were performed (see SI) by following the conversion of ^{14}C-dUMP to ^{14}C-dTMP(18)

indicating that both mutants were still active (only 20 and 400 fold decrease in apparent k_{cat} compared to the wild-type for S88A and S88C, respectively, and a 10-fold decrease in the single-turnover rate constant for S88A, see Table 2.2). Possible contamination by classical *ec*TS was ruled out by a series of control experiments to ensure that mutant FDTS was the source of the observed activity (See SI). The FDTS activity of these mutants and the lack of classical TS activity of S88C demonstrate that the conserved active site serine does not serve as a catalytic nucleophile in the FDTS reaction, in stark contrast to the mechanism proposed hitherto (Figure 2.1B).

Crystal structures of the S88A and S88C mutants were obtained at 1.95 and 2.05 Å resolution, respectively (see data collection/refinement statistics in the SI), and their electron density is compared to that of the wild-type *tm*FDTS (Figure 2.2). The electron densities for both mutants indicate minimal changes in folding and active site configuration. With the Cys88 residue 4.3 Å away from the C6 of the uracil moiety and with no electron density between them (Figure 2.2C), it is clear that there is no covalent bond between the cysteine and dUMP in the crystal. Nevertheless, a MALDI-TOF analysis of the trypsin-digested S88C *tm*FDTS indicated that Cys88 is bound to dUMP (see SI), as previously reported for *hp*FDTS (30). Even in solution, though, cysteine can covalently bind to the C6 position of the uracil moiety (19). These facts together with the low activity of S88C, suggest that the observed Cys88-dUMP complex is not part of the FDTS catalytic cascade, but rather an inhibitory dead-end complex, and that crystallization selects for the small portion in solution that is not covalently linked to the nucleotide.

A critical piece of evidence for the covalent bond between the active site cysteine in classical TS and dUMP is the crystal structure of a covalently bound 5-flouro-dUMP (5F-dUMP) in complex with CH_2H_4folate (PDB 1tls (14)). In contrast to classical TS, FDTS does not covalently bind 5F-dUMP upon incubation with CH_2H_4folate, as confirmed by both MALDI-TOF analysis (see SI), and the crystal structure analysis

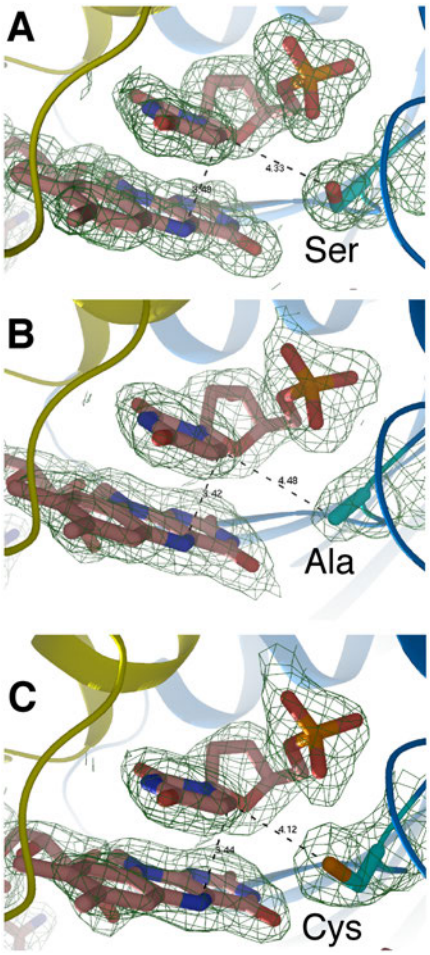

Figure 2.2. Crystal structures of the FDTS-FAD-dUMP complex for: (A) Wild type *tm*FDTS, (B) S88A mutant, and (C) S88C mutant. The distance between the C6 carbon of dUMP and the reducing center of the flavin (N5 of FAD) is 3.4 Å for all three enzymes. The distances of the side-chain of residue 88 to C6 are 4.3, 4.5, and 4.1 Å, for wtFDTS, S88A, and S88C, respectively.

(PDB 1o28 (10)) obtained under similar conditions. Another test for similarities to early stages of the classical TS mechanism (i.e., Michael Addition to the C6 of dUMP) is the dehalogenation of 5Br-dUMP (2, 28). This test resulted in no reactivity with FDTS (see SI). We solved the crystal structures of tmFDTS with FAD and both 5-halogenated-dUMPs (PDB 1o27 and 1o28) and Hol and coworkers solved the 5Br-dUMP-FAD structure for FDTS from *M. tuberculosis* (PDB 2af6) (31). These structures are nearly the same as the complex with dUMP (Figure 2.2A) and the only difference is that with the C6 of 5Br-dUMP is 4.6 Å from the hydroxyl of Ser88 rather than 4.3 Å with dUMP. Whether the results with both 5-halogenated-dUMP derivatives originate from structural differences between FDTS and classical TS, or the differential reactivity of serine relative to cysteine, no nucleophilic attack of enzyme residues on the C6 of dUMP was detected for FDTSs. These observations emphasize the distinctions between the mechanisms of classical TS and FDTS, and in light of the activity of the S88A mutant, support a mechanism in which FDTS does not involve a Michael-addition of an enzymatic nucleophile.

Another way to expose the nature of the FDTS catalyzed reaction is to follow the flow of hydrogens along the catalytic pathway by substituting a specific hydrogen (H) for deuterium (D). We have previously found that when conducting the FDTS reaction in D_2O (50 % D), deuteration of the reduced flavin leads to deuterated dTMP (using ESI-MS analysis), and that reaction with tritiated hydride at 6T-CH_2H_4folate yields 6T-H_4folate (18). These results contrast the same experiments with classical TSs, where reactions performed in D_2O do not incorporate deuterium into the dTMP product and the labeled hydride at the C6 of CH_2H_4folate always transfers to the methyl (C7) of dTMP (17). In the past, we and others (18, 30) suggested that these findings support the mechanism illustrated in Figure 2.1B. The current finding that S88A is catalytically active, however, contradicts the mechanism proposed in Figure 2.1B, which requires an enzymatic nucleophile.

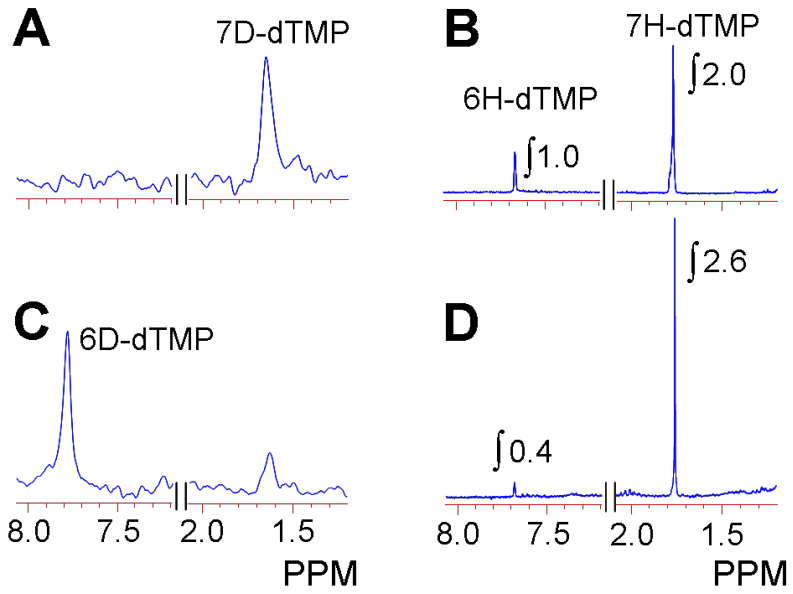

Figure 2.3. ^{2}H-NMR (A & C) and ^{1}H-NMR (B & D) spectra of dTMP produced in the FDTS catalyzed reaction of dUMP in D_2O (Experiment A in Figure 2.4). Spectra A and B were from the reaction at 65 ˚C, and spectra C and D from the same reaction at 37 ˚C. The latter clearly indicate the presence of 6D-dTMP (~60 %).

Here, we examined whether the deuterated dTMP produced by FDTS in D_2O had the deuterium on its methyl group (C7). By repeating the experiment in D_2O (this time > 99.6 % D), and analyzing the product using ESI-MS, ^{1}H-NMR, and ^{2}H-NMR, we found that at 65 °C (close to the physiological temperature of *T. maritima*) the product was indeed deuterated at the C7 position (Figure 2.3 A and B). However, when we performed the same experiment at 37 °C, NMR analyses indicated the formation of both 6D-dTMP (60%) and 7D-dTMP (40%) (Figure 2.3 C and D). This result is quite intriguing, as no mechanism previously proposed for FDTS predicts formation of 6D-dTMP, and such phenomenon has never been reported for any TS reaction.

The lack of an obvious enzymatic nucleophile and the ability to trap deuterium from D_2O at C6 of the product demonstrate that the chemical mechanisms of FDTS and classical TS differ substantially. Without an enzymatic nucleophile, the FDTS catalyzed reaction could proceed *via* Michael-addition of a hydroxide ion or though participation of the flavin prosthetic group. For hydroxide to serve as a nucleophile a water molecule must be activated by a general base in the active site (e.g. the catalytic triad in hydrolytic enzymes). All crystal structures of FDTSs indicate that there is no such basic system available in the active site. Additional experiments using reduced 5-carba-5-deaza-FAD resulted in dTMP formation, excluding the possibility that the reduced N5 of $FADH_2$ is the nucleophile. Importantly, the FDTS mechanism requires a hydrogen transfer to the C6 of the uracil moiety in order to explain the formation 6D-dTMP from reactions performed in D_2O, which is inconsistent with either hydroxyl or flavin as Micheal nucleophiles.

In Figure 2.1C we propose a new chemical mechanism consistent with current data and previous findings (26), wherein a hydride from the N5 of $FADH_2$ is transferred to C6 of dUMP (Fig. 2.1C, step 1). The resulting enolate anion nucleophilically attacks the iminium methylene of CH_2H_4folate, and an elimination of H5 from dUMP and N5 from H_4folate results in a C5=C7 double bond (steps 2 and 3). This exocyclic-methylene intermediate then isomerizes to form the product, dTMP (step 4). The intermediate

proposed here is unique in nucleotide biochemistry, but this isomer of the thymine moiety is chemically feasible and quite stable in solution (36). This mechanism is compatible with our previous findings (26) on the oxidative half-reaction if the equilibrium constant for the first step lies to the left. Since we have no experimental data regarding the methylene transfer and the initial activation (if not H-transfer), steps 2 and 3 are proposed here as a logical path toward the product and step 1 might be preceded by other activation steps.

Since the isomerization of the putative intermediate (Fig. 2.1C, step 4) does not occur rapidly in solution (36), the enzyme could catalyze this transformation by the two mechanisms illustrated in Figure 2.4. An enzymatic acid could catalyze this step *via* an addition-elimination mechanism (AEM), in which a proton is added to the C5=C7 double bond and the intermediate cation loses a proton from C6 to form the product. Alternatively, the thermodynamic driving force (> 6 kcal/mol as estimated from semiempirical QM calculations) could favor a 1,3-sigmatropic rearrangement (1,3-hydride shift) (37). When conducting the reaction in D_2O, an AEM cannot lead to 6D-dTMP unless C7 is also deuterated (Fig. 4, top path). Analysis of the products by ESI-MS (See SI) did not indicate any product with two deuteriums (i.e. 6D,7D-dTMP). Therefore, the possibility of AEM appears unlikely, and a suitable explanation is an enzyme catalyzed isomerization *via* a 1,3-H-shift (Fig. 2.4, lower path).

The finding that two different isotopically labeled products are formed at 37 ˚C was intriguing and warranted further investigation. Thus, we performed the FDTS reactions using dUMP, with D at its C6, in an H_2O buffer at 37 °C (Fig. 2.4, Experiment B). NMR analysis of the product from Experiment B showed the formation of 6D-dTMP (>99%). If any 6H-dTMP was formed it was below our detection limits (<1%). The observations for both experiments (6H-dUMP in D_2O and 6D-dUMP in H_2O) can be explained by reduced stereoselectivity at reduced temperature (37 ˚C). Lack of stereoselectivity has already been observed during the reductive-half reaction of FDTS,

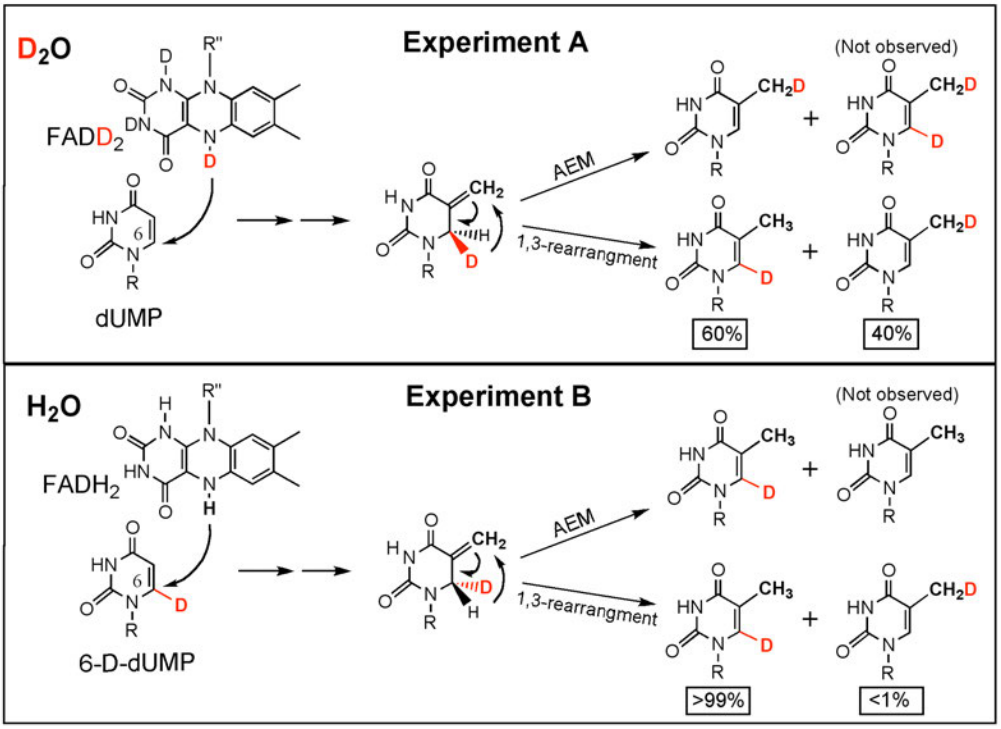

Figure 2.4. Hydride flow. An illustration of two experimental approaches to examine the hydride flow in the reaction catalyzed by the thermophilic *tm*FDTS at reduced temperature (37 °C). Experiment A was performed in a D_2O buffer using 6H-dUMP (i.e., unlabeled, dUMP). Experiment B was performed in an H_2O buffer using 6D-dUMP (see SI). Percentages below each species represent the relative quantities of product formation as indicated by ^1H and ^2H NMR.

which transfers both 4-(*R*) and 4-(*S*) hydride of NADPH (18). The combination of reduced stereoselectivity and a normal kinetic isotope effect (KIE: H reacts faster than the heavier D) rationalizes the findings of both experiments as illustrated in Figure 4. For example, a KIE of 10 (i.e., H is transferred 10 times faster than D) and stereoselectivity of 87 % would result in production of 60:40 C6:C7-dTMP when 6H-dUMP reacts with FDTS in D_2O, and more than 99:1 C6:C7-dTMP produced when 6D-dUMP reacted in H_2O. This model is in good agreement with all available experimental observations (see SI for a more detailed discussion).

Both the nucleophilic addition of deuterium from $FADH_2$ to C6 of dUMP and the subsequent isomerization (steps 1 and 4, Figure 2.1C) could have imperfect stereospecificity and display normal KIEs. Reduced stereospecificity at a temperature that is more than 40 ˚C below the physiological temperature could be due to poor preorganization of the active site, allowing reduced stereo-fidelity in either step 1 or step 4 in Figure 2.1C. Further experiments are needed to determine the origin of the imperfect stereoselectivity and which step has been affected. Nevertheless, a reasonable explanation for formation of 6D-dTMP is a hydrogen transfer to the C6 of dUMP by the deuterated flavin cofactor. This is further supported by the crystal structures of both mutants and wild-type FDTSs, which show a short distance (3.4 Å) between N5 of the flavin ring (the hydride donor in its reduced form) and C6 of dUMP (Figure 2.2).

Hydride transfer from $FADH_2$ to a uracil ring is an atypical chemistry for thymidylate synthases and nucleotide methylation in general, but is not unprecedented in enzymology. For example, dihydrooratate dehydrogenase (DHOD) and old yellow enzyme (OYE) are other flavo-proteins that catalyze the reduction of α,β-unsaturated carbonyl compounds by hydride transfer to the β-carbon and subsequent proton addition to the α-carbon (34, 35). In both the DHOD and the OYE catalyzed reactions, the reduced flavin cofactor transfers a hydride to a position geometrically analogous to the C6 position of uracil.

Our findings suggest that FDTS catalysis occurs without an identified enzymatic nucleophile and is in accordance with a hydride equivalent transfer from the flavin to C6 of dUMP, followed by an isomerization of the exocyclic intermediate to form dTMP *via* a 1,3-H-shift. To the best of our knowledge, neither hydride transfer to the uracil ring, nor an isomerization of such an intermediate has been reported for any thymine biosynthetic pathway or other nucleotide methylations. Importantly, such a chemical mechanism is very different from that of classical TSs, and along with structural differences, may help explain why classical TS inhibitors have a reduced effect on FDTSs (25). The findings and the revised mechanism proposed here (Figure 2.1C), together with the structural differences between these enzymes, suggest that selective inhibition of FDTS should be feasible, and may further alleviate the constraint of an enzymatic nucleophile from structure-based rational drug design efforts. Rationally designed compounds could mimic the non-covalently bound intermediate or the transition states for its formation and isomerization. Such compounds may inhibit FDTS with little effect on classical TSs and thus may serve as leads to selective antibiotics that would not interfere with human thymine biosynthesis.

Materials and methods

Materials

All materials were reagent grade and used without further purification unless specified. 2'-Deoxyuridine-5'-monophosphate (dUMP), reduced nicotinamide adenosine dinucleotide phosphate (NADPH), 5-bromo-2'-deoxyuridine (5Br-dU), 5-fluoro-2'-deoxyuridine-5'-monophosphate (5F-dUMP), trypsin protease, ammonium bicarbonate, tris(hydroxymethyl)aminomethane, D_2, D_2O, phosphocreatine, and creatine kinase were purchased from Sigma. Radiolabed [2-^{14}C]dUMP was obtained from Moravek Biochemicals. N^5,N^{10}-methylene-5,6,7,8-tetrahydrofolate (CH_2H_4folate) was a generous gift from Eprova Inc, Switzerland. The FDTS from *T. maritima* (TM0449, GeneBank

accession number NP228259), and its mutants S88A and S88C were expressed and purified as previously described (3). The thymidine kinase plasmid was obtained from Dr. Robert Stroud's lab at UCSF and expressed and purified as described in ref (43).

Synthesis of 5-bromo-2'-deoxyuridine-5'-monophosphate (5Br-dUMP)

5Br-dUMP was synthesized by phosphorylation of 5Br-dU at 37˚C in a 100 mM Tris, 10 mM $MgCl_2$ buffer at pH = 7.5. The reaction mixture contained 1.5 mM 5Br-dU, 5 mM ATP, 50 mg/mL phosphocreatine, 2 mg/mL creatine kinase and ~1 μM of thymidine kinase. The 5Br-dUMP product was purified by HPLC-UV/Vis (following 280 nm absorbance) and analyzed by ESI-MS.

Purification and activity of FDTS enzymes

The FDTS from *T. maritima* (TM0449, GeneBank accession number NP228259), and its mutants S88A and S88C were expressed and purified as previously described (3). The activities of these enzymes were determined using a [2-^{14}C]dUMP assay which is a modification of the procedure developed and described in ref (18). Mutant reactivity was also determined by oxidation of chemically reduced enzyme by CH_2H_4folate and dUMP under an atmosphere of purified Ar.

Halogenated substrate derivatives

The 5Br-dUMP assay was adopted from ref (28). A TS inhibitor, 5F-dUMP, was assessed as a covalent inhibitor of FDTS by incubating it with the enzyme in the presence of CH_2H_4folate and sodium dithionite, followed by removal of small molecules by ultra filtration. Activities of the incubated enzymes were determined prior to MALDI-TOF analyses.

Mass spectroscopy and NMR analyses

All MALDI-TOF and ESI-MS analyses were conducted at the High Resolution Mass Spectrometry Facility (HRMSF) of the University of Iowa. Enzymes were analyzed following trypsin digestion. NMR analyses were performed at the University of Iowa NMR Central Research Facility using Bruker model Av-300 (for ^{1}H-NMR measurements), and Av-800 (for ^{2}H-NMR measurements) spectrometers.

Following the flow of deuterium during the FDTS reaction in D_2O

Experiments were performed at 65 and 37 °C using dUMP or 6D-dUMP, NADPH, CH_2H_4folate, and enzyme in D_2O or H_2O under anaerobic conditions. The product dTMP was then purified using semi-preparative reverse phase HPLC.

Synthesis of dUMP with deuterium at C6

This procedure was adapted from ref (44). dUMP (225 mg) was dissolved twice in 5 mL of D_2O (>99.96 D-atom) under Ar gas, and evaporated under vacuum (< 50 mTorr) to dryness to reduce proton contamination. The dUMP was then dissolved in 5 mL of D_2O and stirred in the presence of Pt(IV) oxide under 1 atm D_2 gas (>99.96 D-atom) for 3 hours. Vacuum filtration removed the catalyst and the remaining solution was lyophilized to dryness. NMR analysis confirmed >99.5 % D-atom substitution of both the 5 and 6 positions of the uracil ring. A method to substitute the 5D into 5H without affecting 6D has been developed (19), however, such substitution was not used in the current preparation because the TS reaction is a substitution reaction where a methyl group replaces the 5H of dUMP to form dTMP. Since the 5H position is always replaced during the synthesis of dTMP (1, 2, 30) its isotopic labeling can be disregarded.

Analytical methods

All analytical separations were performed on an Agilent series HPLC model 1100, equipped with online degasser, UV/Vis diode array detector and 500TR series Packard flow scintillation analyzer (FSA). Supelco reverse phase column (Discover series 250 mm x 4.6 mm) was used starting with 100 mM KH_2PO_4 (pH = 6.0) followed by a methanol gradient as described elsewhere (18). The enzyme active site concentration was determined by the 454 nm absorbance of bound FAD (ε = 11,300 $cm^{-1}M^{-1}$).

Purification methods

Separation by HPLC was performed using a semi-preparative reverse phase Supelco Column (Discovery series 250 mm x 10 mm). Mobile phase used for separation was a gradient of 100 mM KH_2PO_4 and methanol. Eluent was collected according to the UV spectral absorbance of the purified species and then lyophilized to dryness.

Protein crystallization

The protein-FAD-dUMP complex was prepared by treating 15 mg/mL of the enzyme with around 10 molar excess of dUMP. The well solution for crystallization contained 35 - 45% PEG200 and 0.1M Tris-HCl (pH 8.0) buffer.

Activity assays

The activity assay ([2-^{14}C]dUMP assay) was a modification of the procedure developed and described in ref (18). All experiments were performed in 200 mM tris buffer (exchanged with Ar gas) pH = 8.0 at 65 °C with standard reaction conditions of: 100 μM dUMP (including 0.5 Mdpm [2-^{14}C]dUMP), 200 μM CH_2H_4folate, 5 mM CH_2O (to stabilize CH_2H_4folate) and 5 mM sodium dithionite. Reactions were initiated by addition of 0.1 – 2 μM (final concentration) of enzyme, quenched with HCl (to a final pH = 1) and stored at -80 °C until analysis. HPLC-FSA analysis was used to determine the conversion of [2-^{14}C]dUMP to [2-^{14}C]dTMP.

5Br-dUMP assay

Reactions with either *ec*TS or *tm*FDTS were performed in a 200 mM tris buffer at pH = 8.0, containing 100 μM 5Br-dUMP, 5 mM sodium dithionite, and 5 mM β-mercaptoethanol. Enzyme was added to the reaction mixture which was then incubated at 37 ˚C for 3 hours. Product conversion was determined by HPLC-UV/Vis analysis of the reaction mixtures by following both 256 and 280 nm absorptions for dUMP and 5Br-dUMP, respectively.

Oxidative Half-Reaction of S88A

A solution of oxidized S88A (20 μM) and dUMP (1 mM) was made anaerobic in a sealed cuvette by successive cycles of evacuation and equilibration with an atmosphere of purified Ar. The oxidized enzyme was titrated spectrophotometrically to complete reduction with a solution of dithionite. CH_2H_4folate was added anaerobically from a side-arm to initiate the reaction (25°C). The absorbance spectrum of oxidized enzyme returned before the first scan, indicating a rapid reaction of the mutant enzyme.

Protein digestion

All enzyme digestion reactions were performed in 100 mM ammonium bicarbonate buffer adjusted to pH = 8.0 at 37˚C. Enzyme solutions were diluted to 1 μM protein concentration followed by addition of trypsin to a final concentration of 10 ng/μL. All digestions were allowed to incubate for 3 hours at 37˚C and stored at -20 °C prior to MALDI-TOF MS analysis.

Assessment of 5F-dUMP as a covalent inhibitor of FDTS

These experiments were performed at 37˚C in 200 mM tris buffer at pH = 8.00. Both wt-FDTS and S88A (11 μM active site concentration) were incubated for 30 minutes in the presence of 50 μM 5F-dUMP, 200 μM CH_2H_4folate, and 5 mM sodium dithionite. After incubation, activities of the enzymes were determined using the standard

activity assay conditions (except with a residual 5 μM 5F-dUMP). Samples of native and trypsin-digested enzymes were prepared for MALDI-TOF MS analysis. The remaining enzyme solutions were exchanged with 40 mL of Tris buffer at 4˚C, and concentrated by centrifugal filtration (using a Millipore 10,000 MWCO filtration device) to 11 μM active site concentration. Once concentrated, the activity of both FDTS and S88A were determined using the standard activity assay conditions. As described in the report, no covalent adduct of 5F-dUMP to enzyme was identified and both enzymes recovered 100 % activity after the removal of the 5F-dUMP from the reaction mixture.

Following the flow of deuterium during the FDTS reaction

For studies in D_2O, all substrates in 100 mM tris buffer were exchanged twice by dissolving in D_2O (>99.96 % D-atom) and lyophilizing to dryness prior to use. Experiments were performed in 100 mM tris buffer (99.96 % D_2O or H_2O) pH = 8.0 at 65 and 37 °C using 4 mM dUMP or 6D-dUMP, 8 mM NADPH, and 8mM CH_2H_4folate, under Ar. To maintain anaerobic conditions 10 mM glucose and 100 units of glucose oxidase were added to the reaction mixture. Reactions were initiated by adding enzyme (previously lyophilized and resuspended in D_2O or H_2O) to a final concentration of 1-10 μM. The reaction mixtures were incubated (at 65 or 37 °C) for 20 hours under Ar and stored at -20 °C. The product dTMP was then purified using semi-preparative HPLC, lyophilized, triturated into methanol, and dried under vacuum. The dTMP was dissolved in D_2O or H_2O for ^1H and ^2H NMR analysis, respectively.

Supplementary information

Additional discussion regarding alternative enzymatic nucleophile(s)

If Ser88 is not essential for catalysis, the most straightforward way for another enzymatic nucleophile to participate in the reaction is through a conformational change

which brings a remote nucleophile close to C6 of dUMP. We did not limit our search for alternative nucleophiles to the vicinity of the active site because the binding of CH_2H_4folate may induce an unpredicted conformational change (all the current structures of FDTSs lack the CH_2H_4folate cofactor). These conformational changes should be limited due to the FAD's ADP moiety, which is tightly held at the core of the tetramer and only the isoalloxazine ring has some flexibility proximal to its glycosidic bond (C2-C3 of the ribose).

The only two potential nucleophiles (aside from Ser88) are conserved Ser83 and Tyr91 (Figure 2.5), both within 20 Å of the current coordinates of the electrophilic center of dUMP. Tyr91 is an unlikely nucleophile because it is not strictly conserved and is a Phe in some organisms. In fact, its mutation to Phe in *H. pylori* (*hp*FDTS) results in an enzyme that is 50% **more** active than the wild type (30). The Ser83 residue is 17.7 Å from C6 of dUMP and is hydrogen-bonded to the adenine ring of FAD at the core of the tetramer (11). In *tm*FDTS, FAD remains tightly bound throughout purification and it is very unlikely that the dUMP can displace the adenine ring to become proximal to Ser83. Even in crystal structures where the adenine moiety of $NADP^+$ has substituted FAD, Ser83 is still H-bonded to the adenine ring and is unavailable to activate dUMP. These points diminish the possibility for Ser83 or Tyr91 to act as nucleophiles during the FDTS reaction.

Besides the options presented above (Ser83, Tyr91 and Ser88), the absence of any other possible enzymatic nucleophile is further supported by: (i) The lack of any complexes where 5F-dUMP forms a covalent bond with the enzyme (as described in the report, see Figure S2), which is consistent with similar results reported for FDTSs from *Chlamydia trachomatis* (27) and *Paramecium bursaria* Chlorella Virus-1 (24); and (ii) Lack of reactivity with 5Br-dUMP (a common assay for enzymatic Michael Addition in classical TS). Taken together, these points further support the lack of an enzymatic nucleophile in the FDTS catalyzed reaction.

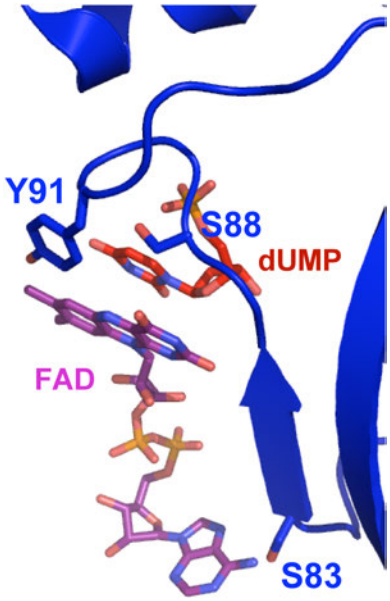

Figure 2.5. Active site of *tm*FDTS. All conserved nucleophilic residues (S83, S88, and Y91), dUMP and FAD are shown as sticks.

Excluding the possibility of a false signature of activity

To eliminate the possibility of a false signature of activity we used an assay which follows the conversion of [2-^{14}C]dUMP to [2-^{14}C]dTMP(18). In contrast to the 340 nm assay that quantifies the consumption of NADPH (sensitive to the side reaction with O_2 due to oxidase activity (33)), or tritium release from [5-^{3}H]dUMP(30) that may occur prior to product formation, the [2-^{14}C]dUMP assay follows the actual formation of dTMP.

MALDI-TOF experiments with tmFDTS

A digested peptide fragment of the wild type (wt) FDTS (IASYNEL**S**GR) was observed at 1109.49 m/z, which is within error of the calculated fragment mass of 1109.56 amu (see Figure S3). A peak at 1093.46 m/z was observed for the S88A, which is in accordance with the loss of oxygen (16 amu). Analysis of the S88C mutant spectrum did not show a peak with the corresponding mass of 1125.5 m/z, however, the 1109.49 m/z peak representing wt FDTS was not present. Further analysis did not identify a dimer (i.e. disulfide bond) of the S88C peptide fragments (2251.1 m/z). The S88C mutant did have a peak at 1433.5 m/z that was not observed in either wt FDTS or S88A spectra. This peak may represent the mass of the mutant fragment plus dUMP (1125.5 + 308 amu). When ref (30) identified a similar covalent adduct for S84C of hpFDTS it was reasonable to conclude that it supported the proposal of S84 (hpFDTS) as the enzymatic nucleophile. However, in the current experiment dUMP was not incubated with the mutant enzymes prior to digestion. Thus, the current finding implies that dUMP was bound to S88C throughout the purification procedures. Together with the activity of S88A, this finding supports our conclusion that such a covalent adduct does not represent a reactive complex but rather an inhibitory dead-end complex.

ESI-MS analysis of dTMP and D-dTMP

Figure 2.8 presents the MS spectra of the dTMP produced in the FDTS reactions conducted in H_2O and D_2O buffers. Spectrum 2.8.B. indicates no detectable doubly deuterated dTMP, which eliminates the possibility of AEM for the isomerization of the proposed intermediate in Figure 2.4.

Stereospecificity and H/D isotope effect

To rationalize the isotopic distribution of D in the dTMP that was produced in the experiments illustrated in Figure 2.4 (i.e., 6H-dUMP in D_2O and 6D-dUMP in H_2O), we employed a simple model involving two unknowns: the percent stereoselectivity and the normal kinetic isotope effect (KIE). Using the measured percentage of D in the C6 and C7 positions of the produced dTMP in both experiments we obtained two equations with two unknowns. A set of solutions was determined by solving these equations within physically reasonable values of percent stereoselectivity and KIE. In the report we present such a solution (percent stereoselectivity = 87 % and KIE = 10) that when applied to both experiments reproduced the measured distribution of D in the product dTMP.

Rate Measurements

This work is qualitative in nature, and the main point is that both mutants S88A and S88C still have FDTS activity and no activity of classical TS. The actual activity measurements were carried in two independent experiments: a. The initial velocity of [2-^{14}C]-dUMP formation under steady-state conditions at 65 ˚C (assuring no classical TS activity), and b. Single turnover pre-steady-state on the oxidative half reaction, by following the formation of FAD 454 nm absorbance (not sensitive to classical TS activity) at 25 ˚C. The activity of S88C at 25 ˚C was too low for quantitative stopped flow measurement. These data are presented in Table 2.2.

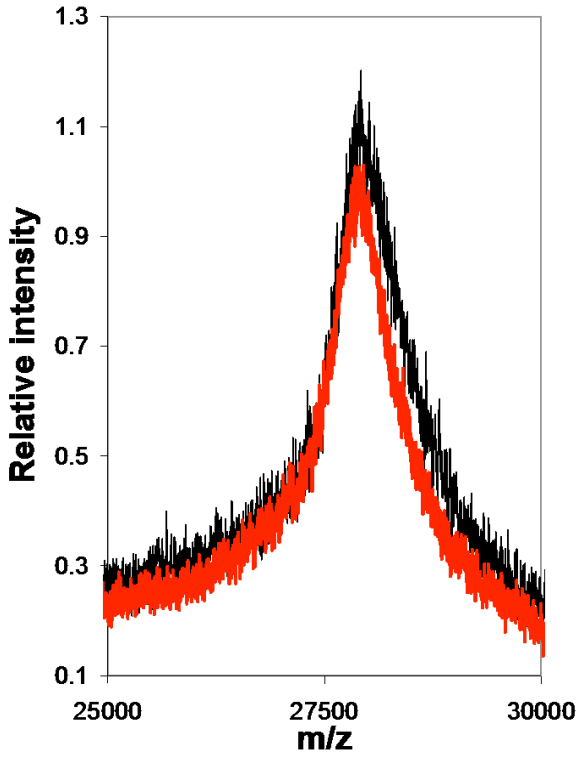

Figure 2.6. Native MALDI-TOF spectra of *tm*FDTS**.** The spectrum presented in red was obtained from enzyme that was analyzed after incubation with the inhibitor 5F-dUMP and the cofactor CH_2H_4folate. The control spectrum presented in black was obtained from analysis of *tm*FDTS complex with FAD (as purified). Upon ternary complex formation (i.e. FDTS-5F-dUMP- CH_2H_4folate), a mass change of >800 amu is expected. As seen from the figure, the control enzyme is indistinguishable from enzyme incubated with the inhibitor and cofactor.

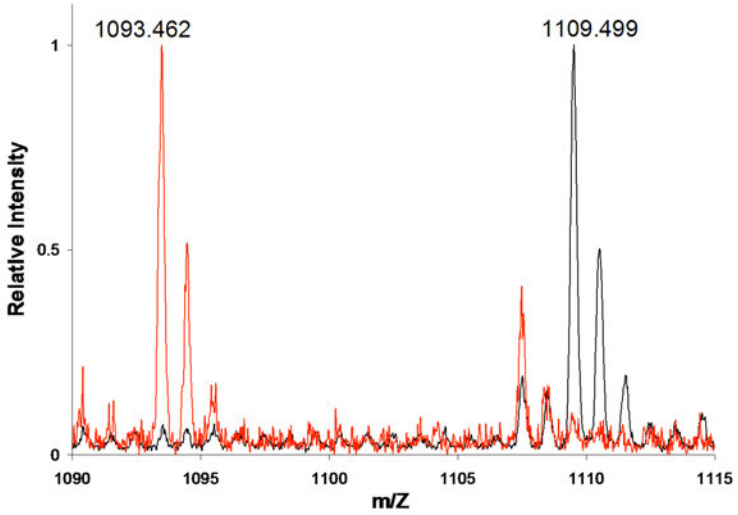

Figure 2.7. MALDI-TOF mass spectra of digested *tm*FDTS. The Wt peptide fragment (IASYNELSGR) has a predicted mass of 1109.5586 amu and is presented in black. The S88A Peptide fragment (IASYNELAGR) has a predicted mass of 1093.5592 amu and is presented in red. A 16 amu difference between fragment masses is consistent with a loss of oxygen, as expected by mutation from Ser to Ala.

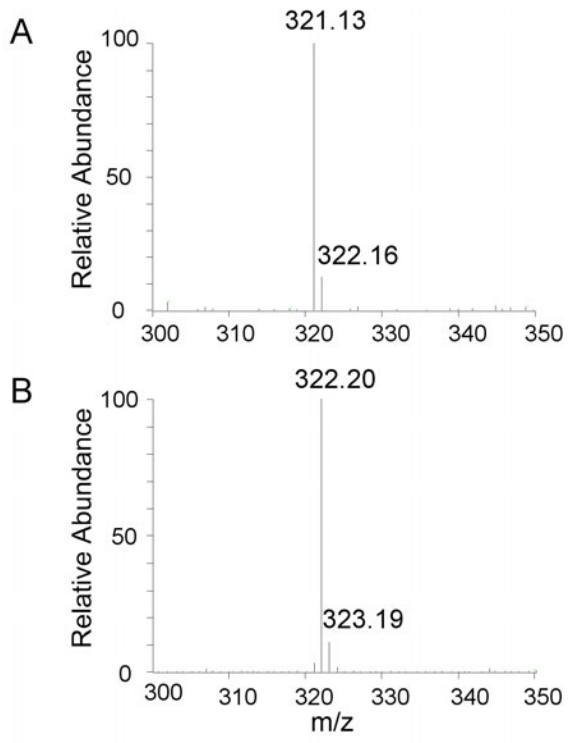

Figure 2.8. ESI-MS spectra of dTMP produced in the FDTS reaction. Reactions were conducted in H_2O (panel A) and D_2O (99.6 %D) (panel B) buffers.

Table 2.1. Data collection and refinement statistics.

	S88A+FAD+dUMP	S88C+FAD+dUMP
Data collection:		
Space group	$P2_12_12_1$	$P2_12_12_1$
Unit cell	53.95, 116.22, 140.73Å	53.90, 116.50, 140.99Å
wavelength (Å)	0.9795	0.9795
resolution (Å)	89.4-1.95 (2.0-1.95)	46.22 – 2.05
no. of reflections	285498	239601
no. of unique reflections	65136	56600
redundancy	4.4 (3.7)	4.2 (4.3)
completeness	99.6 (96.2)	99.9 (100.0)
Rsym (%)	6.6 (69.2)	7.4 (63.0)
I/σ	13.2 (1.5)	12.0 (2.1)
Refinement:		
resolution (Å)	89.4-1.95 (2.00-1.95)	46.2-2.05 (2.1-2.05)
reflections (working)	58490(4330)	50851 (3924)
reflections (test)	3288 (248)	2843 (206)
R_{work} (%)[b]	18.6 (24.6)	20.0 (25.4)
R_{free} (%)[c]	22.2 (30.4)	25.4 (32.9)
no. of protein atoms	7043	6951
no. of ligand atoms	292	292
no. of water atoms	159	167
rms deviations		
bonds (Å)	0.014	0.014
angles (º)	1.59	1.61
average B-factor ($Å^2$)		
protein atoms	36.7	30.2
ligand atoms	35.2	33.0
solvent atoms	40.3	32.6

[a] Values for the outer shell are given in parenthesis.

[b] $R_{work} = \sum_{hkl} ||F_{obsd}| - |F_{calcd}||/\sum_{hkl} |F_{obsd}|$, where F_{obsd} and F_{calcd} are observed and calculated structure factors, respectively.

[c] For R_{free}, the above summation is extended over a subset of reflections (5%) that were excluded from all stages of refinement.

Table 2.2: Apparent kinetic values of *tm*FDTS.

	Apparent k_{cat} (sec^{-1})[a]	**Apparent K_M [μM][a]**	**Pre-steady state (sec^{-1})[b]**
WT	1.2	30	0.18
S88A	0.07	29	0.02
S88C	0.003	29	–

[a.] Measured from steady state initial velocities using the ^{14}C-dUMP assay at 65 ˚C.

[b.] Measured by pre-steady state stopped flow for the oxidative half reaction following the increase in 454 nm absorbance of enzyme bound FAD at 25 ˚C.

[c.] Reaction conditions are stated in *Materials and Methods*. Data were fit using non-linear regression to the equation: $\nu/[E] = k_{cat}[dUMP]/(K_M + [dUMP])$ using Kaleidagraph.

CHAPTER III

TRAPPING OF AN INTERMEDIATE IN THE REACTION CATALYZED BY FLAVIN-DEPENDENT THYMIDYLATE SYNTHASE (FDTS)

This chapter was in full or part published in the Journal of the American Chemical Society, Mishanina, T., Koehn E. M., *et. al*., 2012, *J. Am. Chem. Soc.* 134:4442-4448. Figures and/or content are used with permission from ACS.

Abstract

Thymidylate is a DNA nucleotide that is essential to all organisms and is synthesized by the enzyme thymidylate synthase (TSase). Several human pathogens rely on an alternative flavin-dependent thymidylate synthase (FDTS), which differs from the human TSase both in structure and molecular mechanism. Recently it has been shown that FDTS catalysis does not rely on an enzymatic nucleophile and the proposed reaction intermediates are not covalently bound to the enzyme during catalysis, an important distinction from the human TSase. Here we report the chemical trapping, isolation, and identification of such an intermediate in the FDTS-catalyzed reaction. The chemically modified reaction intermediate is consistent with currently proposed FDTS mechanisms that do not involve an enzymatic nucleophile, and has never been observed during any other TSase reaction. These findings establish the timing of key chemical steps during FDTS catalysis. The presented methodology provides an important experimental tool for further studies of FDTS, which may assist the efforts to rationally design inhibitors as leads for future antibiotics.

Introduction

Thymidylate synthases (TSases) catalyze the last step in the *de novo* biosynthesis of the DNA nucleotide 2'-deoxythymidine-5'-monophosphate (dTMP) by reductively

methylating the uracil moiety of 2'-deoxyuridine-5'-monophosphate (dUMP) (1, 2). There are two currently known classes of TSases that differ in structure, sequence, and cofactor requirements (4). The homodimeric enzymes encoded by the *thy*A gene (the *TYMS* gene in humans) are referred to here as classical TSases. These have been extensively studied, leading to the established kinetic and chemical mechanisms. Classical TSase enzymes use N^5,N^{10}-methylenetetrahydrofolate (CH_2H_4folate) for both the one-carbon methylene and the reducing hydride to form the C7 methyl of the dTMP product (Scheme 1a) (2). The more recently discovered *thy*X-encoded proteins utilize a non-covalently-bound flavin adenine dinucleotide (FAD) prosthetic group to catalyze the redox chemistry and use CH_2H_4folate only as a methylene donor. These flavin-dependent thymidylate synthases (FDTSs) are found primarily in prokaryotes, including several pathogens and biological warfare agents (3, 4). The structural and mechanistic differences between FDTS and classical TSase present an enticing new avenue for the development of antibiotics with a potential for minimal toxicity to humans.

Several mechanism-based drugs targeting classical TSase are available today (e.g. 5-fluorouracil, 5-trifluoromethyl 2'-deoxyuridine, raltitrexed, etc.) (45-47). Development and identification of these compounds relied greatly on the knowledge of the molecular mechanism of catalysis and identification of reaction intermediates for the classical TSase reaction. To emphasize the differences in catalysis from the FDTS enzymes under study here, we present the established chemical mechanism of the classical TSase (Scheme 3.1a). In short, the classical TSase reaction begins with an active site cysteine covalently activating dUMP via Michael addition (step 2), which then undergoes a Mannich-type condensation with the methylene of CH_2H_4folate (step 3). The resulting bridged intermediate eliminates H_4folate (step 4) to form an enzyme-bound exocyclic methylene intermediate, which accepts a hydride from H_4folate (step 5) producing H_2folate and the product dTMP (1, 2). Step 3 of this mechanism is supported by the quenching experiments with wild-type *Lactobacillus casei* TSase (49), the crystal

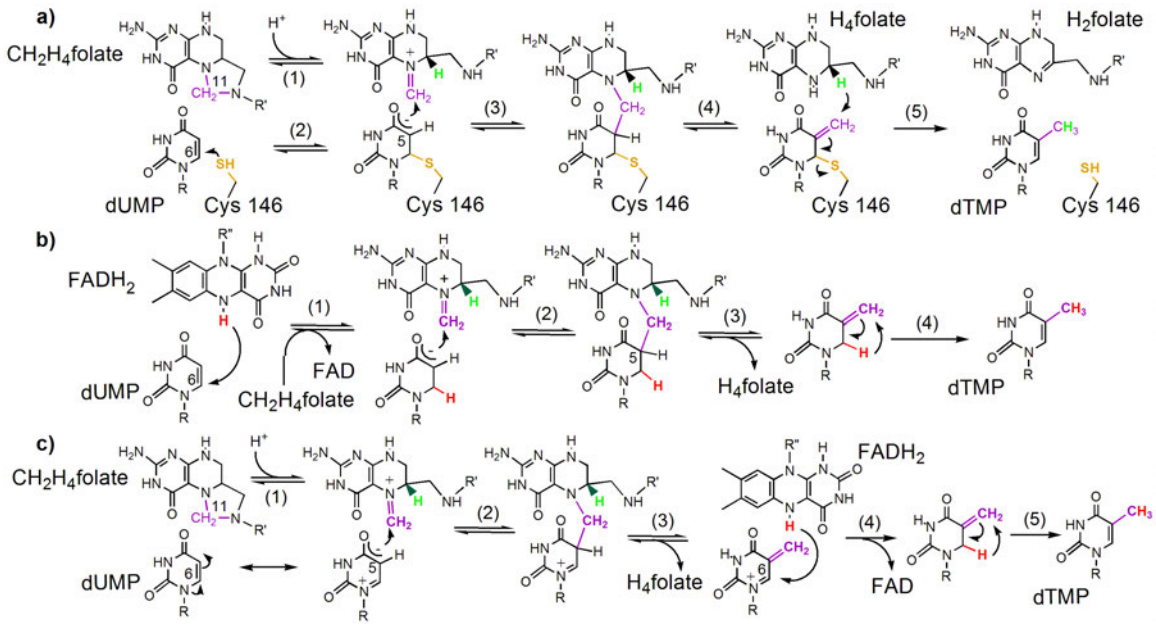

Scheme 3.1. Thymidylate synthase chemical mechanisms. a) The mechanism for classical TSase (1, 2). b) A mechanism proposed for FDTS where dUMP reduction occurs prior to methylene transfer (22). c) An alternative mechanism proposed for FDTS where reduction happens after methylene transfer (48). The enzymatic nucleophile is orange, the methylene is purple, the reducing hydride from H_4folate is green, and the hydride from $FADH_2$ is red. R=2'-deoxyribose-5'-phosphate; R'=(p-aminobenzoyl)-glutamate; R''=adenosine-5'-pyrophosphate-ribityl.

structure of the covalent complex of wild-type *Escherichia coli* enzyme with 5F-dUMP and CH_2H_4folate, and the isolation on SDS-PAGE of the enzyme-bound bridged intermediate (between steps 3 and 4) in reactions of E60A and E60L mutants of *Lc*TSase with radiolabeled substrates (50).The existence of the exocyclic methylene intermediate (between steps 4 and 5) was supported by experiments with a W82Y mutant of *Lc*TSase, which allowed chemical trapping with β-mercaptoethanol under steady state conditions (13).

A few moderate inhibitors of FDTS enzymes have been developed, none of which are mechanism-based nor have shown highly specific inhibition of FDTS over classical TSase (41, 51). Potent inhibitors of classical TSase, such as 5F-dUMP, produce moderate reversible inhibition of FDTS, and crystal structures of FDTS with 5F-dUMP (e.g. P.D.B accession 1tls) present non-covalently bound complexes that do not provide significant information about the catalytic mechanism or intermediate structures (22, 52).

One of the most convincing pieces of evidence for any chemical mechanism is the identification and characterization of reaction intermediates. Although several chemical mechanisms have been proposed for FDTS, direct evidence of the identity of any of the proposed reaction intermediates has been previously unavailable (18, 22, 23, 25, 27, 48, 52). In this chapter we show that a reaction intermediate can be chemically trapped and isolated during a single-turnover oxidative half-reaction of FDTS. The identification of the trapped intermediate described below indicates that it is not covalently bound to the enzyme and already includes the methylene originally carried by the CH_2H_4folate. This finding together with the time course of accumulation and decay of this intermediate limits the options for potential mechanisms and provides a timeframe for key chemical events of FDTS catalysis.

Results and discussion

Acid-quenching of the oxidative half-reaction of FDTS

To determine whether any intermediate(s) accumulate during the FDTS-catalyzed reaction, a series of quench-flow experiments were performed. To increase the chance for intermediate trapping, we used a hyperthermophilic FDTS from *T. maritima* and carried out the reactions at room temperature – significantly below *T. maritima*'s physiological 80°C − possibly enhancing the duration and magnitude of intermediate accumulation. Briefly, the FAD bound to *T. maritima* FDTS enzyme was stoichiometrically reduced with dithionite under anaerobic conditions, allowing $FADH_2$ to serve as the limiting reactant in the oxidative half-reaction under study (i.e., conversion of dUMP to dTMP). The dUMP was bound to the pre-reduced enzyme prior to the reaction since in the catalytic turnover this substrate binds before CH_2H_4folate and probably even prior to the flavin reduction (29, 33, 48). Oxidative FDTS half-reactions were then initiated by rapid mixing with CH_2H_4folate and quenched with 1 M HCl at various reaction times (for details see Materials and Methods).

By quantitatively tracking the substrate dUMP and product dTMP by LC-MS, we were able to construct a time course for the oxidative FDTS half-reaction. Figure 3.1 shows the total ion counts measured at various reaction times for dUMP, dTMP, and their sum (which represents the total amount of material accounted for by these species). It was noticed that for time points between ~ 0.5-10 seconds the sum of the ion counts for dUMP and dTMP was substantially less than at the beginning and the end of the reaction. This observation suggests that a reaction intermediate has accumulated during this time period. This finding is in accordance with the lag in product formation we reported recently (48), but does not reveal the identity of the intermediate, leading to the next set of experiments.

Following intermediate formation using radiolabeled substrates

To characterize the acid-trapped intermediate, it was first necessary to identify this material in the chromatographic analysis. To do so, ^{14}C-radiolabled substrates were used where the labeled carbon was either on the dUMP or the methylene of the CH_2H_4folate. The oxidative turnover of FDTS with the radiolabeled nucleotide, [2-^{14}C]-dUMP, was quenched with acid at various times, as described above and under the Materials and Methods. Figure 3.2a shows an HPLC-radiochromatogram of a reaction quenched at 2 seconds, where under the reaction conditions about 80% of the total radioactivity was in the form of the trapped intermediate. The total radioactive counts (dUMP, dTMP, and the newly identified peak) remained constant at all quenched reaction times, suggesting that all the missing nucleotide observed in the LC-MS analysis above was being accounted for by this single newly developing radioactive peak. It is also noteworthy that the fraction of total radioactivity associated with the new radioactive material accumulates and decays during the course of the singe-turnover half-reaction, a behavior typical of enzymatic intermediates (Figure 3.2c).

To test whether the trapped species already contains the methylene from the cofactor CH_2H_4folate, we performed another crucial experiment wherein the enzyme mixed with non-labeled dUMP was reacted with [11-^{14}C]-CH_2H_4folate under the same conditions as above. By following the radiolabeled methylene we found that when quenching at 2 seconds a new radioactive peak developed that had the same retention time as the peak observed when starting with [2-^{14}C]-dUMP (Figure 3.2b). This clearly shows that the intermediate nucleotide that is being chemically trapped during the acid-quenching has already undergone the condensation with CH_2H_4folate, and the carbon-carbon bond between the C5 of dUMP and the methylene has been formed prior to the formation of that intermediate.

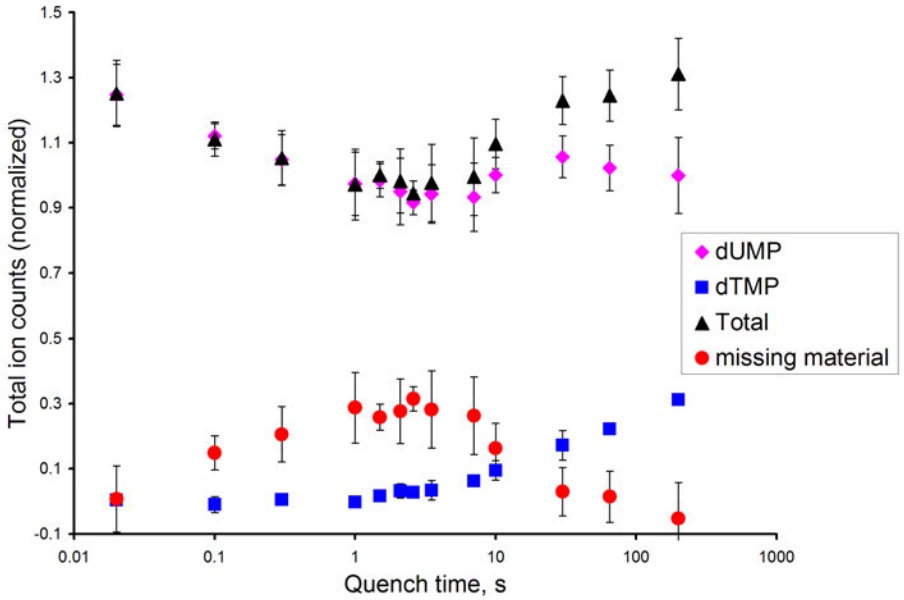

Figure 3.1. Single-turnover FDTS reaction. Total ion counts for dUMP and dTMP determined by LC-MS analysis are given for dUMP in purple and dTMP in blue. Notably, the sum of the counts for dUMP and dTMP is not conserved during the reaction, suggesting the accumulation of an intermediate (in red).

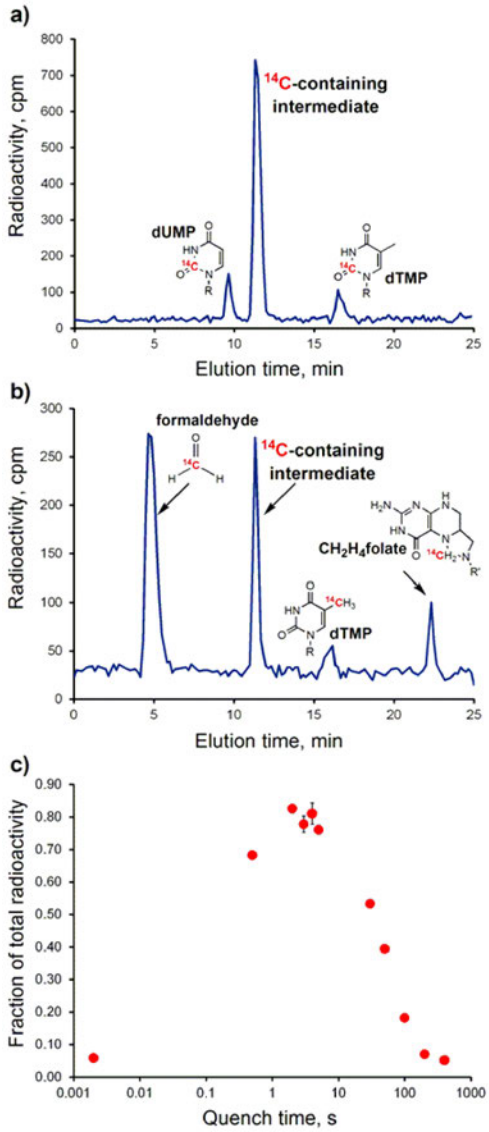

Figure 3.2. Intermediate trapping using ^{14}C-labeled substrates. HPLC radiograms for FDTS reactions quenched at 2 seconds with 1M HCl starting with either (a) ^{14}C-labeled dUMP, or (b) ^{14}C-labeled CH_2H_4folate. The labeled carbon is shown in red. In both cases, ^{14}C-containing trapped intermediate elutes at ~11 minutes, representing the same trapped species. Panel (c) shows the fraction of total radioactivity contained in the trapped intermediate peak for the FDTS reactions with ^{14}C-labeled dUMP as a function of oxidative half-reaction time.

Characterization and identification of the acid-trapped intermediate

Once the chromatographic elution time of the trapped intermediate was known, non-radioactive FDTS reactions were quenched at ~2 seconds, which produced the largest amount of trapped intermediate, and were purified by HPLC. The purified trapped intermediate was analyzed by ESI-MS and high-resolution MS and was found to have an m/z of 337.0432 (M-1 ion), which is consistent with the exact mass and atomic composition of the product dTMP plus a hydroxyl group (i.e., 17 a.m.u.). The possibility of the trapped intermediate being 5-hydroxymethyl-dUMP was tested by the matching of HPLC retention time, HRMS, and MS-MS of the purified trapped intermediate compared to the synthesized 5-hydroxymethyl-dUMP (see Materials and Methods), as shown in Figure 3.3. LC−MS analyses of reactions quenched at short (2 ms) or long (400 s) times did not contain 5-hydroxymethyl-dUMP, indicating that it was not a pre-existing contaminant. Furthermore, the accumulation and decay pattern observed when using radioactive substrates (Figure 2c) was consistent with the accumulation and decay of the intermediate as analyzed by LC−MS (Figure 1).

Mechanistic implications.

Reactions of classical TSase enzymes with the same radiolabeled substrates, as described above, led to accumulation and isolation of the covalent bridged intermediate (Scheme 3.1a, between steps 3 and 4) (50). No such enzyme-bound species was observed with FDTS (see Materials and Methods), and all the radiolabeled trapped material was accounted for in a single, soluble intermediate. Thiol addition to the enzyme-bound exocyclic methylene intermediate in classical TSase mutants (Scheme 3.1a, between steps 4 and 5) resulted in chemical modification at C7 (13). Our efforts to use thiols as trapping reagents (see Materials and Methods) resulted in no trapped species during the

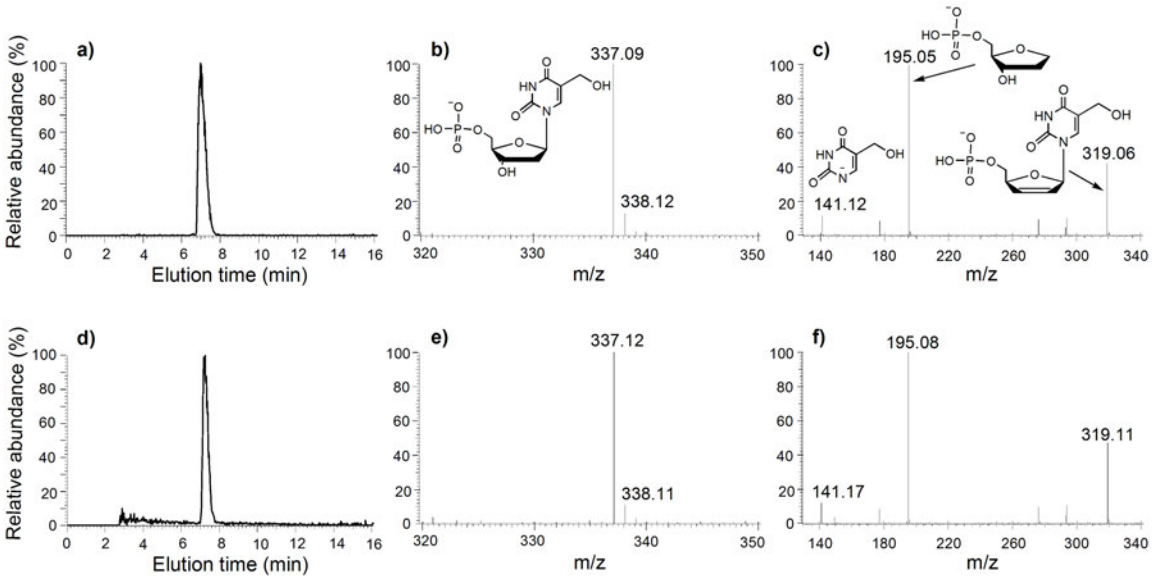

Figure 3.3. LC-ESI data for the synthesized 5-hydroxymethyl-dUMP standard (top panel) and the trapped intermediate (bottom panel). Shown are the chromatograms (a and d), MS spectra (b and e) and MS-MS spectra (c and f) of the standard and the trapped intermediate, respectively. All spectra were collected in the negative-ion mode. The structures of the ions with the observed masses are shown. By these analyses, the synthesized standard was indistinguishable from the trapped intermediate.

FDTS-catalyzed reaction. These observations further emphasize the mechanistic differences between classical TSase and FDTS.

Substantial evidence has been published indicating that the FDTS-catalyzed reaction occurs without participation of an enzymatic nucleophile, a notable deviation from not only classical TSase but also other uridyl-methylating enzymes (22, 52). A recently proposed mechanism for FDTS catalysis is presented in Scheme 3.1b, which was based on mutagenesis and isotope labeling studies with *Tm*FDTS that did not support a nucleophilic attack on dUMP by any enzymatic residue (22). In this mechanism, dUMP accepts a hydride from the N5 of $FADH_2$ (step 1) generating an enolate that attacks the iminium form of CH_2H_4folate (step 2). Elimination of tetrahydrofolate (H_4folate, step 3) results in a putative exocyclic methylene intermediate, which would need to isomerize to form dTMP (step 4). In Scheme 3.2a, we suggest a mechanism for water addition under acidic conditions to the isomer of dTMP proposed in Scheme 3.1b. Notably, if 5-hydroxymethyl-dUMP does originate from treating this isomer of dTMP with acid, it requires oxidation (i.e. loss of a proton and two electrons) to form the acid-trapped species. Molecular oxygen is proposed as a likely hydride acceptor in the last step of mechanism 3.2a because quenched reactions are exposed to oxygen immediately after quenching.

Even more recent studies, following flavin absorbance in an oxidative half-reaction by stopped-flow technique, showed that flavin oxidation is not likely to be the initial step in FDTS catalysis and led to an alternative mechanistic option for FDTS catalysis, presented in Scheme 3.1c (48). In this mechanism, dUMP is electronically polarized upon binding leading to nucleophilic attack from C5 of dUMP with no covalent activation at C6. Methylene transfer can then occur (step 2), followed by elimination of H_4folate (step 3). The resulting exocyclic-methylene cation is then reduced by a hydride from $FADH_2$ (step 4) to form either dTMP (if reduced at C7), or the exocyclic isomer of dTMP (if reduced at the C6 as suggested in ref (22)), which can isomerize to form dTMP

(step 5). The exocyclic-methylene cation proposed to form after step 3 could readily undergo hydroxyl addition in acidic media to yield 5-hydroxymethyl-dUMP, as depicted in Scheme 3.2b.

The mechanism proposed in Scheme 1b requires a hydride transfer from the reduced flavin prior to the formation of a methylene-bridged intermediate, while the mechanism in Scheme 1c offers an option that does not require flavin redox chemistry until after the methylene transfer. In attempt to further distinguish between these two mechanisms, we repeated quenching experiments without pre-reducing the flavin and found no intermediates that accumulate, suggesting that the reduced flavin is required to form the intermediate that we have shown to contain the transferred methylene. While this observation is in accordance with the mechanism proposed in Scheme 3.1b, it does not necessarily eliminate the mechanism in Scheme 3.1c. It is possible that even though the reduced flavin might not participate in redox chemistry until after the elimination of H_4folate (as suggested in Scheme 3.1c), it does play a role in a conformational change in the enzyme, which is needed to bring both substrates in a reactive configuration.

Spectral evidence has also suggested that more than one reaction intermediate may accumulate during the FDTS reaction (48). Yet, at all reaction times analyzed here, only one acid-trapped species was identified. Furthermore, in reactions using radiolabeled substrates, the total radioactive counts are always conserved amongst dUMP, 5-hydroxymethyl-dUMP, and dTMP, and the reaction time-course fits reasonably well to a simple mechanism with one intermediate. The two spectral species and the single acid-trapped intermediate could be consolidated if the acid modification of more than one intermediate leads to the formation of 5-hydroxymethyl-dUMP, e.g., bridged dUMP-CH_2H_4folate species transiently accumulating prior to the formation of the exocyclic methylene intermediate.

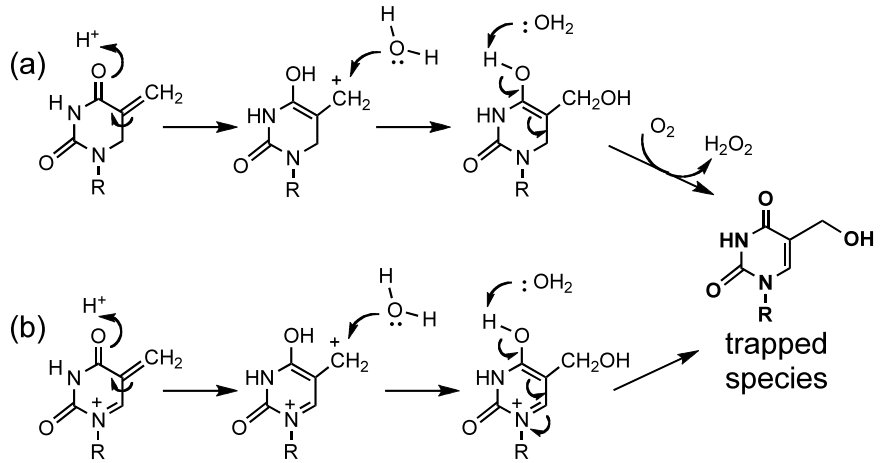

Scheme 3.2. Possible mechanisms for acid trapping of the intermediates proposed in Scheme 1b (a) and c (b).

Conclusions

Rapid acid-quenching experiments with *Tm*FDTS at room temperature resulted in chemical trapping of a reaction intermediate, which was not covalently bound to the enzyme and was identified as 5-hydroxymethyl-dUMP. This provides evidence for the existence of non-covalently bound intermediates (Scheme 1b and 1c) and indicates the timing of carbon bond formation between dUMP and CH_2H_4folate. Importantly, this trapped species has not been isolated from any classical TSase, supporting the notion that the FDTS-catalyzed reaction proceeds via a unique chemical mechanism. The identification of this acid-trapped intermediate adds new restrictions to possible mechanism and eliminates several mechanisms proposed in the past (18, 23, 25, 27, 30). The timing of intermediate(s) accumulation will be crucial for future efforts to characterize the intermediate following different chemical trapping agents, or the unmodified intermediate. While the trapping of 5-hydroxymethyl-dUMP in the FDTS reaction emphasizes the mechanistic distinctions from classical TSase, it is not sufficient to distinguish between two of the currently proposed mechanisms (Scheme 1b and 1c) and both should be considered in future studies and mechanism-based inhibitor design.

Materials and methods

Materials

All chemicals were reagent grade and used as purchased without further purification, unless specified. 2'-Deoxyuridine 5'-monophosphate (dUMP), 5-hydroxymethyl-2'-deoxyuridine (5-hydroxymethyl-dU), glucose oxidase powder, D-glucose, D_2O, and formaldehyde solution (36.5% by weight) were obtained from Sigma. N^5,N^{10}-methylene-5,6,7,8-tetrahydrofolate (CH_2H_4folate) was provided by Eprova Inc. (Schaffhausen, Switzerland). Radiolabeled [2-^{14}C]-dUMP was purchased from Moravek Biochemicals. Radiolabeled [11-^{14}C]-CH_2H_4folate was prepared according to the previously developed chemoenzymatic synthesis procedure (53). Sodium dithionite

powder was purchased from J.T. Baker, and tris(hydroxymethyl)aminomethane was obtained from Research Products International Corp. The FDTS from *Thermatoga maritima* (TM0449, GenBank accession number NP228259) was expressed and purified as previously described (11). Human deoxycytidine kinase mutant dCK-DM was a generous gift from Dr. Arnon Lavie at the University of Illinois-Chicago.

Synthesis of 5-hydroxymethyl-2'-deoxyuridine-5'-monophosphate (5-hydroxymethyl-dUMP).

The synthesis procedure has been previously reported and was adapted from ref (54). More specifically, the 5-hydroxymethyl-dUMP was synthesized by phosphorylation of commercial 5-hydroxymethyl-dU at 37ºC in a 100 mM Tris, 10 mM $MgCl_2$, 100 mM KCl buffer at pH 7.5. The final reaction mixture contained 2 mM 5-hydroxymethyl-dU, 4 mM ATP, and 10 units/mL of deoxycytidine kinase (dCK-DM). The 5-hydroxymethyl-dUMP product was purified by HPLC-UV/Vis and analyzed by LC-ESI-MS and MS-MS (Figure 3.3).

Analytical Methods

Separations were carried out on an Agilent series HPLC, with UV/vis diode array detector and 500TR series Packard flow scintillation analyzer. An analytical reverse phase Supelco column (Discovery series 250 mm X 4.6 mm) was used with 50 mM KH_2PO_4 at pH 6 followed by a gradient of methanol. The concentration of enzyme for rapid-quenching experiments was determined by the 454 nm absorbance of bound FAD (e = 11,300 $cm^{-1}M^{-1}$). Liquid chromatography-mass spectrometry (LC-MS) analysis was performed on UltiMate 3000 Dionex LC system, using an eluent gradient of water and acetonitrile containing 0.1% formic acid, followed by a Finnigan LCQ deca mass spectrometer. High-resolution mass analysis was done on a Waters Q-TOF mass spectrometer.

Purification Methods

The trapped intermediate and 5-hydroxymethyl-dUMP were purified by HPLC using an analytical (Discovery series 250 mm X 4.6 mm) or a semipreparative (Discovery series 250 mm X 10 mm) reverse phase Supelco column, respectively. Mobile phase used for separation was a gradient of 50 mM KH_2PO_4 at pH 6 (for purification of the intermediate) or 100 mM KH_2PO_4 at pH 2 (for purification of synthesized 5-hydroxymethyl-dUMP) and methanol. Elution of the species of interest was followed by UV absorbance (at 267 nm). Eluent containing the purified species was collected, lyophilized to dryness, and dissolved in H_2O for LC-MS, MS-MS, high-resolution-MS analyses.

Acid quenching of FDTS during the oxidative half-reaction

A solution of oxidized FDTS (100 μM) was made anaerobic in a sealed tonometer by cycles of applied vacuum and equilibration with purified argon. The anaerobic enzyme was reduced stoichiometrically with a dithionite solution as followed spectrophotometrically (at 454 nm). The reduced FDTS was then mixed with dUMP (92 mM) from a side-arm of the tonometer and loaded on a KinTek Chemical Quench-Flow instrument (model RQF-3), which had been previously scrubbed of oxygen with a glucose/glucose oxidase solution (50 units/mL). An anaerobic 400 mM CH_2H_4folate solution was prepared containing 50 units/mL glucose oxidase, 10 mM glucose (to assure anaerobic conditions) and 30 mM formaldehyde (to stabilize CH_2H_4folate). FDTS reactions were initiated by rapid mixing of the enzyme/dUMP and CH_2H_4folate solutions in the instrument and quenched at various time points with 1 M HCl. The quenched reactions were analyzed by HPLC with UV-vis diode array, radioactivity flow detection and by LC-MS.

Searching for an enzyme-bound intermediate(s)

The acid-quenched oxidative half-reactions of FDTS with [2-^{14}C]-dUMP were spun in a microcentrifuge, and the radioactivity in supernatant was quantified by liquid-scintillation counting (LSC). The FDTS protein pellets (denatured enzyme) were analyzed on 10% SDS-PAGE. To test for protein-bound radioactive nucleotide, coomassie-stained FDTS bands were excised, solubilized with 30% hydrogen peroxide, and counted by LSC. In a separate analysis, the enzyme pellets were re-suspended in water and filtered to remove the residual soluble radioactivity. Both the filtrate and the washed pellets were then analyzed by LSC.

Searching for intermediates by thiol trapping during the FDTS reaction

Steady-state reactions containing 1 mM FDTS, 100 mM dUMP, 500 mM NADPH, 500 mM CH_2H_4folate and a trace of [2-^{14}C]-dUMP were incubated at 37°C. β-mercaptoethanol (3 M) was added at 1 minute and aliquots were withdrawn at 1.5, 3 and 5 min for analysis. Single turnover FDTS (20 mM) reactions with 10 mM dithionite (excess to ensure a high quantity of reactive thiol), 500 mM CH_2H_4folate and limiting [2-^{14}C]-dUMP (10 mM) where manually quenched with 1 M HCL at 1-2 seconds. The aliquots from both experiments were dried by speed-vacuum and re-suspended in water or neutralized (for HCl samples) and analyzed by HPLC with a radioactivity flow detector.

Data fitting for FDTS reaction kinetics

Mathematica was used to fit the data to a mechanism with one reaction intermediate:

$$\text{dUMP} \xrightarrow{k_1} \text{Intermediate} \xrightarrow{k_2} \text{dTMP}$$

CHAPTER IV

THE FOLATE BINDING SITE OF FLAVIN-DEPENDENT THYMIDYLATE SYNTHASE

This chapter was in full or part published in the Proceedings of the National Academy of Sciences, Koehn E. M., *et. al*., 2012, *Proc. Natl. Acad. Sci. 109:15722-15727*.

Abstract

The DNA nucleotide thymidylate is synthesized by the enzyme thymidylate synthase, which catalyzes the reductive methylation of deoxyuridylate (dUMP) using the cofactor methylene-tetrahydrofolate (CH_2H_4folate). Most organisms, including humans, rely on the *thy*A- or *TYMS*-encoded classical thymidylate synthase (TSase), whereas, certain microorganisms, including all *Rickettsia* and other pathogens, use an alternative *thy*X-encoded flavin-dependent thymidylate synthase (FDTS). Although several crystal structures of FDTSs have been reported, the absence of a structure with folate(s) limits understanding of the molecular mechanism and the scope of drug design for these enzymes. Here we present the first X-ray crystal structures of FDTS with several folate derivatives, which together with mutagenesis, kinetic analysis, and computer modeling shed light on the cofactor binding and function. The new structural data will likely facilitate further elucidation of FDTS's mechanism and the design of structure-based inhibitors as potential leads to new antimicrobial drugs.

Introduction

Unlike other deoxynucleotides, thymidylate (2'-deoxythymine-5'-monophosphate; dTMP) cannot be directly synthesized by a ribonucleotide reductase, and its *de novo* biosynthesis requires the enzyme thymidylate synthase (1, 2, 4). Thymidylate synthases use N^5,N^{10}-methylene-5,6,7,8-tetrahydrofolate (CH_2H_4folate) to

reductively methylate 2'-deoxyuridine-5'-monophosphate (dUMP) producing dTMP. Two general classes of thymidylate synthases are known (22). The enzymes encoded by the *thy*A gene (*TYMS* in humans and other mammals) are well studied and are known as classical thymidylate synthases (TSase) (1, 2). Certain bacteriological and archeological organisms have been found to lack any gene coding for such TSase, as well as dihydrofolate reductase and thymidine kinase (9), yet can survive in thymidine-deprived environments. This observation led to the identification of alternative flavin-dependent thymidylate synthases (FDTSs), which are encoded by the *thy*X gene and have no sequence or structure homology to classical TSase enzymes (3, 4, 11). Furthermore, multiple studies have identified key differences in the molecular mechanism of catalysis between FDTSs and classical TSases (4, 6, 10, 12, 18, 22-24, 27, 29, 30, 33, 38, 55-57). These differences, along with the fact that the *thy*X gene is present in many human pathogens (e.g. bacteria causing Anthrax, Tuberculosis, Typhus, etc.), renders these flavo-enzymes as potential targets for rational inhibitor design, possibly affording compounds that might be effective antimicrobial drugs (6, 25, 58, 59).

The catalytic mechanism of classical TSase is well established and has facilitated in the identification of several inhibitors, some of which are in clinical use as anticancer drugs (e.g., 5-flouro-uracil, tomudex (Raltitrexed)) (2, 46, 60). This is owed greatly to the large amount of chemical, kinetic, and structural information. Numerous X-ray crystal structures have been solved for classical TSase, including ternary complexes with various combinations of substrate and folate cofactor, along with their analogs (1, 2). Studies of the FDTS reaction mechanism on the other hand, are still in their infancy, and critical structures of FDTS with any folate moiety have not been reported. Additionally, FDTS requires a nicotinamide cofactor to reduce the bound flavin, but a reactive binding site for nicotinamide(s) has not been identified or proposed.

FDTS enzymes use a flavin adenine dinucleotide (FAD) prosthetic group to catalyze the redox chemistry, which can be divided into reductive and oxidative-half

reactions. The FAD can be reduced to $FADH_2$ by nicotinamides, ferrodoxin, and other small molecule reductants (e.g. dithionite). Although the reductive half-reaction is activated by dUMP the conversion of dUMP to dTMP occurs during the oxidative half-reaction ($FADH_2 \rightarrow FAD$) (29, 30, 33, 39, 55). In contrast to classical TSase where the cofactor CH_2H_4folate provides both the H^- and methylene, in the FDTS reaction the H^- is provided by the $FADH_2$ and CH_2H_4folate is used only as a source for the methylene moiety (18, 52, 57).

Several different mechanisms for methylene-transfer have been proposed, suggesting either a direct methylene transfer (Fig. 4.1a) from CH_2H_4folate to dUMP (18, 22-25, 29, 30, 38, 55), or transfer of the methylene *via* an arginine residue (Arg174 in *Thermatoga maritima* FDTS; *Tm*FDTS) before its delivery to dUMP (Fig. 4.1b) (27). These studies may have been complicated by the competing oxidase activity ($FADH_2$ reaction with O_2 to form H_2O_2) (29, 33, 39), and by other kinetic complexities such as possible positive cooperativity (23). Published structures of FDTSs (11, 23, 31, 32, 56) have not been reported with folate(s) making further differentiation between these methylene transfer mechanisms difficult. Structural information regarding folate binding would not only provide a better understanding of the methylene transfer step, but will also present a new FDTS binding mode that might serve as a potential target for inhibitor design.

In this chapter we present X-ray crystal structures of *Tm*FDTS in complex with FAD, dUMP, and either CH_2H_4folate, folinic acid, or Tomudex (Raltitrexed; an antifolate). The observed location for folate binding does not allow direct methylene transfer from CH_2H_4folate to dUMP and could be an ideal binding site for NADPH during the reductive-half reaction. The previously proposed mechanism where the methylene is transferred through an arginine residue was tested and eliminated by site directed mutagenesis and kinetic analysis, warranting further examination of direct methylene transfer mechanisms. In the past we hypothesized that the isoalloxazine ring of

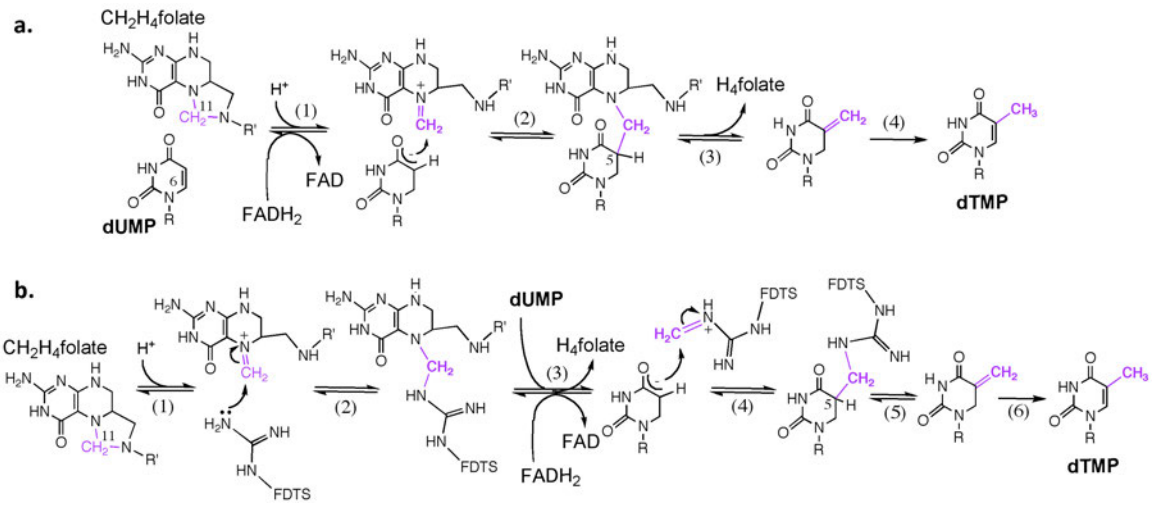

Figure 4.1: Mechanisms for FDTS catalyzed methylene transfer. a. A recently proposed mechanism for FDTS enzymes involving direct transfer of the methylene between CH_2H_4folate and dUMP (22, 55). b. A mechanism proposed for methylene transfer that involves an enzymatic arginine residue (27). Please note that the methylene transfer is the focus of this figure, and the methylene could in principle be transfered to the reduced dUMP (as drawn), to the oxidized dUMP as proposed in ref (55), or to dUMP activated by Michael Addition of Ser to C6 as originally suggested by ref (27). The transferred methylene moiety is labeled in purple. R = 2′-deoxyribose-5′-phosphate; R′ = (p-aminobenzoyl)-glutamate.

the FAD may rotate away from dUMP allowing room for CH_2H_4folate to bind in the active site (18), but it was not clear how this may happen. In the current work, we identified an additional FAD conformation when solving the structures of the E144R and R174K mutants of *Tm*FDTS, indicating that the flavin can occupy more than one conformational state during catalysis. Using the active site configuration of the quaternary complex, and FAD conformation observed in the E144R and R174K mutants, we modeled alternative binding options, and identified a potential configuration where the CH_2H_4folate is bound adjacent to dUMP suitable for direct methylene transfer.

Results

Folate binding pocket

In the FDTS-catalyzed reaction CH_2H_4folate provides the methylene moiety for the conversion of dUMP to dTMP (Fig. 4.1). Although several studies have published structures of FDTS from various organisms in complex with dUMP and dUMP analogs along with FAD (10, 11, 23, 31, 56), and even a nonreactive complex with $NADP^+$ (32), a structure with CH_2H_4folate or any other folate(s) has been an unrealized goal. Here we report the structures of the *Tm*FDTS with the cofactor CH_2H_4folate and other folate derivatives in complex with FAD and dUMP (Fig. 4.2). We solved crystal structures of *Tm*FDTS-FAD-dUMP complex with CH_2H_4folate at 1.39 Å resolution, an intermediate analog (leucovorin or folinic acid) at 1.50 Å resolution, and an antifolate (the anticancer drug Raltitrexed or tomudex) at 1.70 Å resolution (Fig. 4.3; See Methods in the Supporting Information, SI, for experimental details).

In these structures, the pterin moiety is stacked between the isoalloxazine of FAD and the imidizole of His53, and on the opposite side of the flavin relative to the substrate dUMP. It is important to note that without the folate bound, His53 shows weaker electron density and crystallizes in various conformations (10, 11, 31). We mutated this residue to alanine and solved the crystal structure of this mutant with FAD, dUMP, and folate at

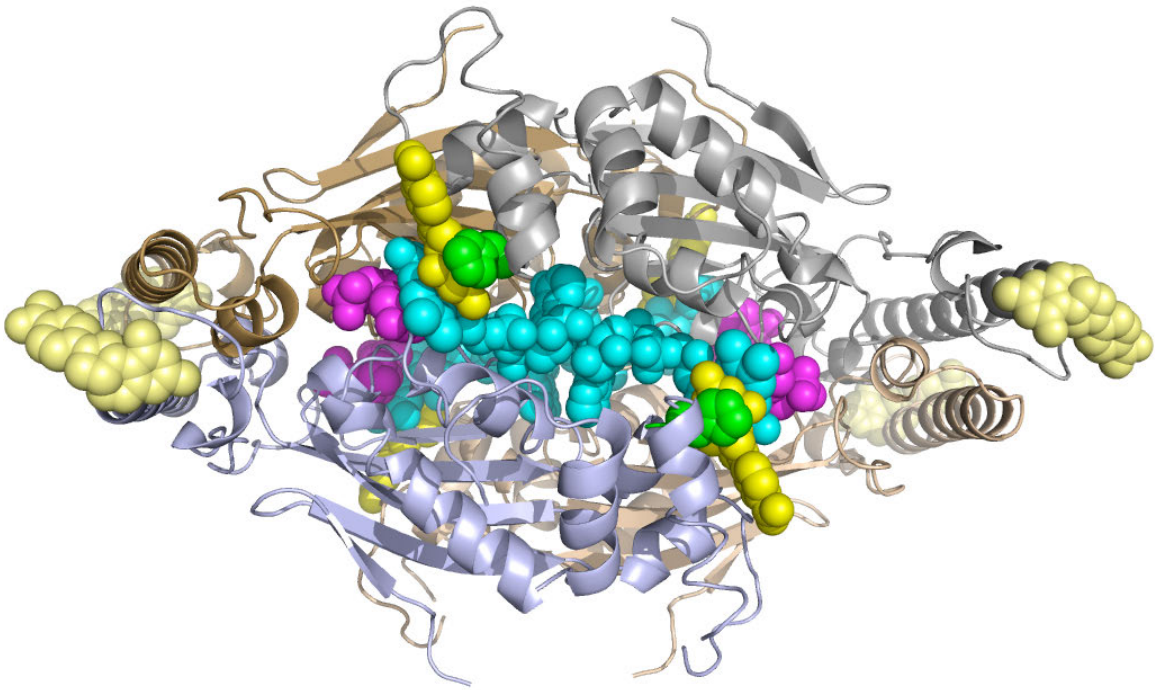

Figure 4.2. A view of the *Tm*FDTS in complex with FAD, dUMP, and CH_2H_4folate. The CH_2H_4folate is in yellow, dUMP in magenta, FAD in cyan, and His53 in green spheres to emphasize the packing of these residues in the active site. Four other CH_2H_4folates per subunit (in lighter yellow illustrating low electron density) are found remote from the active site. These may play allosteric role as discussed in the text.

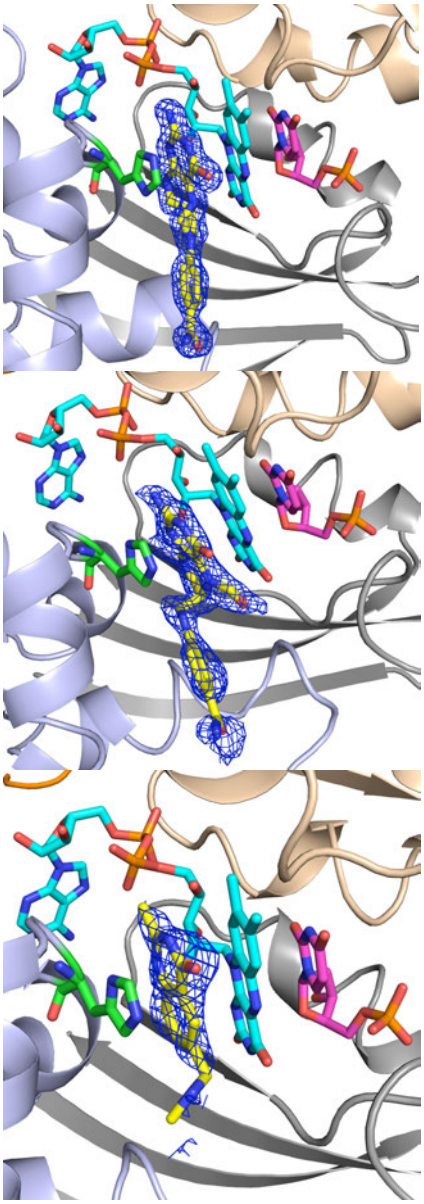

Figure 4.3. An active site view of crystal structures of *Tm*FDTS in complex with FAD, dUMP, and folate derivatives. A view of the omit maps contoured at 3 sigma for CH_2H_4folate a., folinic acid b., and raltitrexed c.. Ribbon drawings for the three protein chains constructing the active site (light gray, light blue, and wheat) and stick representation for FAD (cyan), dUMP (magenta), folate (yellow), and His53 (green).

1.77Å (see Table 4.1 in the SI). The H53A mutant structure showed similar folate binding for the pterin ring (see Figure 4.6 in the SI), but the activity of both H53A and H53D mutants was dramatically reduced (see Table 4.2 in the SI).

The residues near the folate binding site are highly conserved amino acids highlighting the importance of this newly found binding pocket (i.e., Ala27, Arg28, Ser30, Phe31, Leu44, Leu48, His53, Thr55, Pro56, Asn85, and Tyr91, where Ser30 could be Thr). The CH_2H_4folate makes eight H-bonding interactions involving seven water-mediated H-bonds and one direct H-bond to the protein (OG1 of Thr55). The structure with folinic acid (Fig. 4.3b) shows a similar hydrogen bonding pattern with additional hydrogen bonds involving the formyl group. It is important to note that folinic acid is good mimic of the reactive form of CH_2H_4folate in any proposed mechanism (e.g., the N5-iminium, which follows the 1st step in Fig. 4.1 mechanisms). Raltitrexed (tomudex) also binds FDTS in the same binding pocket with similar interactions (Fig. 4.3c). Structural comparison to our previously solved structures of *Tm*FDTS-FAD-dUMP complex (e.g., PDB code 1O26) showed that the positions of FAD and dUMP are not affected by the binding of the different folate compounds.

In addition to the folate bound in the active site, the electron density map also showed evidence for an additional CH_2H_4folate molecule bound in the 108 to 111 loop region (light yellow in Fig. 4.2). While the electron density at this region was weak, the pterin ring of this folate appears to make hydrogen bonding interaction with the main chain atoms of Leu106, Tyr109, and Thr111 and a water molecule (Fig. S2). The 108 – 111 loop is at the N-terminus of the long 25 residue helix of the protein and this loop region also showed weak density in the previously reported dUMP structure of *Tm*FDTS (10). A comparison with the other folate structures in the $I4_122$ space group reported in this paper, suggests that the ordering of the 108 – 111 loop is due to packing effects. The remote folate binding site found here might represent crystallographic trapping (of no functional implications). Alternatively, it could indicate an allosteric binding site with

impact on the reaction kinetics, which may explain some of the kinetic complexity (29, 33, 52, 59) and cooperativity reported for this enzyme (23).

Examination of the protein methylation mechanism (Fig. 4.1b)

The observed folate binding at the active site (Fig. 4.3) places the reactive methylene approximately 8 Å from the C5 of dUMP and does not support a direct methylene transfer mechanism between CH_2H_4folate and dUMP (Fig. 4.1a). This could imply a methylene transfer involving an arginine of the protein as previously suggested (Fig. 4.1b) (27). In this mechanism the iminium form of CH_2H_4folate condenses with the guanidine group of an enzymatic arginine (step 2, Fig. 4.1b), elimination of H_4folate results in an enzymatic Shiff-base (step 3, Fig. 4.1b), which following conformational changes in the protein can, in principle, be attacked by the activated dUMP (step 4, Fig. 4.1b) regenerating the catalytic arginine and completing methylene transfer. In *T. maritima* the residue proposed by ref (27) is Arg174, which is proximal to dUMP in the crystal structures and shares hydrogen bonds with the C4 and C2 carbonyls of dUMP. We tested the activity of both R174K and R174A mutant of FDTS (see Table 4.2 in the SI). Notably, although the activity of R174A mutant was much slower than wild-type FDTS, dTMP was produced (as confirmed by formation of ^{14}C-dTMP) demonstrating this mutant's capability of catalyzing methylene transfer without Arg174. The reduced activity of R174A makes sense in light of the important role of this residue in binding and orientation of dUMP (10, 31). The only other amino acid, beside arginine, that could function as the methylene carrier is lysine, but R174K was not active. The lack of activity of R174K might be attributed to the hydrogen bonds between this Lys174 and His79 leading to active site deformation (Fig. 4.4b). These and other findings (18, 23, 24, 29, 30, 33, 55, 56) seem to eliminate a mechanism where the methylene is transferred

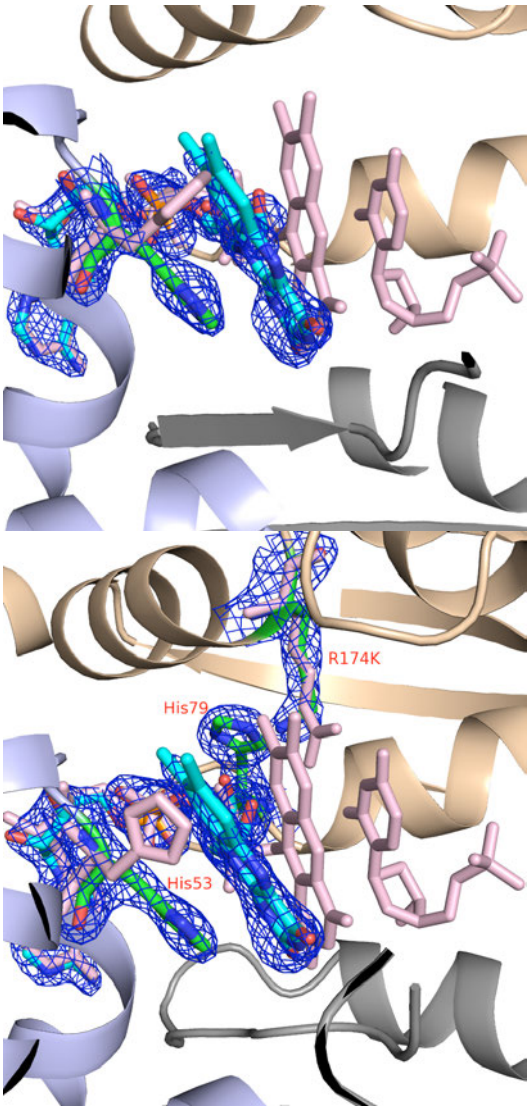

Figure 4.4. An alternative conformation where the flavin is in the opposite side of the active site, and away from the substrate dUMP binding-site. a. The flavin binding mode observed in one of the active sites of E144R mutant, with the 2Fo-Fc electron density contoured at 1.5 sigma. b. The flavin binding mode observed in two of the actives sites of R174K mutant, with the 2Fo-Fc electron density contoured at 1.5 sigma shown for FAD, H53, K174, and H79. Superposition with the wild-type enzyme in complex with dUMP (PDB code: 1O26) is shown in pink.

through a protein residue, and further examination of direct methylene transfer mechanisms was necessary.

Identification of an alternative flavin conformation

For the CH_2H_4folate to bind closer to the dUMP, the isoalloxazine ring would have to move to the other side of the active site as we hypothesized in an earlier mechanistic study (18). While we were determining the structures of various mutants of *Tm*FDTS, two of the mutants (E144R and R174K) in complex with FAD fortuitously showed an additional conformation where the isoalloxazine moiety is stacked with the imidizole of His53, which is rotated relative to its common orientation (Fig. 4.4). Only one of the active sites of the E144R and two of the active sites of the R174K tetramer showed this alternative flavin conformation. Additionally these mutants had greatly reduced, or no FDTS activity (see Table 4.2 in the SI), perhaps due to a loss of the stable wild-type FAD conformation. Nevertheless, the flavin occupying this new conformation showed better electron density than the other isoalloxazine moieties of FAD in the tetramer. As it has been pointed out earlier, the isoalloxazine of FAD is either disordered or shows very weak electron density in structures without dUMP (10, 11, 23, 31, 56). Interestingly, the newly observed binding site of the isoalloxazine moiety is almost identical to the binding site of the pterin moiety of the folate derivatives presented in Fig. 4.3. This finding is consistent with the chemical and structural similarities between these two moieties. From these observations we suggest that conformational switching of the flavin and the folate could be catalytically significant. The stacking of the flavin with the rotated imidizole of His53, as depicted in E144R and R174K mutants, may stabilize the alternative conformation of the isoalloxazine ring, which enables CH_2H_4folate access to the dUMP.

Attempts to get a structure of the folate bound between the flavin, in its newly identified “flipped” conformation, and dUMP were not successful even when attempting

to soak folates into the E144R-FAD crystals. The electron density maps for the resulting structure (see Fig. 4.8 in the SI) showed very weak electron density that could be part of folate bound between the flavin and dUMP, as expected for direct methylene transfer to dUMP. While this observed electron density was too low to be considered significant or conclusive, it did indicate that the appropriate space is available for folates to bind close to dUMP enabling direct methylene transfer.

Modeling of an alternative folate binding mode

To test whether the "flipped" isoalloxazine ring of FAD observed in Fig. 4.4 could facilitate binding of the CH_2H_4folate cofactor proximal to the substrate dUMP, we modeled the iminium form of CH_2H_4folate (the reactive intermediate ready for methylene transfer as illustrated in Fig. 4.1) into the solved FDTS-FAD-dUMP-CH_2H_4folate structure. Then, by rotation of His53, as well as the C2'-C3' and C1'-N10 bonds of FAD, the isoalloxazine ring was moved into a new binding site with the same conformation and functional group interactions as observed in the E144R and R174K structures discussed above. The iminium CH_2H_4folate was modeled into the site previously occupied by the flavin (as described in detail in the SI Methods section). After minimization, the iminium CH_2H_4folate intermediate fits well between FAD and dUMP. Fig. 4.5 presents the preferred binding orientation, and additional conformations with a short encounter distance between the iminium methylene and the C5 of dUMP were found and are presented in Fig. 4.9 in the SI. Notably, the position of dUMP was not significantly modified in any of the minimized structures. The small energy differences between these binding modes suggest a broad and flat binding potential that would enable several orientations where the methylene could be transferred directly to the dUMP. The details of the modeling procedures and methods are described in detail in the SI Methods section.

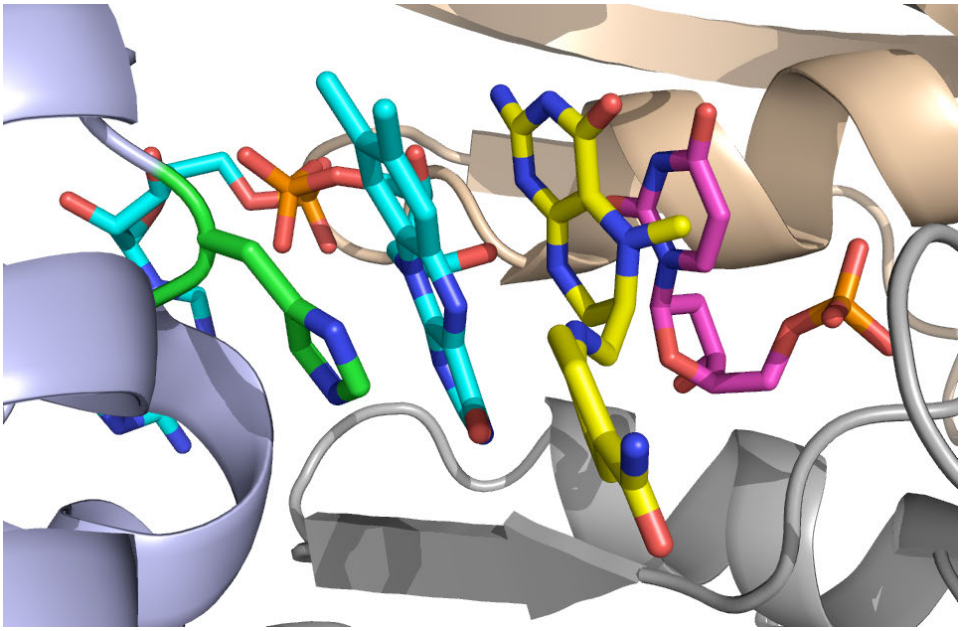

Figure 4.5. Modeled reactive structure for the FDTS-dUMP-FAD-CH_2H_4folate intermediate complex. FAD's isoalloxazine ring and His53 are rotated as in Figure 4.4 and Figure 4.8. The iminium-CH_2H_4folate intermediate is docked into the site as described in the text. Chain A is colored in grey, chain C in purple, and chain D in wheat color.

The outcome of these modeling efforts suggests that such ligand binding conformation is feasible. For all of the ligand binding conformations modeled (Fig. 4.5 and Fig. 4.9 in the SI) the activated methylene of CH_2H_4folate is at a reasonable distance (3.3-3.5 Å) and orientation (N5-CH_2-C5 of 100˚ ±20˚) to enable a direct methylene transfer to the dUMP substrate. The main structural modifications involved are the rotation of the FAD's isoalloxazine ring and His53 (chain C), as well as small rearrangements of residues Asn85 (chain A) and Tyr91 (chain A). The rotated isoalloxazine ring interacts with Asn85 (chain A), Arg78 (chain D), and Thr55 (chain C). These structures are substantially stabilized by the stacking of the FAD's isoalloxazine ring with the imidizole ring of His53, which is rotated as in the crystal structures of the E144R and R174K mutants.

Folate inhibition of TmFDTS-FAD reduction by NADPH.

The folate binding site observed here (the *re*-face of the isoalloxazine of FAD, opposite to the dUMP), could be an ideal site for NADPH binding during the reductive-half reaction. Such binding would accord with other structures of nicotinamide cofactors bound to flavo-enzymes (61). To test this hypothesis we examined the effect of folate moieties on the single reductive-half reaction of FAD with NADPH. Steady state competitive CH_2H_4folate inhibition has been reported for the oxidase activity of FDTS (10, 14), and substrate inhibition of the folate cofactor has been shown for steady state NADPH oxidation and dTMP formation (18, 29, 33). While the observed steady-state competitive inhibition by CH_2H_4folate is consistent with the notion that CH_2H_4folate can occupy the nicotinamide binding-site, it could have several possible interpretations due the cofactor's role in the oxidative half reaction, the reported positive cooperativity (23), and the possible allosteric binding site (light yellow in Fig. 4.2 and Fig. 4.7 in the SI). Consequently, more direct evidence was needed to suggest that folate moieties could inhibit the reductive-half reaction of FAD with nicotinamide cofactors. Such examination

was carried out in the presence of dUMP, since it is a substantial activator of the reductive-half reaction of FAD (29, 30, 33, 39). As a result, we could not use the CH_2H_4folate cofactor, which would react with the dUMP, and used folinic acid to inhibit the reduction of the FDTS-FAD-dUMP by NADPH. These measurements indicated that the rate of flavin reduction decreased over 100-fold in the presence of folinic acid (see Fig. 4.10 in the SI), supporting the hypothesis that folates in Fig. 4.3 are occupying the site where NADPH binds during the reductive half reaction. To further examine this possibility, we modeled NADPH into the space occupied by folate derivatives in the crystal structures presented in Fig. 4.3. Several minimized NADPH orientations (e.g., Fig. 4.11 in the SI) indicated that this pocket can bind NADPH with no steric clashes in more than one way, which is in accordance with the low stereospecificity, binding promiscuity, and high K_M for nicotinamide cofactors (18). Our attempts to grow crystals with $NADP^+$, NADPH, and few other nicotinamide derivatives were not successful, and soaking crystals with $NADP^+$ has been reported to result in the replacement of FAD by $NADP^+$ (32).

Discussion

The structural characterization of folate binding for the classical TSase has enabled understanding of the reaction mechanism and has been extensively exploited for the design of highly specific inhibitors and drugs (1, 2, 45, 46, 60). Similarly, the identification of the folate binding site for FDTS is crucial to understand the reaction mechanism and to develop folate-based inhibitors.

Here we report the first crystal structures of FDTS with CH_2H_4folate and other folate derivatives, together with the commonly observed ligands FAD and dUMP (Fig. 4.2 and Fig. 4.3). These structures show an extended stacking configuration between the pyrimidine, isoalloxazine, pterin and imidazole rings of dUMP, FAD, CH_2H_4folate, and His53, respectively. His53 is highly conserved in FDTSs and has also been suggested to

stabilize the binding of substrates like folate (31). While the mutant H53A enzyme resulted in the same folate binding configuration (Fig. 4.6) and still produced dTMP, its overall catalytic activity was greatly reduced (see Table 4.2 in the SI). Similar stacking of folate pterin ring between the isoalloxazine of FAD and the imidazole of an enzymatic histidine was also observed in the folate/FAD-dependent tRNA T54 methyltransferase (TrmFO) (62). It is notable that TrmFO and FDTS catalyze the same net reductive methylation reaction of an uridyl moiety and therefore this unique stacking could be a general feature of such flavoenzymes. The main difference between the folate binding in the TrmFO enzyme vs. FDTS is that the *si*-face instead of the *re*-face of the flavin is stacked with the folate in the current structure.

Crystal structures of classical TSase have been solved with both CH_2H_4folate, and tomudex (1, 2, 45, 63). A comparison of these structures with the FDTS-folate structures presented here, shows major differences in the folate binding site. The most striking difference is in the relative positions of the methylene donor (pterin ring) and the substrate (pyridmidine ring) (Fig. 4.12 in the SI). The stacking of the pterin ring of the CH_2H_4folate and the pyrimidine ring of dUMP is essential for direct methylene transfer as proposed in Fig. 4.1a. We tested the proposed protein mediated methylene transfer mechanism (Fig. 4.1b) (27) using site directed mutagenesis studies, which in accordance with previous studies (12), identified no strictly conserved arginine residue that is crucial for methylene transfer. Even Arg174 proposed specifically as methylene acceptor (27) when mutated to alanine was still capable of producing dTMP. Additionally, no other strictly conserved residues seem to be capable of catalyzing such chemistry (12). Furthermore, in contrast to the protein methylation suggested in ref (27), we were unable to identify any methylene transfer to the protein using radiolabeled [^{14}C]-CH_2H_4folate and following intermediate formation during the FDTS reaction (55). These findings, along with multiple kinetic data (18, 23, 24, 29, 30, 33, 38, 39), encouraged the

examination of an alternative CH_2H_4folate binding mode that would enable direct methylene transfer to dUMP.

To explore a binding option for direct methylene transfer between the CH_2H_4folate and dUMP, we used the alternative "flipped" FAD conformation observed in our E144R and R174K structures (Fig. 4.4) and modeled new reactive structures with the CH_2H_4folate iminium intermediate now in direct contact with dUMP. The modeled structures (Fig. 4.5 and Fig. 4.9) place the reactive methylene within reasonable distance and angle from the C5 of dUMP for direct methylene transfer. The stacking interaction between dUMP, CH_2H_4folate, FAD, and the imidazole of His53 further emphasize the possible role of His53 in altering the correct configuration of ligands in the active site at different steps of the catalytic cascade. Similar stacking of the uracil of dUMP with the pterin of CH_2H_4folate is also observed for classical TSase (Fig. 4.12b in the SI), and might be a general structural requirement for direct transfer of the methylene.

Comparing the folate binding modes observed for the crystallographic and reactive-modeled structures of FDTS presented here with that of classical TSase indicate additional structural differences. The pterin of the folate in all FDTS structures (Figs. 4.2, 4.3, and 4.5) is situated in an anti-parallel position relative to dUMP, opposite to the classical TS binding configuration (Fig. 4.12 in the SI). Additionally, FDTS structures show folates bound in an extended conformation whereas classical TSase binds folates with the para-aminobenzoyl moiety perpendicular to the pterin ring system. These unique binding differences for folate derivatives might present an avenue for rationally designed selectivity of folate-based inhibitors (i.e., antifolates) between human TSases and pathogenic FDTSs. Needless to say that such selectivity might be key for new antibiotic drugs with low toxicity.

The folate binding site observed in the current crystal structures (Fig. 4.2 and 4.3) could be ideal for nicotinamide binding during the reductive half reaction, where NADPH reduces the dUMP-FAD-FDTS complex prior to CH_2H_4folate binding (30, 33,

55). The current measurements showing that folinic acid inhibits the reduction of the FDTS-FAD-dUMP complex by NADPH (Fig. 4.10) indicate that folate moieties can compete for the nicotinamide binding site. This suggestion is also consistent with the successful docking of NADPH into the newly identified folate binding site (Fig. 4.11), and with the CH_2H_4folate substrate-inhibition reported in the past (23, 24). The current structure also shows a secondary and weaker (as evident form lower electron density) binding site for CH_2H_4folate at the surface of the protein (light yellow in Fig. 4.2 and Fig. 4.7). This secondary binding site might be related to the positive cooperativity that has been reported for certain FDTSs (23), although more studies will be needed to completely understand how folate binding affects both oxidative and reductive-half reactions.

Conclusions

The potential impact of the findings presented here on our understanding of FDTS catalysis, its differences from classical TSase, and the resulting implications for antibiotic drug design are substantial. The crystal structures of *Tm*FDTS with CH_2H_4folate, folinic acid, and tomudex presented here are to our knowledge the first available structures with any folate(s) bound to FDTS. While these structures do not indicate how the methylene can be transferred to the substrate dUMP, a protein mediated transfer was excluded by site directed mutagenesis of relevant residues. Additionally, most of the previously reported kinetic and mutagenic studies are consistent with mechanisms of direct methylene transfer from CH_2H_4folate to dUMP (i.e., a mechanism such as in Fig. 4.1a). Consequently, an alternative binding configuration was explored via computer modeling based on the “flipped” flavin conformation found for the E144R and R174K mutants, which enabled binding of the folate in direct contact with the substrate dUMP (Fig. 4.5). The folate binding site identified in the crystal structures is likely to represent the NADPH binding site during the reductive half reaction, as supported by current and past kinetic data and modeling (Figs. 4.10 and 4.11 in the SI).

In summary, many folate-based inhibitors that target classical TSase enzymes are in clinical use, however, these compounds have low affinity for FDTS enzymes. The development of these compounds for classical TSases has been greatly facilitated by structural studies with folate and its analogs (antifolates). Similarly, it is expected that new compounds taking advantage of the unique folate binding modes presented here for FDTS may provide new avenues for specific inhibitor design.

Supporting information

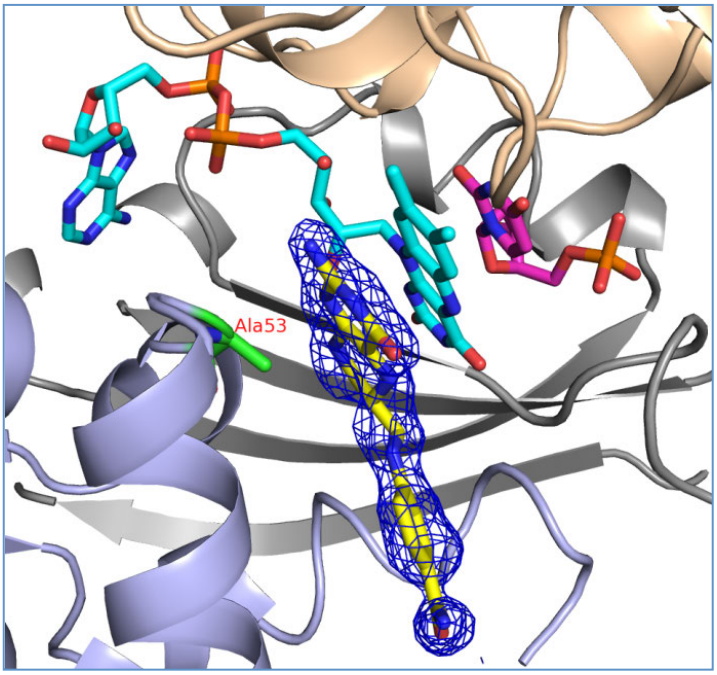

Figure 4.6. The crystal structure of H53A *Tm*FDTS in complex with FAD, dUMP, and folate. A view of the omit map contoured at 3 sigma for the folate. The mutated alanine residue is shown by stick representation in green and the other colors are as in Figure 4.3 from the text.

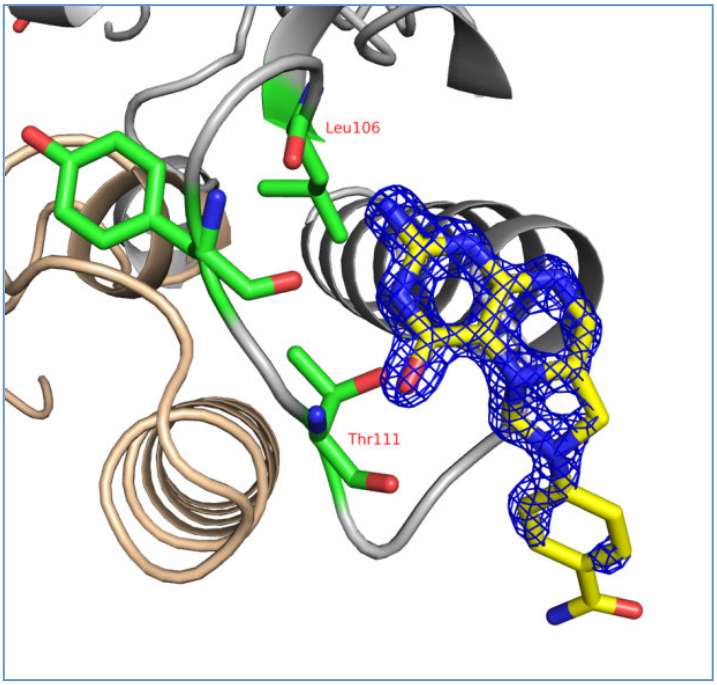

Figure 4.7. Remote folate binding site. A view of the 2Fo-Fc electron density for the 2nd folate contoured at 1.5 sigma. CH_2H_4folate is shown in yellow and the hydrogen bonding residues are shown as sticks.

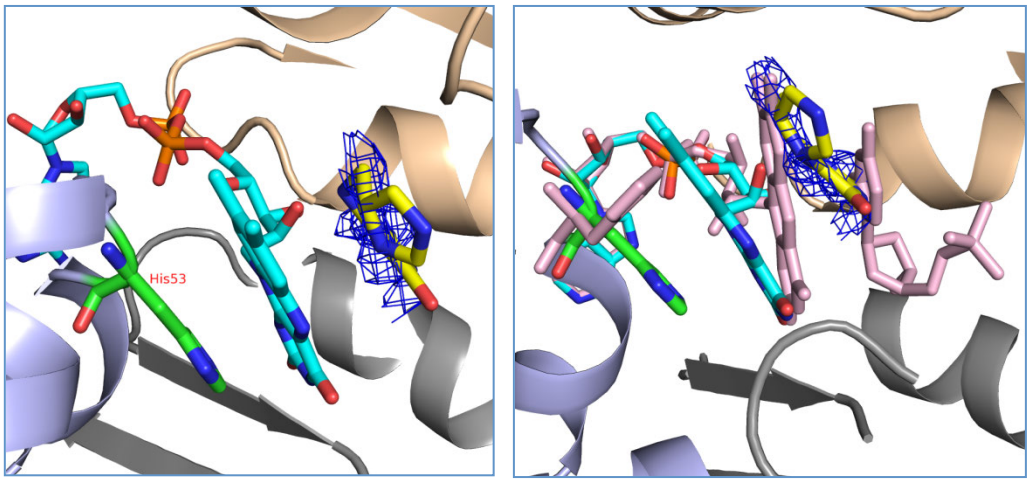

Figure 4.8. A view of the binding mode in the E144R+FAD+folate structure. **a.** The electron density omit map contoured at 2.5 sigma showing the approximate location of the folate. **b.** Comparison of the active sites of the E144R+FAD+folate and wt+FAD+dUMP (PDB code: 1O26, in pink) structures.

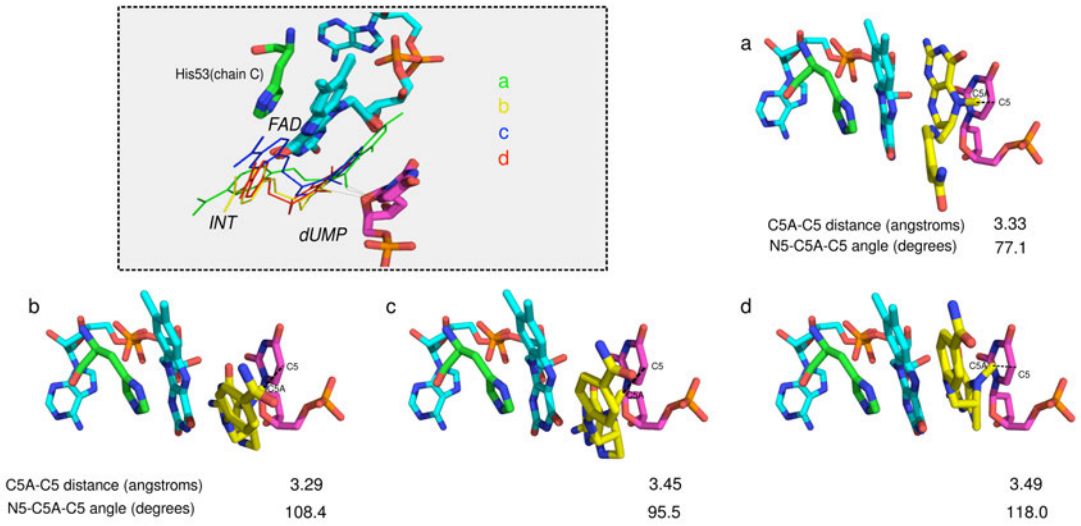

Figure 4.9. Alternative modeled structures for the FDTS-FAD-dUMP-iminium CH_2H_4folate complex where the methylene in close to C5 of dUMP (same color code as in Fig. 4.5). Orientations a, b, c and d are not identical to Figure 4.5, although the docking procedures are the same as described for Figure 4.5. Inset shows the superimposed intermediate docked orientations in different colors: a (green), b (yellow), c (blue) and d (red).

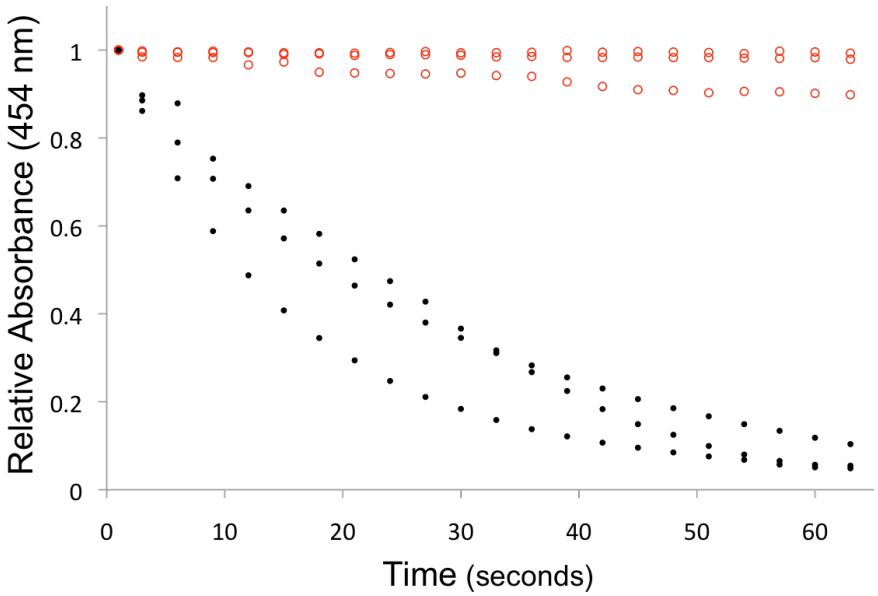

Figure 4.10. Folinic acid inhibition of FAD reduction by NADPH (single reductive half-reaction). The 454 nm absorbance of FAD decreases with reduction to $FADH_2$. A marked decrease in the rate of reduction is observed in the presence of folinic acid (red open circles) versus the control without folinc acid (black solid circles).

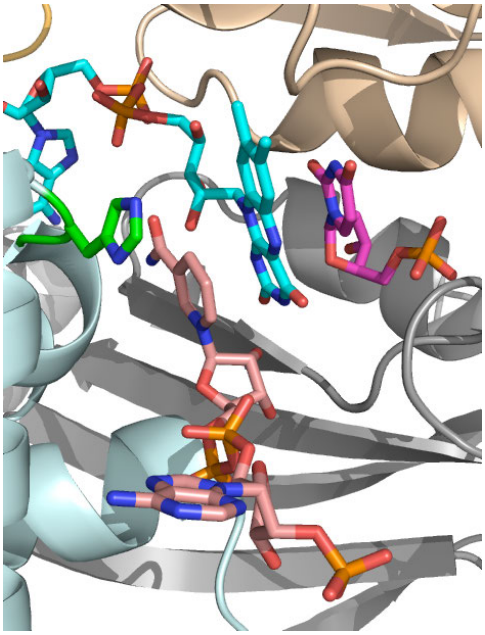

Figure 4.11. $NADP^+$ (in pink) docked into the binding site of folate derivatives found in the crystal structures presented in Figure 4.2 (main text). The binding cavity is wide and could easily accommodate NAD^+, NADPH, NADH, (both substrates of this enzyme) or other reducing agents.

a. b.

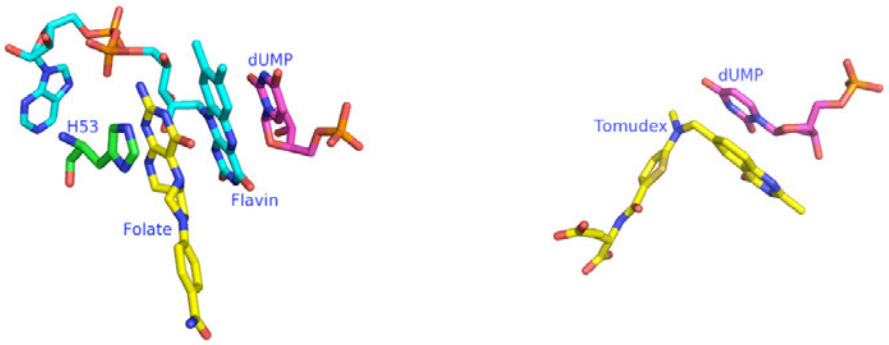

Figure 4.12. Comparison of folate binding modes in FDTS and TSase. a. A view of the stacking of the pterin with FAD and His53 in the *Tm*FDTS enzyme. b. Stacking of the pterin and dUMP in the classical *Ec*TSase. Compounds are shown with stick representation and labeled.

Materials and methods

Chemicals

All chemicals were reagent grade and used as purchased without further purification, unless specified. All reagents not specified below were obtained from Sigma. N^5,N^{10}-methylene-5,6,7,8-tetrahydrofolate (CH_2H_4folate) was provided by Eprova Inc. (Schaffhausen, Switzerland). Radiolabeled [2-^{14}C]dUMP was purchased from Moravek Biochemicals. Sodium dithionite powder was purchased from J.T. Baker, and tris(hydroxymethyl)aminomethane was obtained from Research Products International Corp.

Analytical methods

Separations were carried out on a Beckman series HPLC, with UV/vis diode array detector and 500TR series Packard flow scintillation analyzer (FSA). An analytical reverse phase Supelco column (Discovery series 250 mm X 4.6 mm) was used with 100 mM KH_2PO_4 at pH-6 followed by a gradient of methanol. The concentration of enzyme-bound FAD was determined by the 454 nm absorbance (ε = 11,300 $cm^{-1}M^{-1}$). Single protein spectra and kinetic measurements were performed on a Hewlett Packard Model 8453 diode array UV-Vis spectrophotometer.

Protein expression and purification

The FDTS from *T. maritima* (TM0449, GenBank accession number NP228259), and its H53A, H53D, E144R, E144A, R174K, and R174A mutants were expressed and purified as previously described(3).

Crystallization and structure determination

The crystals involving the folate or folate mimic complexes were crystallized at 22 ˚C in 3 – 6 % PEG 4K (w/v), 200 mM NaCl, 100 mM Na/K phosphate (pH 6.58). These crystals belonged to space group $I4_122$ and contained one monomer per

asymmetric unit. Due to the solubility issues, the Raltitrexed complexes were prepared by soaking the drug into FDTS-FAD-dUMP crystals. Crystals of the E144R mutant with FAD and with FAD and dUMP were crystallized at 22 ˚C in 50 – 60 % (w/v) PEG 200 and 100 mM tris buffer, pH 8.0. These crystals belonged to the $P2_12_12_1$ space group with a tetramer in the asymmetric unit. The E144R+FAD +Folate crystals were prepared by soaking folate into E144R+FAD crystals. The crystals from the PEG 4K condition were transferred stepwise into a cryoprotective solution containing 24 % PEG 4K (w/v), 200 mM NaCl, 100 mM Na/K phosphate, & 10 % glycerol, and flash cooled. The crystals grown from the PEG200 conditions were flash cooled directly from the drop. Diffraction data for all the crystals except E144R+FAD+Folate crystals were collected at the Stanford Synchrotron Radiation Lightsource (SSRL) beamline 9-2 using Mar 325 detector. The diffraction data for the E144R+FAD+Folate crystal were collected at SSRL beamline 12-2 using the Dectris Pilatus 6M detector. The wavelength used for the folate and folinic acid complexes of the native enzyme was 0.9809Å and the others were collected at 0.9795Å. All data were processed using the XDS package(64). Multiple data sets from other crystals were also collected and refined to reasonable R-factors to confirm the binding mode observed for the folate and folinic acid groups.

Structures of the folate derivative complexes were solved by molecular replacement (MOLREP(65)) using the atomic coordinates of the monomer from the *T. maritima* tetramer (PDB code: 1O26). The E144R mutant structures were phased by rigid body refinement implemented in the REFMAC (66) program. All the structures went through several rounds of model building using Coot (67) and refinement using the REFMAC program. The Ramachandran statistics for the refined coordinates showed no outliers. Details of the data collection and refinement statistics are shown in Table 4.1.

Activity determination of FDTS mutants

The activities of H53A, H53D, E144R, E144A, R174K, and R174A mutants of *Tm*FDTS were determined relative to the wild-type as a control using the established [2-^{14}C]dUMP assay (see Table 4.2) as previously described (ref Koehn, 2009, and Agrawal 2004). All experiments were performed anaerobically in 200 mM tris buffer (exchanged with Ar) pH = 8.0 at 65 °C. Reactions contained 100 µM dUMP (including 0.5 Mdpm [2-^{14}C]dUMP), 100 µM CH_2H_4folate, 5 mM CH_2O (to stabilize CH_2H_4folate) and 5 mM sodium dithionite or 500 µM NADPH. Reactions were initiated by addition of 25 nM to 20 µm (final active-site concentration) of enzyme, quenched with HCl (to a final pH = 1), and stored at -80 °C until analysis. HPLC-FSA analysis was used to determine the conversion of [2-^{14}C]dUMP to [2-^{14}C]dTMP.

Inhibition of enzyme-bound FAD reductive half-reaction

All experiments were performed in an anaerobic cuvette using 200 mM tris buffer (exchanged with Ar) pH = 8.0 at 37 °C. Reactions contained ~ 60 uM FDTS (active-site concentration), 100 µM dUMP, with or without 500 µM folinic acid. From the cuvette sidearm 500 µM NADPH was added to initiate the reaction. The 454 nm absorbance was followed as a function of time (See Fig. 4.10). Reduction rates were approximated by linear fitting corresponding to the first 10% fraction conversion.

Modeling system setup

The modeling was performed starting from the crystal structures of wild type *Tm*FDTS complexed with dUMP, FAD, and CH_2H_4folate or folinic acid. The crystal structures contain a total of 216 amino acid residues per subunit, 764 (CH_2H_4folate structure) and 756 (folinic acid structure) crystallographic water molecules, FAD, dUMP and CH_2H_4folate or folinic acid ligands. The structures have missing residues (residues 35, 36, and 37), these residues were not taken into account and fragments ends were constrained. Missing hydrogens were added to the PDB structure using the tleap module

of Amber9 package(68). All solvent molecules and ions were removed. The protonation state for all ionizable residues was set corresponding to pH 7. Thus, His residues were modeled as neutral residues with the proton on Nε or Nδ as determined on the basis of possible hydrogen bond interactions deduced from X-ray crystallographic structure. The amber99 force field (69) parameters were used for all residues.

CH_2H_4folate was replaced by the protonated imine form of CH_2H_4folate (reactive intermediate; INT). The INT ligand was built starting from the folinic acid structure where the 5-formyl was removed and replaced with a methylene having a double bond to the N5 atom. Minimization of INT was done at the HF/6-31G** level of theory using the gaussian09 package(70). Then, the restrained electrostatic potential (RESP) (71)charge approach was used to derived atomic charges. First, the high-density ESP calculation was performed at HF/6-31G** using Merz-Kollman scheme with the gaussian09 package. Then the charges were derived using Antechamber module of Amber9 package, which performed a two-stage fitting. Finally, Gaff force field (72) parameters together with RESP charges were used to generate the parameters file for INT. FAD and dUMP RESP charges and parameters were obtained from R.E.DD.B. (71).

Ligand docking and minimizations

FDTS is a homotetramer with four active sites each located in the interface of three subunits. The whole tetramer was considered in the minimizations. Minimizations were done using the Sander module of the Amber9 package. CH_2H_4folate or folinic acid was removed from all active sites. INT was manually docked into one active site. One short minimization for the entire system was done, and then was followed by a local minimization with restraints. Restraints were applied to all residues outside a radius of 15 Å from N1 atom of dUMP molecule, in order to keep them fixed at their original positions. Only residues within 15 Å radius from N1 atom of dUMP were allowed to move. The Generalized Born solvation approach was used (73-75).

Table 4.1. Data collection and refinement statistics.

	FAD+dUMP+Folate	FAD+dUMP+Folinic Acid	FAD+dUMP+ Raltitrexed
Data collection			
Space group	$I4_122$	$I4_122$	$I4_122$
Cell dimensions			
a,b,c (Å)	110.3, 110.3, 120.6	110.3,110.3,121.0	110.6,110.6,121.7
α,β,γ (°)	90.0,90.0,90.0	90.0,90.0,90.0	90.0,90.0,90.0
Resolution (Å)	25.6–1.39 (1.43-1.39)	40.0-1.50 (1.54-1.50)	40.0-1.70 (1.74-1.70)
R^a_{sym} or R_{merge}	4.3 (87.6)	4.7 (95.3)	5.0 (83.1)
I/σI	27.7(2.7)	24.3 (2.4)	21.0 (2.1)
Completeness (%)	99.6(99.9)	99.8 (100.0)	99.0 (99.9)
Redundancy	8.4(8.4)	8.4 (8.5)	6.6 (5.3)
Refinement			
Resolution (Å)	27.6-1.39	39.0 – 1.50	39.1 – 1.70
No. reflections	70453	56486	39174
R^b_{work}/R_{free}	15.2/16.4	16.4/17.9	17.1/18.3
No. atoms			
Protein	1845	1920	1830
Ligand/ion	121/1	98/1	88/1
Water/buffer atoms	209/4	189	126
B-factors			
Protein	22.3	30.0	36.2
Ligand/ion	23.1/25.3	22.9/29.2	30.5
Water/buffer atoms	34.4/46.5	39.5	42.6/32.0
R.m.s deviations			
Bond lengths (Å)	0.015	0.018	0.017
Bond angles (°)	1.756	1.796	1.740

Table 4.1. contd.

	E144R+FAD	E144R+FAD+dUMP	E144R+FAD+Folate
Data collection			
Space group	$P2_12_12_1$	$P2_12_12_1$	$P2_12_12_1$
Cell dimensions			
a,b,c (Å)	54.1,117.1,142.1	54.6,117.4,142.6	54.7,117.1,141.9
α,β,γ (°)	90.0,90.0,90.0	90.0,90.0,90.0	90.0,90.0,90.0
Resolution (Å)	30.0-1.97 (2.02-1.97)	30.0-1.76 (1.81-1.76)	40.0-1.89 (1.94-1.89)
R_{sym} or R_{merge}	6.0 (88.6)	6.1 (98.8)	8.2 (97.0)
I/σI	16.4 (1.6)	21.9 (2.0)	14.5 (1.7)
Completeness (%)	98.6 (99.6)	99.8 (99.9)	99.2 (99.4)
Redundancy	4.2 (4.3)	6.6 (6.4)	5.4 (3.7)
Refinement			
Resolution (Å)	29.3-1.97	29.4-1.76	38.5-1.89
No. reflections	60636	86827	69504
R_{work}/R_{free}	19.3/23.6	17.9 (21.5)	18.4 (21.0)
No. atoms			
Protein	7263	7174	7246
Ligand/ion	194	292	206
Water	265	373	167
B-factors			
Protein	41.7	40.3	39.7
Ligand/ion	48.2	38.6	49.1
Water	44.0	42.8	41.7
R.m.s deviations			
Bond lengths (Å)	0.016	0.017	0.018
Bond angles (°)	1.638	1.684	1.666

Table 4.1. contd.

	H53A+FAD+dUMP +Folate	R174K+FAD
Data collection		
Space group	$I4_122$	$P2_12_12_1$
Cell dimensions		
a,b,c (Å)	109.8,109.8,122.3	53.8,116.5,141.2
α,β,γ (°)	90.0,90.0,90.0	90.0,90.0,90.0
Resolution (Å)	40.0-1.77 (1.82-1.77)	40.0-2.17 (2.23-2.17)
R_{sym} or R_{merge}	6.0 (96.9)	6.5(85.9)
I/σI	23.3 (2.7)	18.1(1.9)
Completeness (%)	99.9 (100.0)	99.8(99.5)
Redundancy	9.1 (9.2)	5.0(4.6)
Refinement		
Resolution (Å)	38.8-1.77	38.1-2.17
No. reflections	34763	45284
R_{work}/R_{free}	16.3/18.3	18.9/24.0
No. atoms		
Protein	1864	7233
Ligand/ion	96/1	141
Water	124	81
B-factors		
Protein	34.3	34.2
Ligand/ion	27.9/38.3	59.4
Water	41.3	46.7
R.m.s deviations		
Bond lengths (Å)	0.016	0.015
Bond angles (°)	1.699	1.697

[a] $R_{sym} = \sum | Iavg - Ii| / \sum Ii$

[b] Rfactor = $\sum|Fp - Fpcalc| / \sum Fp$, where Fp and Fpcalc are observed and calculated structure factors; R_{free} is calculated with 5% of the data.

Table 4.2. Thymidylate synthase activity of FDTS mutants.

FDTS enzyme	[^{14}C]dTMP formation	Rate (min^{-1}) (10^{3})	% Relative activity
WT	YES	2135 ± 16	100.0 ± 0.8
E144A	YES	2.42 ± 0.04	0.113 ± 0.002
E144R	YES	0.34 ± 0.03	0.016 ± 0.002
R174A	YES	0.017 ± 0.003	0.0008 ± 0.0002
R174K	NO	ND	ND
H53A	YES	29.6 ± 0.4	1.39 ± 0.02
H53D	YES	ND	ND

[a.] Reactions contained 100 μM dUMP (including 0.5 Mdpm [2-^{14}C]dUMP), 100 μM CH_2H_4folate, and 5 mM sodium dithionite or 500 μM NADPH. FDTS activity was assessed by quantifying [2-^{14}C]dTMP formation. Average rates and their standard deviations were determined from three independent measurements.

[b.] ND: denotes that the average rates were not determined.

CHAPTER V

THE RELATIONSHIPS BETWEEN OXIDASE AND SYNTHASE ACTIVITIES OF FDTS

This chapter was in full or part published in Chemical Communications, Chernyshev A, Fleischmann T, Koehn E, Lesley SA, & Kohen A (2007) *Chem. Commun.*:2861-2863. Figures and/or content are used with permission from RSC

Abstract

New findings lead to a revised understanding of the substrates' binding order, the role of the substrate as an activator, and the observed lag phase in the FDTS catalyzed reaction.

Research report

Thymidylate synthases catalyze the reductive methylation of 2´-deoxyuridine-5´-monophosphate (dUMP) to 2´-deoxythymidine-5´-monophosphate (dTMP), one of the DNA building blocks. While the mechanism of the classical thymidylate synthase (TS) is well established (1, 2, 42), the mechanism of the newly discovered flavin dependent thymidylate synthase (FDTS) (3, 4, 11) is not well understood (25). Several experimental observations reported in recent years led to two intriguing suggestions regarding the mechanism of FDTS. The first study (24) examined the oxidation of reduced nicotinamide-adenine dinucleotide 2'-phosphate (NADPH) under aerobic conditions, by following the decrease in 340 nm absorption in the presence or absence of different reactants. This study concluded that the substrate dUMP serves as an activator in the reductive half reaction (involving reduction of oxidized flavin adenine dinucleotide: FAD→ $FADH_2$). This conclusion was of substantial interest as dUMP only reacts during the oxidative half reaction ($FADH_2$→ FAD). A second study (39) examined the oxidized flavin reduction (following 454 nm absorption) and the findings agreed with the

conclusions of ref (24). Additionally, ref (39) suggested that the reductive half reaction presents a lag phase whose duration depends on dUMP concentration. This was quite intriguing as such long lag phases are rare in most chemical and enzymatic reactions and could present a unique kinetic phenomenon. In the current communication, new findings indicate a revised binding order of ligands to the enzyme. Apparently, dUMP is not involved in the reductive half reaction but it does activate the oxidative half reaction even in the absence of the methylene donor (5,10-methylene-5,6,7,8-tetrahydrofolate, CH_2H_4folate). The new data also clarify the origin of the dUMP-dependent lag phase and reinforce the reported activation constant of dUMP (K_f). In contrast to previous interpretations (24, 39), dUMP actually serves as an oxidation activator, rather than a reduction activator.

Classical thymidylate synthase (TS, EC 2.1.1.45) catalyses the reductive methylation of dUMP and CH_2H_4folate, yielding dTMP and 7,8-dihydrofolate (H_2folate). This enzyme is a target of several cytostatic drugs (chemotherapeutics and antibiotics) (25). The alternative TS is a flavin dependent thymidylate synthase (FDTS, EC 2.1.1.148). The gene encoding for FDTS (ThyX) is present in several severe human pathogens and thus FDTS represents a new antibiotic target (4, 10, 24, 25, 27). FDTS is a homotetramer that contains one tightly bound FAD cofactor per subunit (3, 18, 23, 24, 26, 31, 39). In contrast to TS, the CH_2H_4folate in the FDTS reaction is not the reducing agent. During the reductive half reaction, oxidized FAD (yellow, due to an absorbance band at 454 nm) is reduced to colorless $FADH_2$ by nicotinamides, dithionite, or other reducing agents. It remains largely unclear how the methylene group is transferred from CH_2H_4folate to dUMP, but this enigma is beyond the scope of this communication. Instead, we focus on the relationship between the two half reactions and between the two competing reactants: the natural cofactor, CH_2H_4folate, which leads to production of dTMP, and oxygen (O_2), which leads to production of hydrogen peroxide (H_2O_2). The second reaction, denoted oxidase activity, while common to most flavin containing

enzymes (40), is likely to be a side reaction because several studies, including the current one, examined FDTS from the anaerobic hyperthermophile *Thermotoga maritima* (23, 24, 39).

Recently, we measured the single turnover reduction of FDTS from *T. maritima* by NADPH under oxygen depleted conditions (23) in the absence of CH_2H_4folate and with various concentrations of dUMP. The reduction of enzyme-bound FAD by NADPH was measured (454 nm absorbance) over time and a sigmoidal lag phase was observed (39). The duration of the lag-phase decreased with increasing concentration of dUMP leading to the determination of effective binding constant (K_f), at 37 and 80 ˚C (the optimal growth temperature of *T. maritima).* Since the observed lag-phase in FAD reduction may result from residual oxygen in the reaction mixture (21, 76, 77), we repeated the same experiments, in the presence of an *in situ* oxygen-consuming system (10 mM glucose, 60 units of glucose oxidase under purified Ar). Under these strictly anaerobic conditions, no lag phase was detected and FAD reduction was independent of dUMP concentration (Figure 5.1). Contrary to previous suggestions (24, 39), dUMP does not appear to be involved in the FAD reduction and there is no indication that it binds before NADPH. However, the rate of the oxidase activity ($O_2 \rightarrow H_2O_2$) was clearly dependent on the concentration of dUMP (Figure 5.2). We determined the functional constants for dUMP binding (K_f) by measuring the decrease in 340 nm absorbance as probe for NADPH oxidation under aerobic conditions using 0.1 mM NADPH, and various concentration of dUMP. The initial velocities were fitted to single activator kinetics with finite rates at low and high concentrations of dUMP (lines in Figure 5.2):

$$V = V_0 + V_\infty \cdot [dUMP] / (K_f + [dUMP]) \qquad [5.1]$$

where V_0 and V_{oo} are the reaction rates with no dUMP and at saturating dUMP, respectively. The values of K_f at 37 and 65 ˚C were 1.6 ±0.3 mM and 2.7 ±0.6 mM, respectively. These K_fs are within experimental errors from those obtained in ref (39)

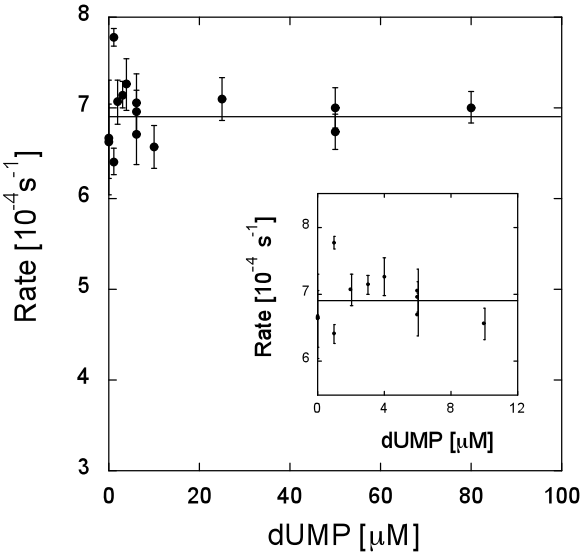

Figure 5.1. Single turnover FDTS-bound FAD's reduction rate vs. dUMP concentration under anaerobic conditions at 37 ºC. Insert, the 0-12 μM range, where the dUMP effect on steady state rates is pronounced (see Figure 5.2 and ref (39)).

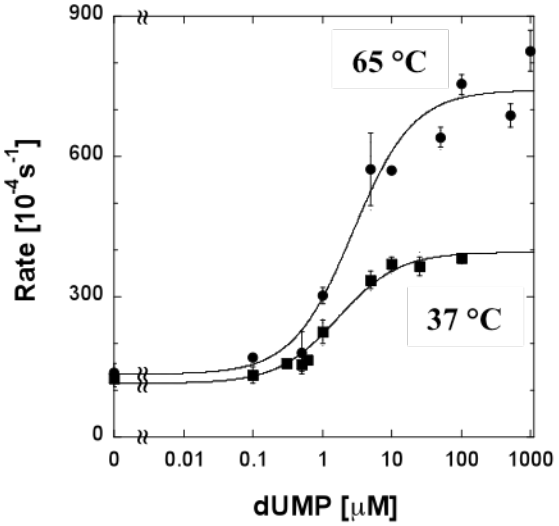

Figure 5.2. The dependence of FDTS's oxidase activity on dUMP concentration at 37 ºC (squares) and 65 ºC (circles).

using the duration of the apparent lag phase (1.4 ±0.1 mM and 2.1 ±0.1 mM at 37 ˚C and 80 ˚C, respectively). The similarities in the values of K_f determined from the duration of the lag phase and from the oxidase activity are consistent with a common origin. The fact that the lag phase was not observed under strictly anaerobic conditions indicates that this phenomenon primarily stems from the kinetics of the oxidase reaction, rather than from other factors, like conformational rearrangements of the enzyme (39) or reorientation of the substrates (23), as was previously proposed.

Additional experiments resulted in several other important findings: (i) The possibility that dUMP serves as a substrate in an oxygenase reaction was eliminated by conducting the FDTS catalyzed reaction with [2-^{14}C]dUMP, NADPH, and oxygen (no CH_2H_4folate). The products were analyzed using HPLC and no new radioactive peak developed during the reaction even after all the oxygen and NADPH were consumed; (ii) The formation of H_2O_2 was confirmed using the Amplex Red/horseradish peroxidase assay (78). Unfortunately, this assay could not be used quantitatively because NADPH is also oxidized by H_2O_2 under the assay conditions; (iii) The apparent K_M for O_2 was determined to be 9.0 ±0.5 mM by measuring initial velocities of NADPH oxidation in the absence of CH_2H_4folate, with varying concentrations of O_2, and saturating dUMP (100 mM); and (iv) Previous findings (24, 39) indicated that dUMP binding to FDTS in the absence of CH_2H_4folate increases the rate of NADPH oxidation by a factor of about ten.

All the observations discussed above can be understood within the model illustrated in Figure 5.3. At the top, the blue lines represent the dUMP dependent O_2 reduction to H_2O_2 by NADPH (detected by following 340 nm absorbance). At the bottom, the red lines represent the oxidation state of the enzyme bound flavin (detected by following 454 nm absorbance). Since the FAD reduction is rate limiting, the 454 nm absorbance does not decrease significantly in the presence of O_2. The FAD is reduced (at a dUMP independent rate) only after the O_2 concentration drops below its K_M, leading to apparent lag-phase (red lines). This finding suggests that the reductive half reaction does

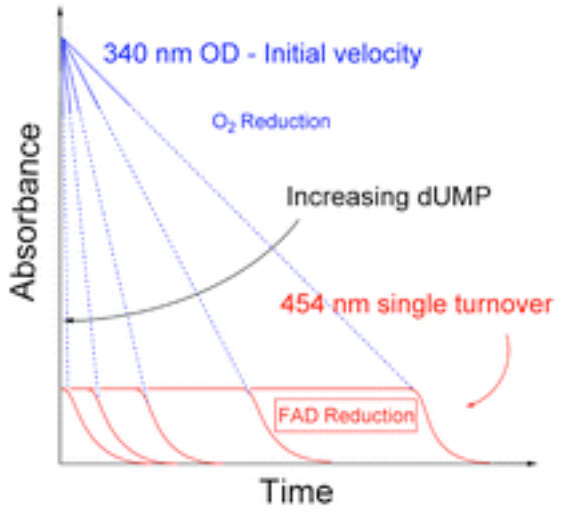

Figure 5.3. Illustration of the relationship between rate of NADPH oxidation (340 nm absorbance, in blue) and the lag phase observed in ref (39) (454 nm absorbance, in red). While consuming the oxygen the 340 nm absorbance decreases (blue lines), but the 454 nm absorbance is hardly affected indicating that the FAD is still oxidized, and in accordance with the reductive half reaction being rate limiting (39). Only after the oxygen is mostly consumed, is FAD reduced. The oxidative half reaction (red) is dUMP dependent, but the reductive half reaction (black) appears independent of dUMP concentration.

not require dUMP, and a new examination of the substrates binding order is presented below.

The fact that dUMP appeared to enhance NADPH consumption led Myllykallio, Liebl, and their co-workers to propose that dUMP binds to the free, oxidized, enzyme and enhances the reductive half reaction (24). They proposed an ordered binding mechanism that is illustrated in Scheme 5.1A. McClarty and co-workers, on the other hand, conducted steady state studies by following tritium release from [5-^{3}H]dUMP, and reported that their kinetic examination of the two natural substrates, dUMP and CH_2H_4folate, resulted in parallel pattern in a double reciprocal plot analysis (Lineweaver Burke) (27). That pattern suggested that CH_2H_4folate binds to the reduced ($FADH_2$) enzyme, transfers its methylene to the enzyme, and that the product H_4folate is released before dUMP binds. These observations lead to the kinetic scheme illustrated in Scheme 5.1B (27).

We conducted similar steady state experiments while following [2-^{14}C]dUMP conversion to [2-^{14}C]dTMP and an intersecting double reciprocal plot of dUMP vs. CH_2H_4folate suggested that these two substrates bind sequentially as illustrated in Scheme 5.1C (79). Similar analysis of the relationship between NADPH and dUMP or CH_2H_4folate also indicated that the product of the reductive half reaction ($NADP^+$) is not released from the enzyme until both dUMP and CH_2H_4folate bind, and presumably until the end of the oxidative half reaction. Scheme 5.1D illustrates this mechanism, where the bottom path (oxidase activity) is faster than the top path (TS activity) (24). We suggest that O_2 and CH_2H_4folate compete for the reduced enzyme (FDTS bound $FADH_2$) after dUMP binding. dUMP enhances the rate of the oxidative half reaction and while the oxidase reaction is faster than the reaction with CH_2H_4folate, this cofactor slows down the consumption of NADPH in the presence of O_2 (24), in accordance with substrate competition.

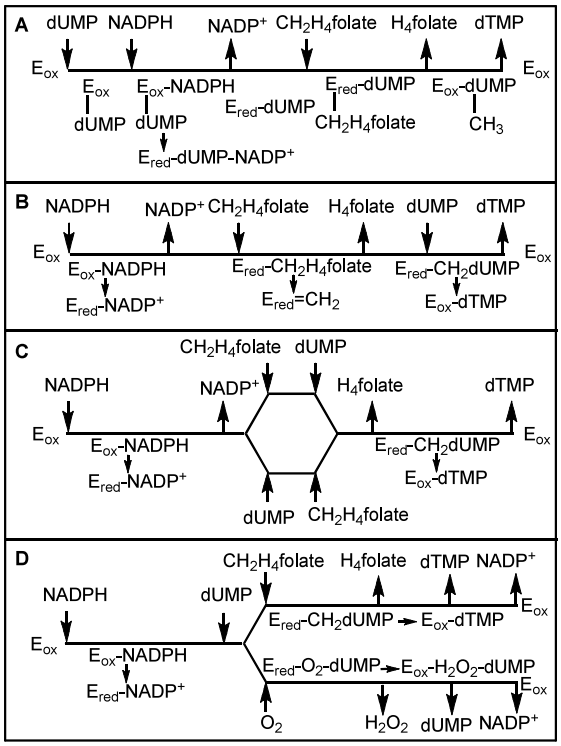

Scheme 5.1. Proposed kinetic mechanisms for FDTS A. Graziani *et al.* (2006) (23), B. Griffin *et al.* (2005) (27), C. Agrawal *et al.* (2004) (18). D. This work (see text).

In summary, two new sets of experiments were conducted in order to examine the role of dUMP as an activator, rather than a substrate of FDTS. In contrast to previous reports, the substrate of the oxidative half reaction (dUMP) does not affect the reductive half reaction (Figure 5.1). In the absence of the second substrate (CH_2H_4folate), dUMP enhances the reaction of molecular oxygen with the reduced enzyme (Figure 5.2) with an "effector" binding constant (K_f) close to 2 mM. This constant presented a weak temperature dependency (e.g., about 1 mM per 30 ˚C). This relatively tight binding with a weak temperature dependency is typical of entropy driven processes. A plausible molecular explanation may involve a dUMP induced protein rigidity prior to O_2 reduction. The lower oxidase activity in the absence of dUMP may result from multiple conformations with only a small fraction of reactive conformations. The binding of dUMP may induce conversion of the protein into the more reactive ensemble of conformations.

Future efforts will examine whether dUMP also activates its reaction with CH_2H_4folate. Allosteric substrate (dUMP) activation will be pursued under anaerobic conditions with CH_2H_4folate as the oxidizing agent (Hill constant values larger than unity may indicate such substrate activation). Additionally, the nature of the competition between CH_2H_4folate and O_2 for the reduced enzyme will be examined via kinetic analysis of their mutual inhibition. While the oxidase activity might not be natural to FDTS from the anaerobic *T. maritima*, it may serve as a probe for hidden features such as the tight binding of dUMP to the reduced enzyme, a much stronger interaction than predicted from K_M values of dUMP (23).

CHAPTER VI

CONCLUSIONS

The studies presented herein have greatly shaped the view of the molecular mechanism of FDTS catalysis and provided evidence for an unprecedented enzymatic methylation reaction. Previously known catalytic strategies for pyrimidine methylation via covalently bound enzyme intermediates do not apply to the FDTS reaction. Instead, FDTS seems to catalyze the reductive methylation by non-covalent protein interactions and cofactor chemistry as shown in chapter II. This remarkable feature of FDTS enzymes has rendered the overall catalytic mechanism quite challenging to access, as certain chemical transformations seem to be unique among biological catalysts. While we have made significant progress in determining aspects of FDTS that are substantially different from classical TS, a unified view of FDTS catalysis is still missing. Nevertheless, the striking differences between FDTS and classical thymidylate biosynthesis enzymes present a unique opportunity to selectively target the flavin-dependent enzyme function and expand the repertoire of methylation enzymes in general.

An important direction for further determination of the mechanism of FDTS will be the chemical trapping of intermediates. To date only one chemically trapped intermediate has been identified, which was isolated after acidic quenching and presented in chapter III. This study has shown a time-course for intermediate formation, and confirmed that several intermediates accumulate during the reaction and are accessible by suitable chemical modification. Other quenching reagents could possibly isolate additional chemical species by modification of reaction intermediates. For example, quenching with base, organic solvents, reducing agents, or nucleophilic compounds could react to give additional trapped derivatives, which might shed light on the structure of the true intermediates that accumulate during catalysis. Future mechanistic studies will be greatly facilitated by these intermediate identification experiments and any

accompanying spectral data reporting on the electronic structure of the flavin during accumulation of these intermediates.

Crystal structures of enzymes mimicking reactive complexes are invaluable when predicting enzyme mechanism and function. Unfortunately, while several crystal structures of FDTS enzymes have been reported, none gives a clear picture of a reactive complex. The findings presented in Chapter IV are the first structures of FDTS with folate moieties bound; however, these appear to represent an inhibitory binding configuration. Additionally, attempts by others to crystallize FDTS with bound nicotinamide resulted in the substitution of the coenzyme FAD, and thus a structure with a non-reactive configuration. It is noteworthy that no crystal structures have been obtained with reduced flavin, which could greatly affect the geometry and electrostatics of this coenzyme's binding in the active site and is more relevant to catalysis than its oxidized form. To this end, crystals should be grown anaerobically under reducing conditions with different ligand combinations. Furthermore, mutant enzymes that enable greater flexibility of the flavin in the active site (i.e. those studied in Chapter IV, E144R, R174K, etc.) could also provide structures that trap a configuration of the flavin relevant to catalysis. These studies might provide the necessary pieces of the puzzle to better understand the function of FDTS and could reveal unique binding modes important for inhibition.

One of the principal goals of studying FDTS enzymes is to identify selective inhibitors with low cross-reactivity with other enzymes (i.e., classical thymidylate biosynthesis enzymes). One of the most accessible resources to achieve such selectivity is through a mechanistic approach taking advantage of the unique intermediates and transition-states formed during FDTS catalysis. To this end, the most distinguishing feature of FDTS is that it does not rely on an enzymatic nucleophile for catalysis. Therefore, compounds that mimic non-covalent binding modes relevant to catalysis could be one possible avenue for inhibition. Some of the non-covalent intermediates proposed

in the FDTS mechanisms presented in chapter II and III are predicted to be stable in neutral aqueous solutions (e.g. the exocyclic-enone isomer of dTMP) and therefore could be synthesized and tested directly with the enzyme. This would help establish the actual intermediates formed during catalysis. Additionally, compounds that structurally mimic these unique intermediates or transition-states along the reaction are likely to bind to FDTS with high affinity, yet lack reactivity and therefore act as inhibitors. Furthermore, since these compounds take advantage of key mechanistic features of the FDTS reaction they might not bind to classical TS and could represent the first step towards antibiotic drugs selectively targeting pathogenic thymidylate biosynthesis.

Since we have found the reaction catalyzed by FDTS to be remarkably different from classical TS, it is reasonable to question mechanisms proposed for other flavoenzymes that methylate pyrimidines. For example, TrmFO methylates the uridyl base in position 54 of tRNA to form a thymidyl moiety, which is the same net reaction catalyzed by FDTS. Further investigation into TrmFO and other flavoenzyme methylases could expose similarities to the FDTS reaction. Thus an additional impact of establishing a mechanism for FDTS enzymes will come from applying the knowledge and experimental tools gained from its study to other methylation systems. Only when additional studies comparing all thymidyl biosynthetic enzymes are complete will we really know if FDTS is truly a unique catalyst, or alternatively, a model for flavoenzyme pyrimidine methylation.

REFERENCES

1. Carreras CW & Santi DV (1995) The catalytic mechanism and structure of thymidylate synthase. *Annu. Rev. Biochem.* 64:721-762.

2. Finer-Moore JS, Santi DV, & Stroud RM (2003) Lessons and conclusions from dissecting the mechanism of a bisubstrate enzyme: thymidylate synthase mutagenesis, function and structure. *Biochemistry* 42:248-256.

3. Lesley SA*, et al.* (2002) Structural genomics of the *Thermotoga maritima* proteome implemented in a high-throughput structure determination pipeline. *Proc. Natl. Acad. Sci. U.S.A.* 99:11664-11669.

4. Myllykallio H*, et al.* (2002) An alternative flavin-dependent mechanism of thymidylate synthesis. *Science* 297:105-107.

5. Murzin AG (2002) BIOCHEMISTRY: DNA Building Block Reinvented. *Science* 297:61-62.

6. Costi MP & Ferrari S (2009) Biochemistry: Anchors away. *Nature* 458:840-841.

7. Escartin F, Skouloubris S, Liebl U, & Myllykallio H (2008) Flavin-dependent thymidylate synthase X limits chromosomal DNA replication. *Proc. Natl Acad. Sci. USA* 105:9948-9952.

8. Leduc D*, et al.* (2007) Flavin-Dependent Thymidylate Synthase ThyX Activity: Implications for the Folate Cycle in Bacteria. *J. Bacteriol.* 189:8537-8545.

9. Myllykallio H, Leduc D, Filee J, & Liebl U (2003) Life without dihydrofolate reductase FolA. *Trends Microbiol.* 11:220-223.

10. Mathews II*, et al.* (2003) Functional analysis of substrate and cofactor complex structures of a thymidylate synthase-complementing protein. *Structure* 11:677-690.

11. Kuhn P*, et al.* (2002) Crystal structure of Thy1, a thymidylate synthase complementing protein from *Thermatoga maritima* at 2.25 A resolution. *Proteins: Struct. Funct. Genet.* 49:142-145.

12. Ulmer JE, Boum Y, Thouvenel CD, Myllykallio H, & Sibley CH (2008) Functional analysis of the Mycobacterium tuberculosis FAD-dependent thymidylate synthase, ThyX, reveals new amino acid residues contributing to an extended ThyX motif. *J. Bacteriology* 190:2056-2064.

13. Barrett JE, Maltby DA, Santi DV, & Schultz PG (1998) Trapping of the C5 methylene intermediate in thymidylate synthase. *J. Am. Chem. Soc.* 120:449.

14. Hyatt DC, Maley F, & Montfort WR (1997) Use of strain in a stereospecific catalytic mechanism: crystal structures of Escherichia coli thymidylate synthase bound to FdUMP and methylenetetrahydrofolate. *Biochemistry* 36:4585-4594.

15. Johnson EF, Hinz W, Atreya CE, Maley F, & Anderson KS (2002) Mechanistic Characterization of Toxoplasma gondii Thymidylate Synthase (TS-DHFR)-Dihydrofolate Reductase. *J. Biol. Chem.* 277:43126-43136.

16. Atreya CE & Anderson KS (2004) Kinetic Characterization of Bifunctional Thymidylate Synthase-Dihydrofolate Reductase (TS-DHFR) from Cryptosporidium hominis. *J. Biol. Chem.* 279:18314-18322.

17. Hong B & Kohen A (2005) Microscale synthesis of isotopically labeled 6R-N5, N10 methylene-5, 6, 7, 8-tetrahydrofolate. *J. Labelled Comp. Radiopharm.* 48:759-769.

18. Agrawal N, Lesley SA, Kuhn P, & Kohen A (2004) Mechanistic studies of a flavin-dependent thymidylate synthase. *Biochemistry* 43:10295-10301.

19. Hong B, Maley F, & Kohen A (2007) The role of Y94 in proton and hydride transfers catalyzed by thymidylate synthase. *Biochemistry* 46:14188-14197.

20. Delk AS, Nagle D. P, Jr., & Rabinowitz JC (1980) Methylenetetrahydrofolate-dependent biosynthesis of ribothymidine in transfer RNA of Streptococcus faecalis. *J. Biol. Chem.* 255:4387.

21. Delk AS, Nagle DP, Rabinowitz JC, & Straub KM (1979) The methylenetetrahydrofolate-mediated biosynthesis of ribothymidine in the transfer-RNA of Streptococcus faecalis: Incorporation of hydrogen from solvent into the methyl moiety. *Biochemical and Biophysical Research Communications* 86:244-251.

22. Koehn EM*, et al.* (2009) An unusual mechanism of thymidylate biosynthesis in organisms containing the thyX gene. *Nature* 458:919-923.

23. Graziani S*, et al.* (2006) Catalytic mechanism and structure of viral flavin-dependent thymidylate synthase *Thy*X. *J. Biol. Chem.* 281:24048-24057.

24. Graziani S*, et al.* (2004) Functional Analysis of FAD-dependent Thymidylate Synthase ThyX from Paramecium bursaria Chlorella Virus-1. *J. Biol. Chem.* 279:54340-54347.

25. Chernyshev A, Fleischmann T, & Kohen A (2007) Thymidyl biosynthesis enzymes as antibiotic targets. *Appl. Microbiol. Biotechnol.* 74:282-289.

26. Gattis SG & Palfey BA (2005) Direct observation of the participation of flavin in product formation by thyX-encoded thymidylate synthase. *J. Am. Chem. Soc.* 127:832-833.

27. Griffin J, Roshick C, Iliffe-Lee E, & McClarty G (2005) Catalytic mechanism of Chlamydia trachomatis flavin-dependent thymidylate synthase. *J. Biol. Chem.* 280:5456-5467.

28. Wataya Y & Santi DV (1975) Thymidylate synthase catalyzed dehalogenation of 5-bromo-and 5-iodo-deoxyuridylate. *Biochem. Biophys. Res. Commun.* 67:818-823.

29. Wang Z*, et al.* (2009) Oxidase activity of a flavin-dependent thymidylate synthase. *FEBS Journal* 276:2801-2810.

30. Leduc D*, et al.* (2004) Functional evidence for active site location of tetrameric thymidylate synthase X at the interphase of three monomers. *Proc. Nat. Acad. Sci. U.S.A.* 101:7252–7257.

31. Sampathkumar P*, et al.* (2005) Structure of the *Mycobacterium tuberculosis* flavin dependent thymidylate synthase (*Mtb*ThyX) at 2.0 resolution. *J. Mol. Biol.* 352:1091-1104.

32. Sampathkumar P, Turley S, Sibley CH, & Hol WGJ (2006) NADP+ Expels both the Co-factor and a Substrate Analog from the Mycobacterium tuberculosis ThyX Active Site: Opportunities for Anti-bacterial Drug Design. *J. Mol. Biol.* 360:1-6.

33. Chernyshev A, Fleischmann T, Koehn E, Lesley SA, & Kohen A (2007) The relationships between oxidase and synthase activities of flavin dependent thymidylate synthase (FDTS). *Chem. Commun.*:2861-2863.

34. Brown BJ, Deng Z, Karplus PA, & Massey V (1998) On the active site of Old Yellow Enzyme. Role of histidine 191 and asparagine 194. *J. Biol. Chem.* 273:32753-32762.

35. Fagan RL, Nelson MN, Pagano PM, & Palfey BA (2006) Mechanism of flavin reduction in class 2 dihydroorotate dehydrogenases. *Biochemistry* 45:14926-14932.

36. Kloetzer W (1973) Two isomers of thymine. *Monatsh. Chem.* 104:415-420.

37. Carey FA & Sundberg RJ (2000) Advanced Organic Chemistry, Part A. (Macmillan Publishers Limited. All rights reserved).

38. Hunter JH, Gujjar R, Pang CK, & Rathod PK (2008) Kinetics and ligand-binding preferences of Mycobacterium tuberculosis thymidylate synthases, ThyA and ThyX. *PLoS ONE* 3:e2237.

39. Mason A, Agrawal N, Washington MT, Lesley SA, & Kohen A (2006) A lag-phase in the reduction of flavin dependent thymidylate synthase (FDTS) revealed a mechanistic missing link. *Chem. Commun.*:1781-1783.

40. Mattevi A (2006) To be or not to be an oxidase: challenging the oxygen reactivity of flavoenzymes. *Trends in Biochemical Sciences* 31:276-283.

41. Esra Önen F*, et al.* (2008) Design, synthesis and evaluation of potent thymidylate synthase X inhibitors. *Bioorg. Med. Chem. Lett.* 18:3628-3631.

42. Stroud RM & Finer-Moore JS (2003) Conformational dynamics along an enzymatic reaction pathway: Thymidylate Synthase, the Movie. *Biochemistry* 42:239.

43. Waldman AS, Haeusslein E, & Milman G (1983) Purification and characterization of herpes simplex virus (type 1) thymidine kinase produced in Escherichia coli by a high efficiency expression plasmid utilizing a lambda PL promoter and cI857 temperature-sensitive repressor. *J. Biol. Chem.* 258:11571-11575.

44. Burdzy A, Noyes KT, Valinluck V, & Sowers LC (2002) Synthesis of stable-isotope enriched 5-methylpyrimidines and their use as probes of base reactivity in DNA. *Nucleic Acids Res.* 30:4068-4074.

45. Sotelo-Mundo RR*, et al.* (1999) Crystal structures of rat thymidylate synthase inhibited by Tomudex, a potent anticancer drug. *Biochemistry* 38:1087-1094.

46. Takemura Y & Jackman AL (1997) Folate-based thymidylate synthase inhibitors in cancer chemotherapy. *Anticancer Drugs* 8:3-16.

47. Touroutoglou N & Pazdur R (1996) Thymidylate synthase inhibitors. *Clin. Cancer Res.* 2:227-243.

48. Conrad JA, Ortiz-Maldonado M, Hoppe SW, & Palfey BA (2011) Oxidative Half Reaction of the FAD-dependent Thymidylate Synthase from Thermotoga maritima. *JACS (accepted and enclosed for reviewers only)*.

49. Moore MA, Ahmed F, & Dunlap RB (1986) Trapping and partial characterization of an adduct postulated to be the covalent catalytic ternary complex of thymidylate synthase. *Biochemistry* 25:3311-3317.

50. Huang W & Santi DV (1994) Isolation of a covalent steady-state intermediate in glutamate 60 mutants of thymidylate synthase. *J. Biol. Chem.* 269:31327-31329.

51. KoÃàgler M*, et al.* (2011) Synthesis and Evaluation of 5-Substituted 2,Ä≤-deoxyuridine Monophosphate Analogues As Inhibitors of Flavin-Dependent Thymidylate Synthase in Mycobacterium tuberculosis. *J. Med. Chem.* 54:4847-4862.

52. Koehn EM & Kohen A (2010) Flavin-dependent thymidylate synthase: a novel pathway towards thymine. *Arch. Biochem. Biophys.* 493:96-102.

53. Agrawal N, Mihai C, & Kohen A (2004) Microscale synthesis of isotopically labeled *R*-[6-^{x}H]N^{5},N^{10}-methylene-5,6,7,8-tetrahydrofolate as a cofactor for thymidylate synthase. *Anal. Biochem.* 328:44-50.

54. Hazra S, Ort S, Konrad M, & Lavie A (2010) Structural and kinetic characterization of human deoxycytidine kinase variants able to phosphorylate 5-substituted deoxycytidine and thymidine analogues. *Biochemistry* 49:6784-6790.

55. Mishanina TV*, et al.* (2012) Trapping of an intermediate in the reaction catalyzed by flavin-dependent thymidylate synthase (FDTS). *J. Am. Chem. Soc.* 134:4442-4448.

56. Wang K*, et al.* (2011) Crystal structure and enzymatic characterization of thymidylate synthase X from Helicobacter pylori strain SS1. *Protein Sci* 20:1398—1410.

57. Leduc D*, et al.* (2004) Two distinct pathways for thymidylate (dTMP) synthesis in (hyper)thermophilic Bacteria and Archaea. *Biochem. Soc. Trans.* 32:231-235.

58. Fivian-Hughes AS, Houghton J, & Davis EO (2012) Mycobacterium tuberculosis thymidylate synthase gene thyX is essential and potentially bifunctional, while thyA deletion confers resistance to p-aminosalicylic acid. *Microbiology* 158:308-318.

59. Mishanina TV, Koehn EM, & Kohen A (2011) Mechanisms and inhibition of uracil methylating enzymes. *Bioorg. Chem.*:In Press.

60. Cunningham D*, et al.* (1996) 'Tomudex' (ZD1694): a novel thymidylate synthase inhibitor with clinical antitumour activity in a range of solid tumours. 'Tomudex' International Study Group. *Ann. Oncol.* 7:179-182.

61. Berkholz DS, Faber HR, Savvides SN, & Karplus PA (2008) Catalytic Cycle of Human Glutathione Reductase Near 1Å Resolution. *Journal of Molecular Biology* 382:371-384.

62. Nishimasu H*, et al.* (2009) Atomic structure of a folate/FAD-dependent tRNA T54 methyltransferase. *Proc Natl Acad Sci U S A* 106:8180-8185.

63. Phan J*, et al.* (2001) Human thymidylate synthase is in the closed conformation when complexed with dUMP and raltitrexed, an antifolate drug. *Biochemistry* 40:1897-1902.

64. Kabsch W (2010) XDS. . *Acta Crystallogr. D Biol. Crystallogr.* 66:125-132

65. Vagin AaT, A. (1997) MOLREP: an automated program for molecular replacement. *J. Appl. Cryst.* 30:1022-1025.

66. Murshudov GN, Vagin AA, & Dodson EJ (1997) Refinement of macromolecular structures by the maximum-likelihood method. *Acta Crystallogr. D Biol. Crystallogr.* 53:240-255.

67. Emsley PaC, K. (2004) Coot: model-building tools for molecular graphics. *Acta Crystallogr. D Biol. Crystallogr.* 60:2126-2132.

68. Case DA*, et al.* (2006) AMBER 9. *University of California: San Francisco*.

69. Cheatham TE, Cieplak P, & Kollman PA (1999) A modified version of the Cornell et al. force field with improved sugar pucker phases and helical repeat. *J. Biomol. Struct. Dyn.* 16(4):845-862.

70. Frisch MJ*, et al.* (2009) Gaussian 09, Revision A.02. *Gaussian, Inc., Wallingford CT*.

71. Dupradeau F-Y*, et al.* (2008) R.E.DD.B.: A database for RESP and ESP atomic charges, and force field libraries. *Nucl. Acids Res. (Database issue)*:D360-D367.

72. Wang J, Cieplak P, & Kollman PA (2000) How well does a restrained electrostatic potential (RESP) model perform in calculating conformational energies of organic and biological molecules? *J. Comput. Chem.* 21:1049-1074.

73. Bashford D & Case DA (2000) Generalized Born Models of Macromolecular Solvation Effects. . *Ann. Rev. Phys. Chem.* 51:129-152.

74. Simonson T (2001) Macromolecular electrostatics: continuum models and their growing pains. *Curr. Opin. Struct. Biol.* 11:243-252.

75. Tsui V & Case DA (2001) Theory and applications of the generalized Born solvation model in macromolecular simulations. . *Biopolymers* 56:275-291.

76. Gibson QH, Swoboda BE, & Massey V (1964) Kinetics and mechanism of action of glucose oxidase. *J. Biol. Chem.* 239:3927-3934.

77. Neujahr HY & Kjellen KG (1978) Phenol hydroxylase from yeast. Reaction with phenol derivatives. *J. Biol. Chem.* 253:8835-8841.

78. Zhou M, Diwu Z, Panchuk-Voloshina N, & Haugland RP (1997) A stable nonfluorescent derivative of resorufin for the fluorometric determination of trace hydrogen peroxide: Applications in detecting the activity of phagocyte NADPH oxidase and other oxidases. *Anal. Biochem.* 253:162-168.

79. Agrawal N, Hong B, Mihai C, & Kohen A (2004) Vibrationally enhanced hydrogen tunneling in the E. coli thymidylate synthase catalyzed reaction. *Biochemistry* 43:1998.